

RESONANCE CONES AND MODE CONVERSION IN A WARM MAGNETIZED
BOUNDED PLASMA

Thesis by
Crockett L. Grabbe

In partial fulfillment of the requirements
for the degree of
Doctor of Philosophy

California Institute of Technology
Pasadena, California

1978

(Submitted August 29, 1977)

ACKNOWLEDGMENT

I would like to thank my advisor, Dr. Roy Gould, for his guidance during the course of this work and for his instructive comments on plasma physics.

I am also grateful to Dr. Hans Kuehl, for the interesting and useful discussions I had with him during his short stay at the institute, and to Dr. Mario Simonutti, for his informative comments and help while he was a research fellow at the institute.

To the electromagnetic theory group, Dr. C. H. Papas and his students Walter de Logi, Dwight Jaggard, and Alan Mickelson, I am grateful for occasional chats on electromagnetic theory and related problems in physics, some of which touched on this work.

I greatly appreciate the support from the U.S. Energy Research and Development Administration (initially the Atomic Energy Commission) for their support which made this research possible.

To Ruth Stratton and others I owe thanks for help in preparing the manuscript.

Finally, the moral support and encouragement of family and friends is gratefully acknowledged.

ABSTRACT

The warm plasma resonance cone structure of the quasistatic field produced by a gap source in a bounded magnetized slab plasma is determined theoretically. This is initially determined for a homogeneous or mildly inhomogeneous plasma with source frequency lying between the lower hybrid frequency and the plasma frequency. It is then extended to the complicated case of an inhomogeneous plasma with two internal lower hybrid layers present, which is of interest to radio frequency heating of plasmas.

In the first case, the potential is obtained as a sum of multiply-reflected warm plasma resonance cones, each of which has a similar structure, but a different size, amplitude, and position. An important interference between nearby multiply-reflected resonance cones is found. The cones are seen to spread out as they move away from the source, so that this interference increases and the individual resonance cones become obscured far away from the source.

In the second case, the potential is found to be expressible as a sum of multiply-reflected, multiply-tunnelled, and mode converted resonance cones, each of which has a unique but similar structure. The effects of both collisional and collisionless damping are included and their effects on the decay of the cone structure studied. Various properties of the cones such as how they move into and out of the hybrid layers, through the evanescent region, and transform at the hybrid layers are determined. It is found that cones can tunnel through the evanescent layer if the layer is thin,

and the effect of the thin evanescent layer is to subdue the secondary maxima of cone relative to the main peak, while slightly broadening the main peak and shifting it closer to the cold plasma cone line.

Energy theorems for quasistatic fields are developed and applied to determine the power flow and absorption along the individual cones. This reveals the points of concentration of the flow and the various absorption mechanisms.

TABLE OF CONTENTS

CHAPTER I: INTRODUCTION	1
1.1 Review of Resonance Cone Theory	1
1.2 Review of the Theory of Mode Conversion	11
1.3 Model	17
1.4 Purpose of This Work	29
CHAPTER II: RESONANCE CONE STRUCTURE FOR HOMOGENEOUS PLASMA	32
2.1 Model and Approximations	
2.2 Equation for the Potential	33
2.3 Guided Wave Solutions	37
2.4 Resonance Cone Solutions and Properties	39
2.5 Damping of the Resonance Cones	53
2.6 Analysis of Assumptions	62
2.7 Inhomogeneous Plasma	65
CHAPTER III: RESONANCE CONES IN INHOMOGENEOUS PLASMA WITH LOWER HYBRID LAYERS :	70
3.1 Lower Hybrid Density Model	70
3.2 Dispersion Relation near Lower Hybrid	77
3.3 WKB Solutions	79
3.4 Resonance Region Solutions	86
3.5 Connections Between WKB and Hybrid Layer Solutions	99
3.6 Calculations of Coefficients	103
3.7 Expansion into Resonance Cone Form	110

3.8 Discussion and Illustration of Resonance Cones	123
CHAPTER IV: DAMPING, ENERGY FLOW, AND ABSORPTION	135
4.1 Damping of the Cones	135
4.2 Energy Conservation Theorems for Quasistatic Fields	151
4.3 Energy Flow and Absorption along the Cones	163
CHAPTER V: SUMMARY AND CONCLUSIONS	179
Suggestions for Further Work	188
APPENDIX A: TABLE OF NOTATION	190
APPENDIX B: DERIVATION OF WKB SOLUTIONS	193
REFERENCES	195

CHAPTER I: INTRODUCTION

1.1 Review of Resonance Cone Theory

Wave propagation in plasmas exhibits a variety of physical phenomena, which is enriched and increased in complexity by the presence of anisotropies (produced by a background magnetic field), finite temperature, inhomogeneities, collisions, and boundaries in the plasma. One such physical phenomenon which may occur in magnetized plasmas which has been of interest in the last few years is that of resonance cones produced by a driven source in the plasma. In the special case of a point source, simple cold plasma theory predicts that for ranges of the driving frequency such that $K_{\parallel}K_{\perp} < 0$, where K_{\parallel} is the equivalent dielectric constant along a static, homogeneous background magnetic field and K_{\perp} is the dielectric constant in the direction perpendicular to that field, the fields produced by the source become singular along a surface emanating from the source. For a homogeneous plasma this surface is that of a double-cone concentric with the magnetic field, hence the name resonance cones (see Fig. 1.1.) The singularities in the fields for such a plasma were first discussed in detail by H. Kuehl,¹ although others had previously noted the singularities.

In the quasistatic approximation, the potential of a source harmonically driven at a frequency ω in a cold homogeneous plasma with static magnetic field $\vec{B} = B_0 \hat{z}$ taken along the z axis is given by the Poisson equation

$$K_{\perp}(\omega) \frac{\partial^2 \phi(\rho, z)}{\partial \rho^2} + K_{\parallel}(\omega) \frac{\partial^2 \phi(\rho, z)}{\partial z^2} = \frac{\rho_{\text{ext}}}{\epsilon_0} e^{-i\omega t} \quad (1.1)$$

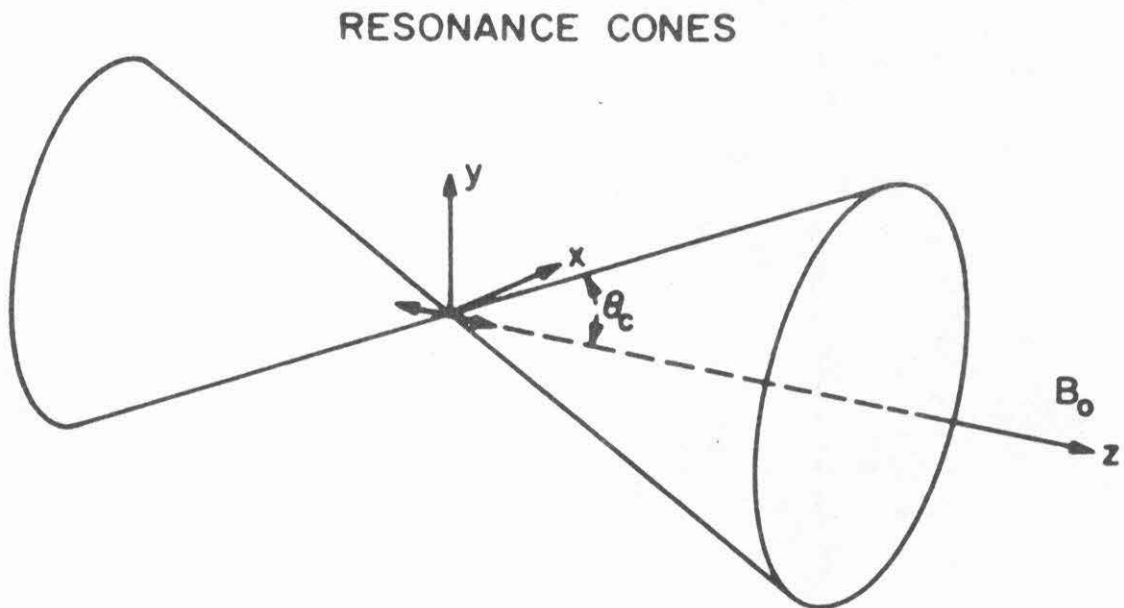


Fig. 1.1 Double cone surfaces along which the fields produced by a point source in a magnetized plasma become singular in cold plasma theory. θ_c is the resonance cone angle [after Fisher²].

in terms of cylindrical coordinates (ρ, ϕ, z) , where ρ_{ext} is the source charge density. The solution for an oscillating point source of charge q at the origin $\rho = z = 0$ is given by

$$\phi(\rho, z) = \frac{q e^{-i\omega t}}{4\pi\epsilon_0 (K_{\perp}^2 K_{\parallel})^{1/2} [\rho^2/K_{\perp} + z^2/K_{\parallel}]^{1/2}} \quad (1.2)$$

It is clear that when $K_{\parallel} K_{\perp} < 0$ there is a singularity in ϕ which occurs along the resonance cone angle θ_c given by

$$\tan \theta_c = \frac{\rho}{z} = \left[\frac{-K_{\perp}}{K_{\parallel}} \right]^{1/2} \quad (1.3)$$

and this angle defines the double-cone surface.

The form of the dielectric tensor components for the "cold" plasma is

$$K_{\perp} = 1 - \frac{\omega_{pe}^2}{\omega^2 - \omega_{ce}^2} - \frac{\omega_{pi}^2}{\omega^2 - \omega_{ci}^2} \quad (1.4)$$

$$K_{\parallel} = 1 - \frac{\omega_{pe}^2}{\omega^2} - \frac{\omega_{pi}^2}{\omega^2}$$

where $\omega_{pe} = \frac{ne^2}{\epsilon_0 m_e}$ and $\omega_{pi} = \frac{ne^2}{\epsilon_0 m_i}$ are the electron and ion plasma frequencies, $\omega_{ce} = Be/m_e$ and $\omega_{ci} = Be/m_i$ are the electron and ion cyclotron frequencies, n is the plasma density, e is the electronic charge, and m_i and m_e are the ion and electron masses. From these one sees the cold plasma resonance cones occurring for $K_{\perp} K_{\parallel} < 0$ exist for three frequency ranges of ω (see Fig. 1.2):²

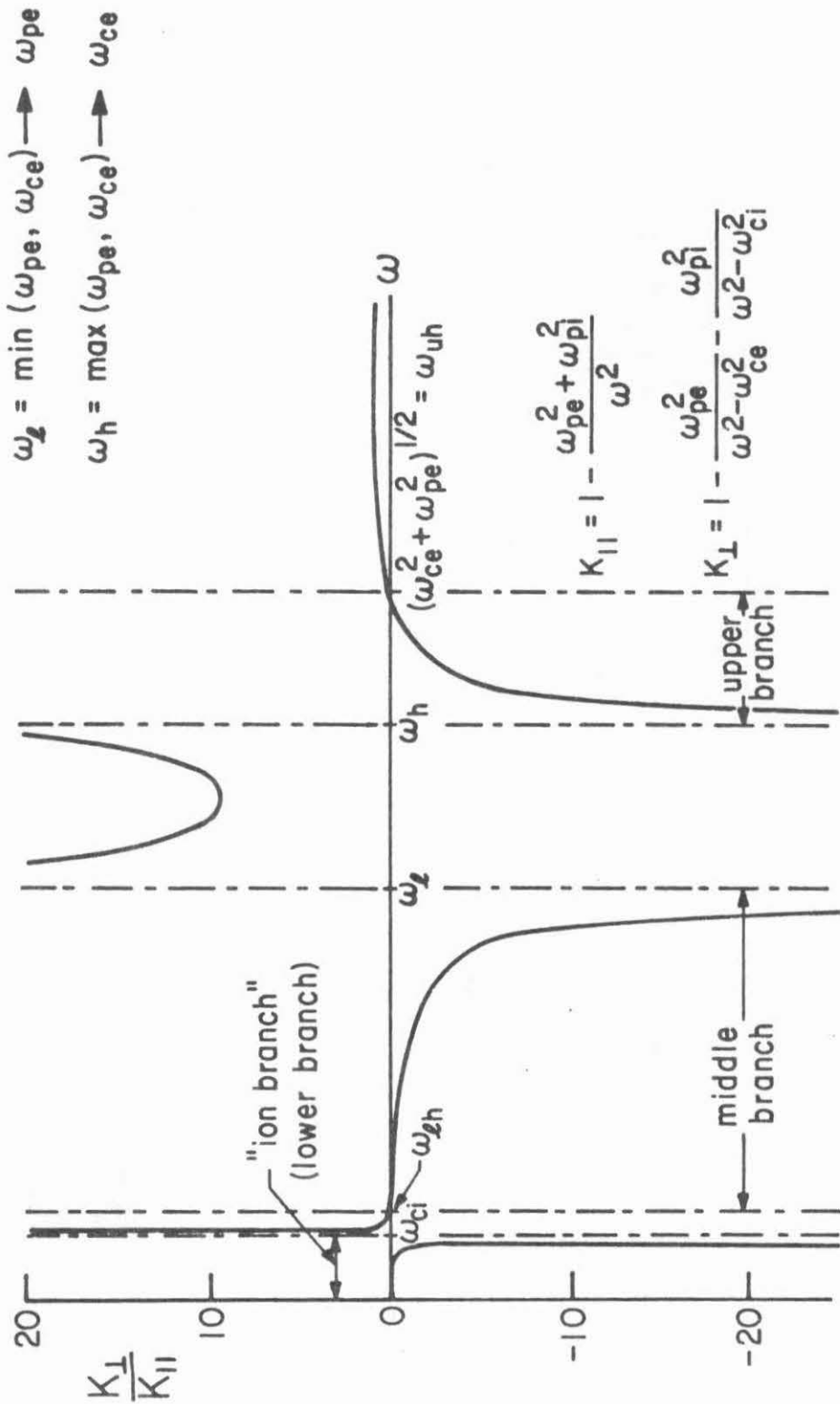


Fig. 1.2 Three frequency branches of the resonance cones predicted by cold plasma theory, occurring when $K_{\parallel} K_{\perp} < 0$ [after Fisher²].

$$(1) \quad 0 < \omega < \omega_{ci}$$

$$(2) \quad \omega_{lh} < \omega < \min(\omega_{pe}, \omega_{ce})$$

$$(3) \quad \max(\omega_{pe}, \omega_{ce}) < \omega < \omega_{uh} \quad ,$$

where $\omega_{lh} = \left[\frac{(\omega_{pi}^2 + \omega_{ci}^2)\omega_{ci}\omega_{ce}}{\omega_{pi}^2 + \omega_{ci}^2 + \omega_{ci}\omega_{ce}} \right]^{1/2}$ is the lower hybrid frequency

and $\omega_{uh} = (\omega_{pe}^2 + \omega_{ce}^2)^{1/2}$ is the upper hybrid frequency. It is the middle branch of the cones which we will be primarily concerned with in this work.

The reason for the occurrence of resonance cones is clearly seen from Eq. (1.1). When $K_{||}$ and K_{\perp} are of opposite sign, that equation has characteristics propagating from the source. Thus when we assume a point source, which implies a singularity in the field at that source, that singularity propagates out along the characteristics, and the resonance cones are just the characteristic surfaces. The occurrence of resonance cone singularities is not surprising, since it is a basic mathematical property of the simple plasma model which arises from an unphysical assumption. The inclusion of physical effects in the model such as finite temperature, collisions, or a finite source will eliminate these singularities. The important point from a physics standpoint is that in physical approximations to this idealized model, namely in plasmas with small temperatures, small sources, and small collision frequencies, the fields may be unusually large or concentrated along the resonance cone direction and have a structure which is dependent upon parameters of the

plasma, particularly on those properties which are most important in limiting the size of the field. It is these large field structures which occur along or near the cold plasma characteristic directions which have more generally come to be called resonance cones, and will be what I will refer to as resonance cones.

In this more general definition of the cones, the criterion for the existence of the cones of $K_{\parallel}K_{\perp} < 0$ is not always a valid criterion. This is because that criterion gives the condition under which the fields are singular for cold collisionless plasmas, and not for the finite field cone structures in a warm plasma. If one considers the warm plasma cones going from a region where $K_{\parallel}K_{\perp} < 0$ to one where $K_{\parallel}K_{\perp} > 0$ in an inhomogeneous plasma, the cones in the more general sense may not disappear, but rather, the large field structures may remain, although they usually spread out and decrease in size very rapidly in that region because the waves are evanescent there.

The physical phenomenon of resonance cones is just another manifestation of the existence of resonances in a plasma, where the index of refraction of a magnetized plasma becomes infinite in cold collisionless plasma theory for a wave of a given frequency.³ It is well known that quasistatic waves experience a resonance for phase velocities along an angle ψ given by

$$\tan \psi = \frac{k_x}{k_z} = \sqrt{\frac{-K_{\parallel}}{K_{\perp}}} \quad (1.5)$$

As pointed out by Fisher and Gould,² this angle is perpendicular to the resonance cone direction, because along the cones the phase velocity is

perpendicular to the group velocity. Thus resonance cones are just group velocity surfaces associated with waves propagating at resonance in a magnetized plasma.

R. Fisher² first observed the resonance cones experimentally and measured the cone field patterns. He found that the maxima of the field occurred inside the cold plasma resonance surface along with an oscillating interference structure (see Fig. 1.3). Such a cone field structure is predicted by warm plasma theory, i.e., thermal effects were very important in determining the physical resonance cone fields for that experiment (see Fig. 1.4). The upper frequency branches of the cones have also been observed by A. Gonfalone,⁴ R. Briggs and R. R. Parker for propagation into the lower hybrid layer,⁵ K. Burrell,⁶ P. Colestock,⁷ and P. Bellan and M. Porkolab.⁸ P. Bellan,⁹ and Ohmura, Kuwabara, Shibatu, and Adachi,¹⁰ have observed the low frequency branch of the cones.

Resonance cones are of interest for a couple of reasons other than just being interesting phenomena associated with wave propagation in plasmas. The first is their potential use as a plasma diagnostic under the right conditions. As seen from Eqs. (1.3) and (1.4), the cone angle is a unique function of the plasma frequency and hence the density. Thus by measuring the trajectory of the resonance cones one may deduce the density profile, as pointed out by Fisher and Gould.² Also, the interference spacing in the cone field structure as in Fig. 1.4 is a unique function of the electron temperature. Fisher and Gould calculated the angular interference spacing of the interference structure inside the cone for a point charge source in a homogeneous plasma with ion motions

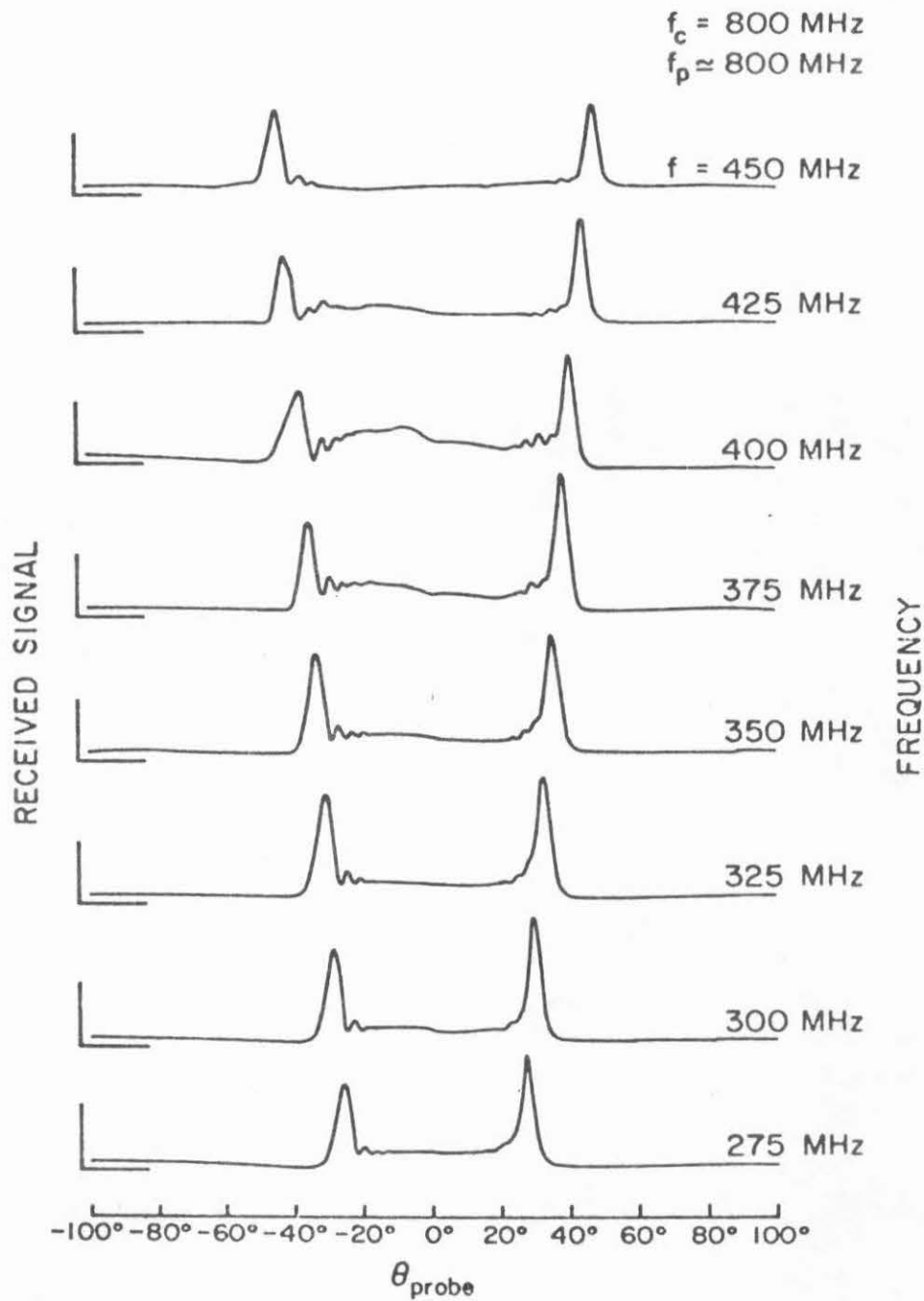


Fig. 1.3 Typical signal traces observed by Fisher, showing a strong peak along the resonance cone directions

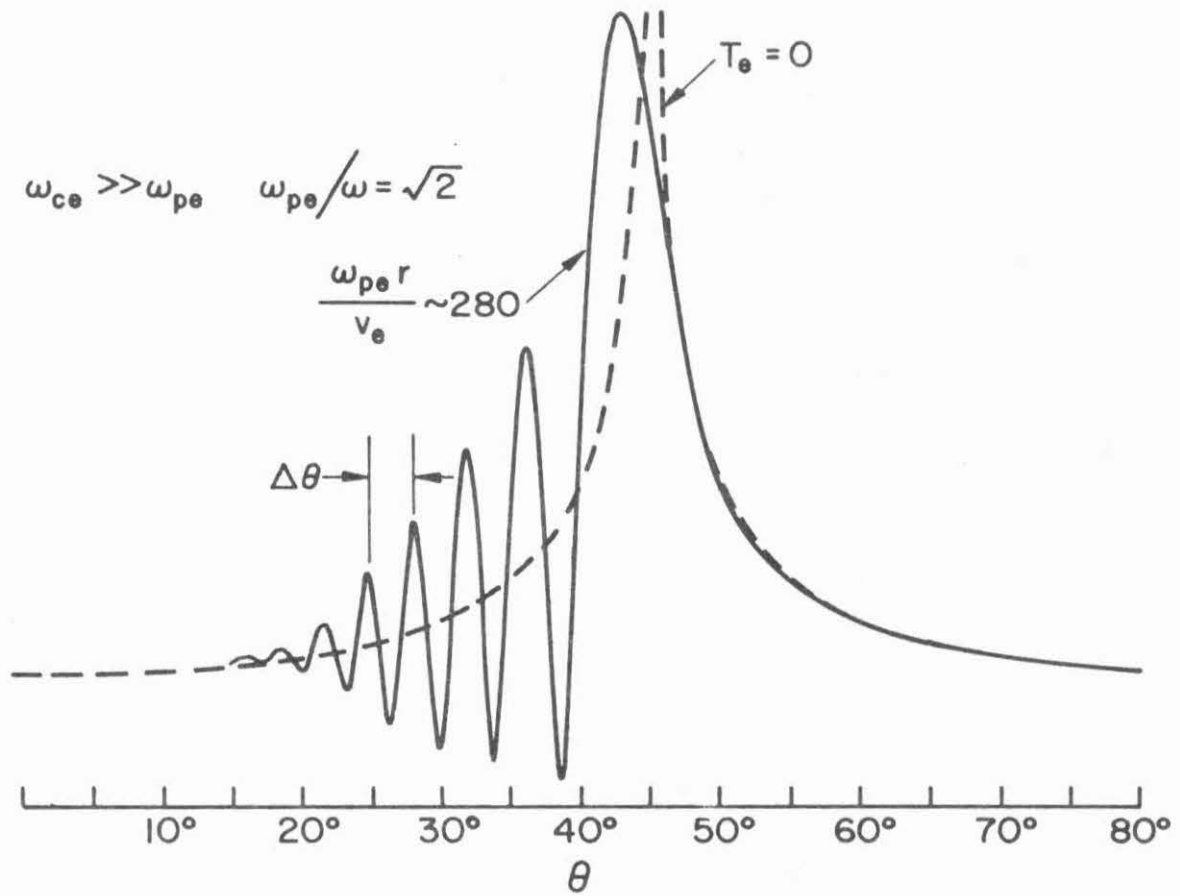


Fig. 1.4 Predicted warm plasma resonance cone pattern compared with the cold plasma pattern for a point charge source (made by Fisher and Gould²).

neglected to be

$$\Delta\theta = 5.8^\circ \left(\frac{200}{\omega_{pe} r/v_e} \right)^{2/3} \tan^{1/3} \theta_c \quad (1.6)$$

where r is the distance from the source and v_e is the electron thermal velocity. There are advantages to using the resonance cones as a diagnostic. While sheath effects at the transmitting and receiving antenna and probe geometry may significantly affect the amplitude of the received signal, they should not affect the resonance cone trajectory or the interference spacing, and hence not the measured temperature and density. Also, although Langmuir probe measurements can in principle be used to measure density and temperature, the theory is not very well developed for magnetized plasmas. Thus resonance cone measurements would provide a useful and in some cases more reliable supplement to Langmuir probe measurements of temperature and density.

Second is their importance in being channels along which energy flow is concentrated. This is of particular interest in understanding the transport of energy to the lower hybrid resonance in lower hybrid heating studies. Briggs and Parker⁵ showed that energy flow from an electrostatic wave source to the lower hybrid layer in an inhomogeneous plasma is confined to the narrow resonance cone channels, and near the hybrid layer the cones are aligned at a small angle $\sim (m_e/m_i)^{1/2}$ with respect to the magnetic field. The wave energy travels along the cones until it is absorbed or changed by damping, nonlinear effects, or mode conversion (to be discussed in the next section). For a linear open-ended device, the energy may reach the end of the plasma before it has been

totally absorbed at the hybrid layer because the cone is oriented almost parallel to the magnetic field (the density gradient being assumed to be perpendicular to the magnetic field) and thus be lost at the end. For a closed device such as a tokamak, the cones will circulate around the torus at the small angle until the lower hybrid layer is reached and the energy is absorbed or changed. The resonance cones excited by a ring source have been observed in a toroidal geometry in WII stellarator by P. Javel, G. Müller, U. Weber, and R. Weynants.¹¹

1.2 Review of the Theory of Mode Conversion

It has long been known that a wave in a magnetized plasma may experience a "resonance" in the plasma, i.e., a region where the index of refraction for the wave goes to infinity in cold collisionless plasma theory.³ For wave propagation perpendicular to the magnetic field in the extraordinary mode [for $\psi = \pi/2$ in Eq. (1.5)], there are two such resonances: the lower and upper hybrid resonances. That is, if $\omega = \omega_{\ell h}$ or $\omega = \omega_{uh}$ for the value of $\omega_{\ell h}$ or ω_{uh} for the local density and magnetic field of the plasma, the wave experiences a resonance at that point. These resonances have been of interest for wave heating of plasmas. The original idea was that a wave propagating into a resonance layer in an inhomogeneous plasma should have its phase velocity slow to zero and its energy density begin to diverge as suggested by cold plasma theory, and be completely absorbed by damping processes there. The wave energy would then go into heating of ions and electrons. If the damping processes were not present, however, the wave should be reflected at the resonance layer, since the wave becomes evanescent there (see Fig. 1.5).

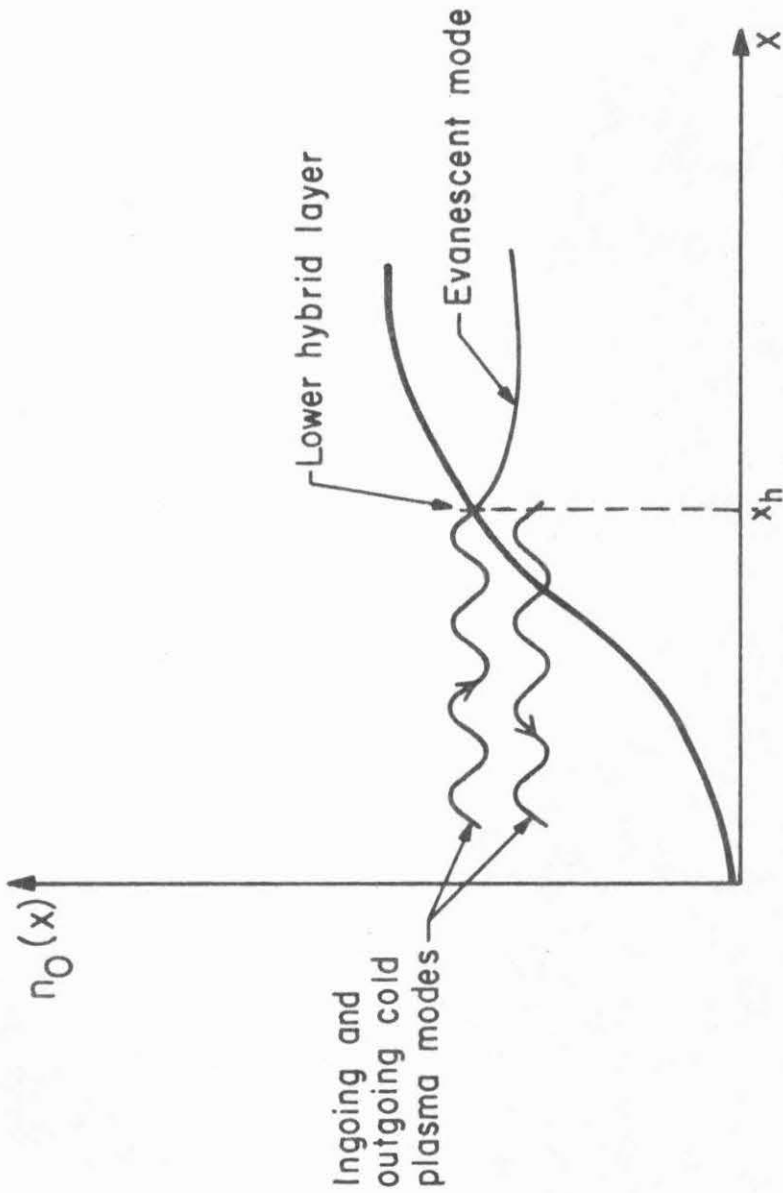


Fig. 1.5 Wave propagation into lower hybrid layer $x = x_h$ in cold plasma theory. The cold plasma mode becomes evanescent at the hybrid layer, and may reflect in the same mode if it is not completely absorbed near the layer by damping processes.

When the problem of wave propagation into a lower hybrid layer was considered from a warm plasma point of view, it was found that a finite temperature changes this picture.¹² The effect of temperature in a plasma is to add more possible modes of wave propagation, in principle an infinite number, but in practice only a few are important--the least damped root or roots which arise in Vlasov theory.¹³ Stix showed that theoretically an electrostatic extraordinary wave (see dispersion relation in Fig. 1.6) propagating into a lower hybrid resonance layer will not actually reach the layer but will convert into a purely thermal mode (an ion thermal or Bernstein mode¹⁴) just before the resonance layer and propagate out on the same side (see Fig. 1.7). Two exponentially decaying modes continue into the evanescent side of the resonance layer. It was concluded that for a large evanescent region, all of the power coming into the resonance layer should convert to the thermal short wavelength mode coming out of the layer. This mode would be much more highly damped than the mode coming into the resonance layer, and would rapidly decay away with its energy going to thermal energy of the ions and electrons. Thus it was thought that mode conversion at the lower hybrid would be a method of heating the plasma by waves.

It was shown by Stix³ that only those k_z excited by the source that are sufficiently large will reach the hybrid layer and be able to convert to the other mode, because the smaller k_z encounter substantial intermediate regions where k_x is imaginary. Stix gave the criterion $k_z \gtrsim 2\omega/c$ for accessibility and Golant¹⁵ gave the stronger condition

$$k_z \gtrsim \omega/c (1 + \omega_{pe}/\omega_{ce})^{1/2} \quad (1.7)$$

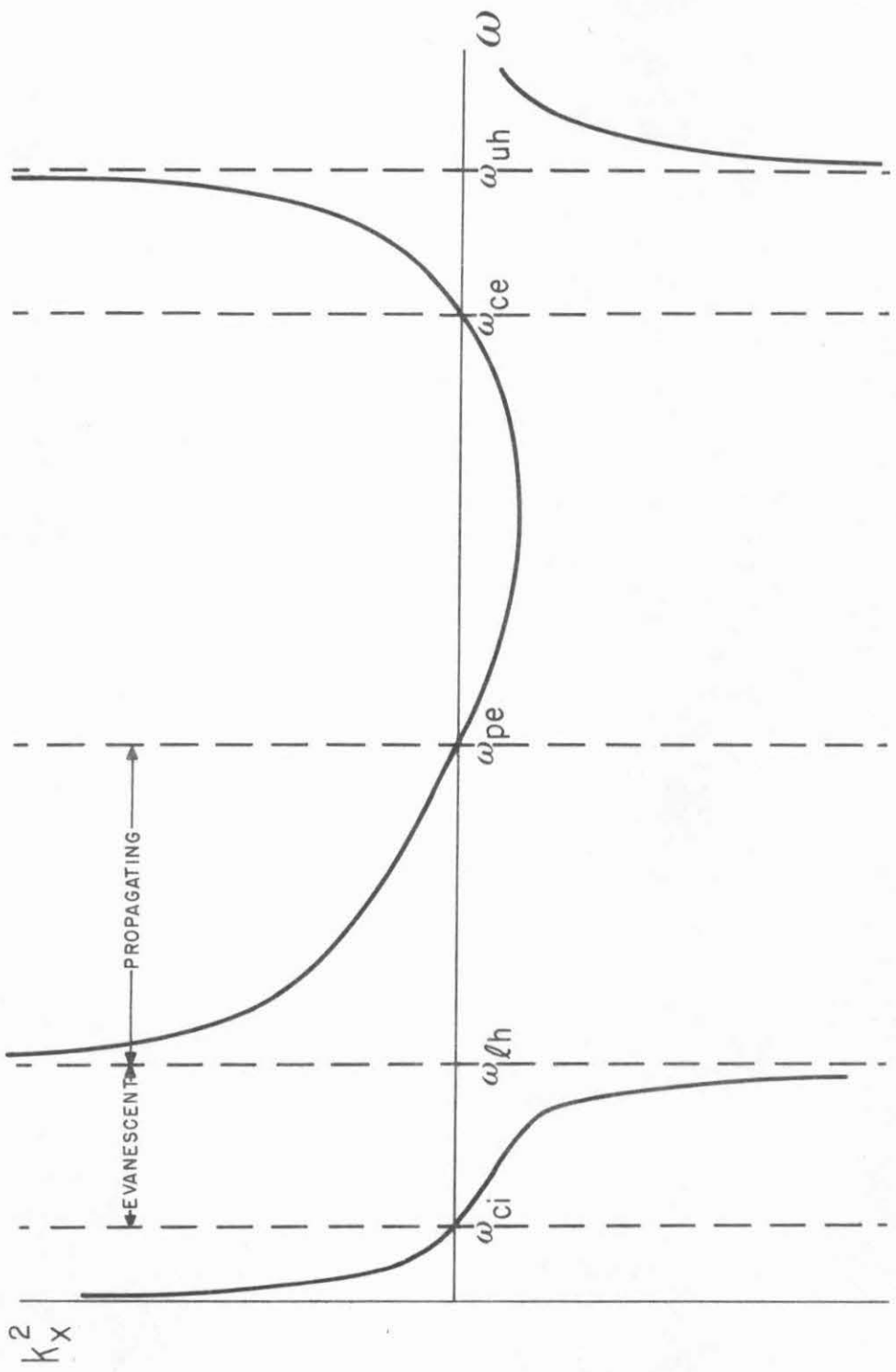


Fig. 1.6 Sketch of dispersion relation for the extraordinary mode in the cold plasma quasistatic approximation, showing propagating and evanescent regions near the lower hybrid

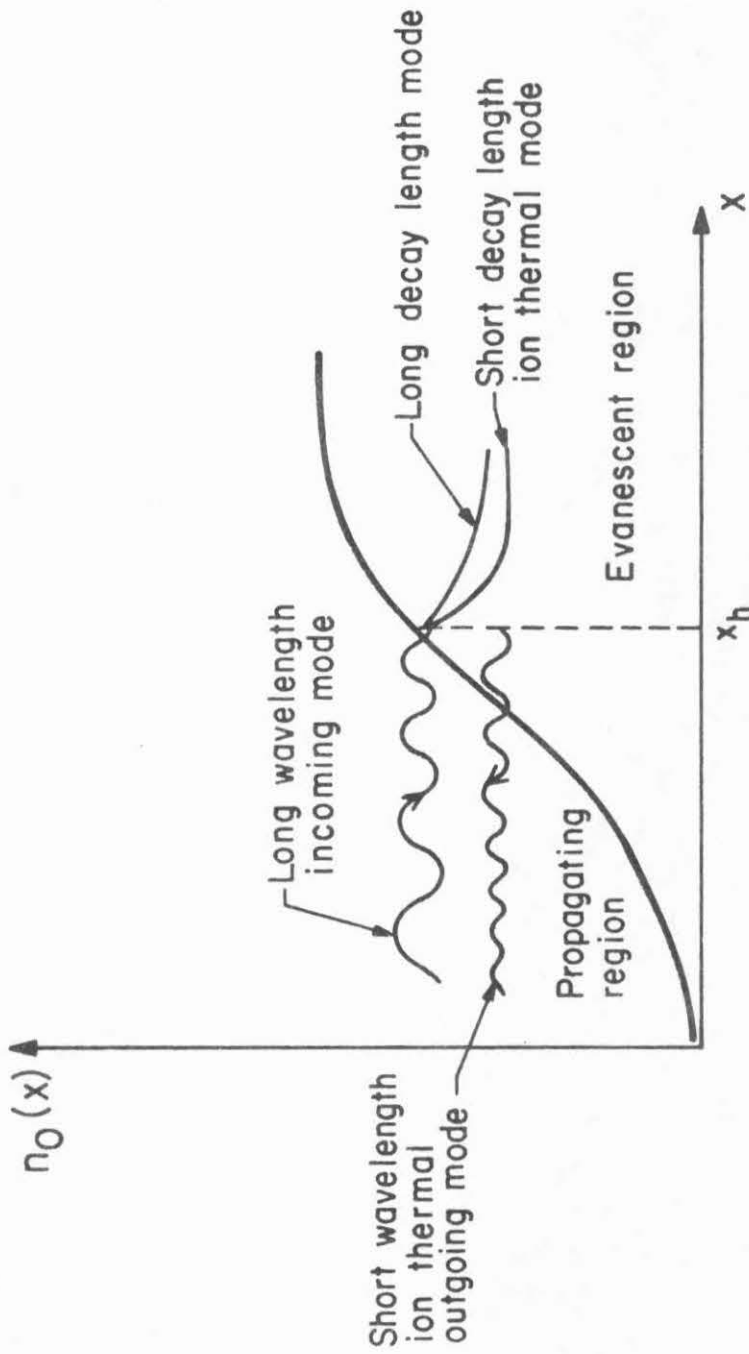


Fig. 1.7 Mode conversion of ingoing mode to an outgoing thermal mode at the lower hybrid layer $x = x_h$ predicted by warm plasma theory

The theory of mode conversion for a single k_z component was studied in greater detail by B. Moore and M. Oakes,¹⁶ who studied the form of the solution very near the hybrid layer (the "conjugate" regions) and gave an expression for mode conversion efficiency in terms of the damping and density inhomogeneity. Similarly, I. Fidone has studied mode conversion at the lower hybrid, both linear and nonlinear.¹⁷ R. Briggs and R. Parker showed that energy flow into the lower hybrid resonance from a source was concentrated along the resonance cones.⁵ Mode conversion from the resonance cone point of view has been studied numerically by M. Simonutti,¹⁸ for finite sources by P. Bellan and M. Porkolab,¹⁹ and by K. Ko and H. Kuehl,²⁰ who discussed the thermal effects on the cone structures.

The reason for mode conversion is that near the lower hybrid the X mode and the ion thermal mode become coupled because their phase velocities become approximately equal, whereas away from this layer they each can exist as independent modes. As the X mode propagates in, it has a frequency in the electron frequency range in the low density and the wave drives predominately the electrons. As the wave moves into higher density regions, ion motion becomes more important. Because of finite temperature, thermal effects are important in the ion motion, and at the mode conversion point, ion thermal effects on the X-mode and the effects of electron motion on the purely ion thermal mode have caused the two modes to be coupled, matching in wavelength, phase and group velocity, \vec{E} -field components, etc. Thus, once the wave has reached the coupling point where there is no distinction between the two modes, the

wave can come out in a different mode.

In linear plasma devices, one usually has an approximately constant background B-field, with an approximately circular cross-section with highest density at radius $r=0$, and a fall-off in density as the radius increases out to the boundary. In such devices the lower hybrid layer, if it is present, occurs at an approximately constant radius where the density is the right value. A waveguide source would lie on or near the boundary. The slab model to be used in this work, which will be discussed in the next section, would be a model of this case, where $x = a/2$ corresponds to the high density plasma at radius $r = 0$, with the x axis corresponding to the radius and the y axis to the azimuthal angle. In tokamaks there is an added complication not present in this model, in that such devices contain an inhomogeneous background magnetic field. Thus the lower hybrid is not at a constant minor radius in tokamaks, and the proximity of the wave frequency to the ion cyclotron harmonics varies with position, so that one might expect important physical processes to be present in such devices for lower hybrid mode conversion studies that would not be present in this model.

1.3 Model

This work is a theoretical study of the quasistatic resonance cone fields and of the process of mode conversion in a simple model of a warm bounded magnetized plasma which has many of the characteristics of plasmas encountered in the laboratory. The model we will use is that of a slab plasma, extending from $x=0$ to $x=a$, and from $-\infty$ to ∞ in the y

and z directions. A background magnetic field $\vec{B} = B_c \hat{z}$ is taken in the z direction, and conducting plane boundaries parallel to this field are assumed at $x=0$ and $x=a$. A gap source is assumed at $x=z=0$ which extends to infinity in both directions along the y axis. This enables us to treat the problem in two dimensions, i.e., in the x-z plane (see Fig. 1.8). The plasma is assumed to be homogeneous in the z direction, with all inhomogeneities in the density being in the x direction.

We will use the quasistatic approximation

$$\vec{E} = -\nabla\phi \quad (1.8)$$

to calculate the fields produced by the gap source for a warm plasma. As pointed out by T. Stix,³ the electrostatic approximation assumes

$$c^2|k|^2/\omega^2 \gg |K_{ij}| \quad (1.9)$$

for all i and j, where k is the wavenumber of the wave and K_{ij} is any component of the dielectric tensor. The source is assumed to be driven harmonically at a frequency ω , so the time dependence of the source and all the fields produced by it are taken to be $e^{-i\omega t}$. The resonance cones we will be interested in are of the middle branch, for which

$\omega_{lh}(x) < \omega < \omega_{pe}(x)$. However, in our consideration of the lower hybrid mode conversion problem, in which the density is inhomogeneous along x, there will be a thin high density layer in the center of the plasma for which $\omega < \omega_{lh}(x)$, and there may be a thin layer in the low density region near the boundaries where $\omega > \omega_{pe}(x)$. We take the range of plasma parameters to be $\omega_{ci}^2 \ll \omega^2 \ll \omega_{ce}^2$, and $\omega_{ci} < \omega_{pi} < \omega_{pe} < \omega_{ce}$,

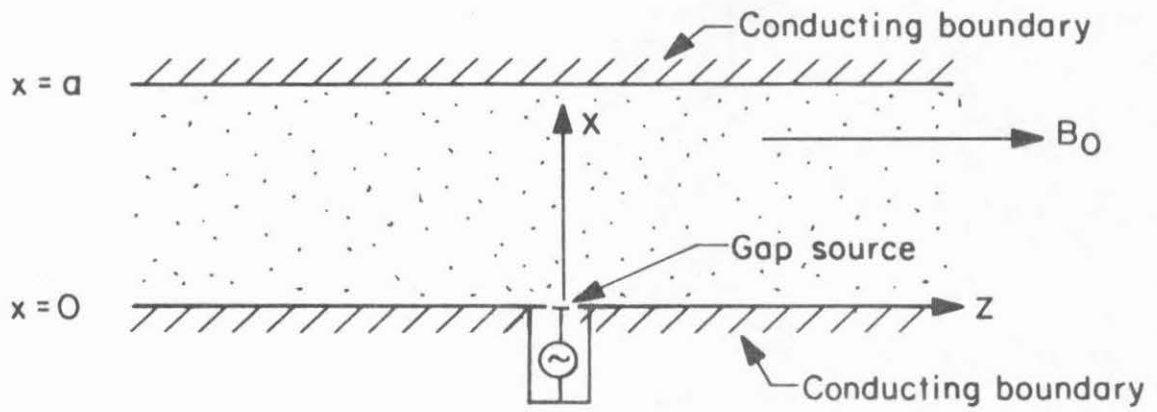


Fig. 1.8 Plasma geometry

which is typical of tokamak plasmas and fields, and a large number of other experiments. Under these approximations the lower hybrid frequency is given by

$$\omega_{\text{lh}}(x) \approx \omega_{\text{pi}}(x) / [1 + \omega_{\text{pe}}^2(x)/\omega_{\text{ce}}^2]^{1/2} \quad (1.10)$$

i.e., is just slightly below the ion plasma frequency.

In addition to the "strong magnetic field" assumption, we assume small electron and ion temperatures: $T_i \lesssim T_e$ so $v_i < v_e \ll \omega/k_z$ where $v_\alpha = [2kT_\alpha/m_\alpha]^{1/2}$ is the thermal velocity and k_z is the wavenumber component along z for the waves of interest. Our approximations mean $r_{\text{ce}} \ll \lambda_{\text{De}} \ll \lambda$, where $r_{\text{ce}} = v_e/\omega_{\text{ce}}$ is the electron cyclotron radius, $\lambda_{\text{De}} = v_e/\sqrt{2} \omega_{\text{pe}}$ is the electron Debye length, and λ is the wavelength of the waves. This means that for all practical purposes we can assume that the electrons are tied to the magnetic field lines because the Larmor radius is much smaller than any other relevant physical quantity.

The ions, on the other hand, are only very weakly tied to the field lines (i.e., have a much smaller Lorentz acceleration than the electrons), and have a rather large Larmor radius. It has been shown by M. Simonutti,²¹ and M. Brambilla²² that near the lower hybrid the large ion Larmor radius approximation is valid, $k_x v_i/\omega_{\text{ci}} \gg 1$ or $r_{\text{ci}} \gg \lambda$. This assumption along with the small thermal velocity assumption will be used in obtaining the approximate form of the dielectric tensor to be used in this work. It assumes that the ions travel in approximately straight line orbits.

The small size of the electron Larmor radius helps ensure that it does not significantly affect the boundary. Also, the ions will, for the most part, be repelled by the sheath at the boundary and the few energetic ones which penetrate the sheath will undergo simple specular reflection at the boundary since they are not strongly held in their orbit. Thus, finite ion Larmor radius effects do not significantly affect the boundary. This assures us that we may use the boundary conditions appropriate for the interface between a dielectric medium and a conductor.

We will assume the plasma to be in thermal equilibrium except for the small perturbation from equilibrium produced by the waves from the source, so the background particle velocity distribution can be assumed to be Maxwellian. We will characterize the plasma by the warm plasma dielectric tensor, which may be expanded to first order in thermal terms for $v_i < v_e \ll \omega/k_z$. This takes the form:

$$\underline{K} \approx \begin{bmatrix} K_{\perp} & K_{xy} & K_{xz} \\ -K_{xy} & K_{\perp} & K_{xz} \\ -K_{xz} & -K_{xy} & K_{\parallel} \end{bmatrix} \quad (1.11)$$

The forms of the dielectric tensor components obtained from Vlasov theory for a Maxwellian plasma are^{3,23}

$$K_{\parallel} = 1 - \sum_{\alpha} \frac{\omega_{p\alpha}^2}{k_z^2 v_{\alpha}^2} Z' \left(\frac{\omega}{k_z v_{\alpha}} \right) \quad (1.12a)$$

$$K_{\perp} = 1 + \sum_{\alpha} \sum_{n=-\infty}^{\infty} \frac{2\omega_{p\alpha}^2 \omega_{c\alpha}^2 n^2}{\omega k_z k_x^2 v_{\alpha}^3} e^{-\lambda_{\alpha}} I_n(\lambda_{\alpha}) Z(\zeta_n) \quad (1.12b)$$

$$K_{xy} = i \sum_{\alpha} \sum_{n=-\infty}^{\infty} \frac{n \epsilon_{\alpha} \omega_{p\alpha}^2}{\omega k_z v_{\alpha}} e^{-\lambda_{\alpha}} [I_n'(\lambda_{\alpha}) - I_n(\lambda_{\alpha})] Z(\zeta_n) \quad (1.13a)$$

$$K_{xz} = - \sum_{\alpha} \sum_n \frac{2\omega_{p\alpha}^2 \omega_{c\alpha} n}{\omega k_z k_x v_{\alpha}} e^{-\lambda_{\alpha}} I_n(\lambda_{\alpha}) [1 + \zeta_n Z(\zeta_n)] \quad (1.13b)$$

$$K_{yz} = i \sum_{\alpha} \sum_n \frac{\epsilon_{\alpha} \omega_{p\alpha}^2 k_x}{\omega \omega_{c\alpha} k_z} e^{-\lambda_{\alpha}} [I_n(\lambda_{\alpha}) - I_n'(\lambda_{\alpha})] [1 + \zeta_n Z(\zeta_n)] \quad (1.13c)$$

where α runs over the species i and e , $\lambda_{\alpha} = k_{\perp}^2 v_{\alpha}^2 / 2\omega_{c\alpha}^2$, $I_n(\lambda)$ is the modified Bessel function of the first kind, $\epsilon_{\alpha} = \pm 1$ is the charge, $Z(\zeta)$ is the plasma dispersion function,²³ and $\zeta_n = (\omega + n\omega_{c\alpha}) / k_z v_{\alpha}$. These forms do not include collisional effects, but those can be included by adding a phenomenological collision frequency in the cold plasma terms when the components are expanded.

We want an expansion for K_{\perp} and K_{\parallel} to first order in temperature for $k_z^2 v_{\alpha}^2 / \omega^2 \ll 1$, which includes collisional corrections. The latter may be added by substituting a phenomenological collision frequency ν into the cold plasma terms in K_{\perp} and K_{\parallel} of the form

$$\frac{\omega_{p\alpha}^2}{\omega^2} \rightarrow \frac{\omega_{p\alpha}^2}{\omega(\omega + i\nu_{\alpha})} \approx \frac{\omega_{p\alpha}^2}{\omega^2} - \frac{i\nu_{\alpha} \omega_{p\alpha}^2}{\omega^3} \quad (1.14)$$

where we have expanded for $\nu_{\alpha} \ll \omega$. Thus from the large argument expansion of the plasma dispersion function²³

$$Z(\zeta) \approx -\frac{1}{\zeta} - \frac{1}{2\zeta^3} + i\sqrt{\pi} \exp(-\zeta^2) \quad (1.15)$$

we obtain

$$K_{\parallel} \cong 1 - \frac{\omega_p^2}{\omega^2} - \frac{3}{2} \frac{k_z^2 v_e^2 \omega_{pe}^2}{\omega^4} + i \left\{ \frac{\nu \omega_p^2}{\omega^3} + 2\sqrt{\pi} \left(\frac{\omega_p^2 \omega}{k_z^3 v_e^3} \right) e^{-\omega^2/k_z^2 v_e^2} \right\} \quad (1.16)$$

where $\omega_p^2 = \omega_{pe}^2 + \omega_{pi}^2$, and ion thermal terms that are negligible compared with the electron thermal terms were dropped.

To get an expression for K_{\perp} we must use the approximation $k_x^2 v_i^2 / \omega_{ci}^2 \gg 1$ (along with $k_z^2 v_e^2 / \omega_{ce}^2 \ll 1$ and $k_z^2 v_i^2 / \omega^2 \ll 1$). This assumption is that the ion Larmor radius is large compared with the perpendicular wavelength. For frequencies considerably above the lower hybrid ($\omega^2 \gg \omega_{lh}^2$) this approximation may break down for the extraordinary mode, since $k_x v_i / \omega_{ci}$ may become ≤ 1 in some cases, but when it does, the ion thermal effects on the X-mode are masked by the electron thermal effects, so the approximation does not give a problem. The assumption was shown to give an ion thermal correction to the real part of K_{\perp} which is equivalent to assuming straight line orbits by M. Brambilla²² and M. Simonutti.²¹ Since $k_z^2 v_e^2 \ll \omega^2$ and $\omega \gg \omega_{ci}$, it gives the same result for the real part of K_{\perp} as the opposite limit $k_x^2 v_i^2 / \omega_{ci}^2 \ll 1$, implying that as long as the former approximations are satisfied, the thermal correction form is not very sensitive to the magnitude of $k_x v_i / \omega_{ci}$. From the small and large argument forms for the Bessel functions²⁴

$$e^{-\lambda} I_n(\lambda) \stackrel{\lambda \ll 1}{\sim} \frac{1}{n!} \left(\frac{\lambda}{2}\right)^n + \mathcal{O}(\lambda^{n+1}) \quad (1.17a)$$

$$e^{-\lambda} I_n(\lambda) \stackrel{\lambda \gg 1}{\sim} (2\pi\lambda)^{-1/2} + \mathcal{O}(\lambda^{-3/2}) \quad (1.17b)$$

we obtain

$$\text{Re } K_{\perp} \approx 1 - \frac{\omega_{pi}^2}{\omega^2} + \frac{\omega_{pe}^2}{\omega_{ce}^2} - \frac{3}{2} k_x^2 \left[\frac{v_i^2 \omega_{pi}^2}{\omega^4} + \frac{v_e^2 \omega_{pe}^2}{4\omega_{ce}^2} \right] \quad (1.18)$$

The form of $\text{Re } K_{\perp}$, obtained under the assumption that the ion Larmor radius $\rho_i = v_i / \sqrt{2} \omega_{ci}$ is much larger than the perpendicular wavelength $\lambda_x = 2\pi/k_x$, has the same form as it would if the ions were unmagnetized, which is to be expected, since the ions orbit with effectively infinite Larmor radii. From our discussion above, this form is pretty much independent of the size of $k_x^2 v_i^2 / \omega_{ci}^2$ when $\omega_{ci}^2 \ll \omega^2$. However, for $\text{Im } K_{\perp}$, the size of that quantity is important, and is not the same form as for unmagnetized ions. The contributions to $\text{Im } K_{\perp}$ involve ion Landau, cyclotron and collisional damping, and these are influenced by a finite cyclotron period. The reason for this is related to the well-known fact that Bernstein waves are undamped in collisionless plasmas when $k_z = 0$, even when the wave frequency is quite close to cyclotron harmonic frequency.¹⁵ The reason is that even though cyclotron harmonic wave particle interaction occurs and causes phase mixing over time periods much larger than the wave period and much smaller than the cyclotron period, the phase is restored after a whole cyclotron period and no net damping results.²⁵ However, if the restoration of phase correlation over a cyclotron period is impeded by a $k_z \neq 0$ component, or by collisions, then net damping may result.

The correct form of $\text{Im } K_{\perp}$ for the large ion Larmor radius case can be obtained from M. Brambilla²² for $v_i < \omega_{ci}$, and is

$$\text{Im } K_{\perp} = \frac{\pi^{3/2} \omega_{pi}^2 \omega v_i e^{-\omega^2/k_x^2 v_i^2}}{k_x^3 v_i^3 \omega_{ci} \sin(\frac{\pi\omega}{\omega_{ci}})} + \frac{2\omega_{pi}^2 \omega_{ci}^3 e^{-\omega^2/k_x^2 v_i^2}}{\omega k_z k_x^3 v_i^4} \sum_n n^2 e^{-\frac{(\omega - n\omega_{ci})^2}{k_z^2 v_i^2}} \quad (1.19)$$

The first term is collisional damping, which is modulated by a perpendicular ion Landau damping term and by proximity of ω to an ion cyclotron harmonic. This is expected because for $v < \omega_{ci}$ there is less than one ion collision per cyclotron period, so the primary role of collisions in that case is to produce net phase mixing over several cyclotron periods, and the net damping is thus sensitive to how large the ion cyclotron wave-particle interaction is, i.e., the proximity of ω to some $n\omega_{ci}$. The second term is a cyclotron harmonic damping, also in combination with perpendicular Landau damping. [The correct form of the cyclotron harmonic contribution to $\text{Im } K$ differs from that obtained by direct expansion and evaluation from the imaginary part in Eq. (1.13) by the factor $e^{-\omega^2/k_x^2 v_i^2}$.] Note that for $k_z = 0$, this contribution is zero, thus giving Bernstein waves which are undamped for perpendicular propagation in a collisionless plasma.

The collisional contribution to $\text{Im } K_{\perp}$ given above is not correct for $v \gg \omega_{ci}$, i.e., for highly collisional plasmas. In that case, an ion undergoes many collisions before it completes a cyclotron orbit. In that case, the finite ion Larmor radius effects should not significantly affect the collisional damping, since the ion motion is much more

strongly influenced by collisions than by the magnetic field, and a simple phenomenological collisional model of the form in Eq. (1.14) should be adequate. Thus for $v \gg \omega_{ci}$

$$\text{Im } K_{\perp} = \frac{v_i \omega_{pi}^2}{\omega^3} + \frac{2\omega_{pi}^2 \omega_{ci}^3}{\omega k_z k_x^3 v_i^4} e^{-\omega^2/k_x^2 v_i^2} \sum_n^{\infty} n^2 e^{-\frac{(\omega - n\omega_{ci})^2}{k_z^2 v_i^2}} \quad (1.20)$$

The K_{xy} and K_{yz} will not be important in our calculations because of the two-dimensional nature of our problem. The K_{xz} have no cold plasma contributions, and have a thermal contribution which gives rise to terms in the dispersion relation that are negligible compared to the thermal contributions from K_{\parallel} and K_{\perp} to the dispersion relation. When $\omega \gg \omega_{lh}(x)$, the contribution of K_{xz} to the dispersion relation is negligible compared with the contribution of the thermal terms of K_{\parallel} , and when $\omega \sim \omega_{lh}(x)$, that contribution is small compared with that of the thermal terms of K_{\perp} in the dispersion relation. Thus the K_{xz} may be considered "higher order" and will be neglected in the field equation.

We have given the components of \bar{K} in \vec{k} -space. We can represent \bar{K} in \vec{r} -space as an operator form which is the Fourier transform of the \vec{k} -space representation by replacing k_z by $-i \frac{\partial}{\partial z}$ and k_x by $-i \frac{\partial}{\partial x}$. This replacement can be done uniquely for homogeneous plasmas, but since we are allowing for possible inhomogeneities in the x-direction, there is an ambiguity in the replacement of the k_x since the coefficients of k_x^2 in \bar{K} are density dependent, and thus a function of x. The proper form

of the replacement for an inhomogeneous plasma can be derived from the Boltzmann-Vlasov equation, from which the form of the dielectric tensor for the warm plasma was originally derived. Thus, for example, the correct replacement of the thermal terms βk_x^2 in K can be obtained from the form of Poisson's equation in L. Pearlstein and D. Bahdra, derived directly from the Boltzmann-Vlasov equation²⁶, that is

$$\beta k_x^2 \rightarrow \frac{\partial}{\partial x} [\beta(x) \frac{\partial}{\partial x}] \quad (1.21)$$

The two principal approximations used in our model are the electrostatic approximation for the field and the small thermal velocity approximation for expanding the dielectric tensor. By combining the criteria for the electrostatic approximation, Eq. (1.9), with the electrostatic dispersion relation, given by Fourier transforming Poisson's equation for a charge-free plasma and requiring that there be nontrivial solutions for the potential:

$$k_x^2 K_{\perp}(k_x) + k_z^2 K_{\parallel}(k_z) = 0 \quad (1.22)$$

we obtain a window on the k_z components for which both approximations are valid:

$$\frac{\omega^2 |K_{ij}|}{c^2 |1 - K_{\parallel}/K_{\perp}|} \ll k_z^2 \ll \omega^2 / v_e^2 \quad (1.23)$$

In our model the point source excites the whole k_z spectrum, and we will consider the whole k_z spectrum when calculating the fields by Fourier transforming in the z direction. The field components for k_z out of

the range given by Eq. (1.23) will not be correct, so our approximations assume that those components make a small contribution to the total field, or are of minor importance to the resonance cone field structures that we will investigate. The lower bound region is very small and negligible everywhere except for a thin region near the source if the source is assumed to be in the vacuum outside the plasma, and the approximation is even better if the source lies in the plasma low density region. We shall see that the upper bound region contributes primarily to the small rapidly oscillating structure of the resonance cones which is far removed from the primary and first few secondary maxima of the cones, so that if we concentrate on the central part of the cones and ignore the small fine structure far removed from it, we eliminate the contributions above the upper bound.

There are conditions on the laboratory plasma that help insure that k_z components outside the range given by (1.23) are not important. First, a real source is finite so that $k_z \geq L^{-1}$, where L represents the characteristic source size, is not excited to any significant amplitude by the source. Also, the very large k_z components are highly Landau damped, and thus become increasingly unimportant as one moves away from the source. We will concentrate on the point source, but will include damping in our calculations of the resonance cone field structures, which decrease the importance of the very large k_z 's contributing to the cone.

Near the lower hybrid, the accessibility condition ensures $k_z \geq \omega/c (1 + \omega_{ce}/\omega_{pe})^{1/2}$ so that none of the k_z outside the lower limit

of (1.23) make it into the hybrid layer. Also, Troyan and Perkins²⁷ have shown that only components of k_z such that $k_z \lesssim \omega/4.5 v_e$ make it into the lower hybrid layer without being virtually damped away. This gives a window on the k_z which make it into the lower hybrid layer from the source:

$$\omega^2(1 + \omega_{ce}/\omega_{pe}) / c^2 < k_z^2 < \omega^2 / (20v_e^2) \quad (1.24)$$

This means that for studying mode conversion, the k_z 's that are important lie easily in the range given by (1.23).

An important point about our use of a point gap source is that it serves as a Green's function for any finite gap type source. Thus, even though our field calculations will contain extraneous contributions from k_z outside the range in (1.23) for any source for wave heating that concentrates energy into k_z inside that range, our fields serve as accurate Green's functions from which the field for that source can be obtained by integrating the source over the Green's function.

1.4 Purpose of This Work

One purpose of this work is to see the effects of boundaries on warm plasma resonance cones, which we will do for the slab model just discussed. We will do this by studying the fields produced by the gap source from the resonance cone approach as an alternative to the guided wave approach. The resonance cone approach can give new physical insights that are not apparent in the guided wave approach. The cones are localized structures near the source, so normally only a few cones contribute significantly to the fields at a given point, in contrast to the

guided wave approach, in which many guided wave modes contribute. Thermal effects will be seen to cause the cones to spread out (de-localize) as they move away from the source. We want to see how they spread for the bounded plasma. We will see that thermal effects and spreading cause interference between nearby cones, most significantly for relatively large cone angles with respect to the magnetic field. We want to study the nature of this interference. We also want to see the effect that collisions and Landau damping has on the cones.

We will be primarily interested in the middle branch of the cones [$\omega_{\ell h}(x) < \omega < \omega_{pe}(x)$], and are particularly interested in the lower end of the branch, where $\omega \approx \omega_{\ell h}(x)$, from the standpoint of plasma heating by waves. A major portion of this work, then, will be concerned with the case of an inhomogeneous plasma where $\omega \rightarrow \omega_{\ell h}(x)$ at some point internally in the plasma, so that we have a pair of lower hybrid layers present in the plasma, for a symmetrical density profile. The purpose will be to see how a gap source (a model of a waveguide source) couples the cones into the lower hybrid layer of interest to lower hybrid heating, and to study the process of mode conversion near the lower hybrid from a resonance cone point of view. We want to obtain the warm plasma cone structure near the lower hybrid layers. We also want to see what the boundary effects on the wave processes involved in mode conversion are, and the resonance cone picture is more useful than the guided wave approach for this.

With the two lower hybrid layers present, there is a high density region in the center of the plasma between the hybrid layers where the

waves are evanescent. We want to study the case that the evanescent layer between the hybrid layers is relatively thin to see if tunneling of the cones takes place. We will see how the cones transform as the hybrid layer is approached from the evanescent or propagating side and their structure and trajectory. We will study how the energy flows in and out of the hybrid layer and across the evanescent region from the resonance cone picture. We want to see how mode conversion depends on damping, inhomogeneities, and size of the evanescent region. Finally, we want to see how the energy is absorbed by the plasma along the resonance cones.

In Chapter II, we consider the structure of the warm plasma resonance cones in the geometry of our model for homogeneous or mildly inhomogeneous plasmas for the middle branch of the cone for frequencies not too close to the lower hybrid or plasma frequency turning points. With insights obtained from this case, we attack the harder problem of the case that lower hybrid layers exist in the inhomogeneous plasma in Chapter III. This will give us information on the cone structure and trajectories near the lower hybrid layer and evanescent region. In Chapter IV we study the damping of the cones, and the power flow and energy absorption along the cones by developing an energy conservation theorem for quasistatic fields. The results are summarized in Chapter V.

CHAPTER II: RESONANCE CONE STRUCTURE FOR HOMOGENEOUS PLASMA

2.1 Model and Approximations

Our first objective will be to determine the structure of the middle branch of the warm plasma resonance cones for our bounded slab plasma with the gap source (Fig. 1.8) for a homogeneous plasma or for a weakly inhomogeneous plasma in which there are no turning points. The density is assumed to drop suddenly to zero at the boundaries. It is well known that such a model supports guided wave modes for the same frequency ranges that cold plasma resonance cones exist, the nature of which is determined by the plasma dielectric properties, including thermal effects. R. Gould²⁸ has shown that the fields produced by the source in such a geometry in cold plasma theory can be looked on as a sum of multiply-reflected singular resonance cones as well as the usual superposition of guided modes. In this chapter we will use and extend this concept to warm plasmas and study the detailed properties of the warm plasma resonance cones in this geometry.²⁹

We will work with frequencies such that

$$\omega_{\ell h}^2(x) \ll \omega^2 \ll \omega_{pe}^2(x) \quad (2.1)$$

everywhere in the plasma, where $\omega_{\ell h}$ is given by Eq. (1.10), to avoid complications in the problem introduced by proximity to the turning points (the effect of the lower hybrid turning point will be studied extensively in the next chapter). For this range of frequencies, the thermal terms of the dielectric tensor components K_{\parallel} and K_{\perp} are much

smaller than the cold plasma parts so that appropriate expansions may be made. More precisely, these approximations are [see Eqs. (1.16,18)]:

$$1 - \omega_p^2/\omega^2 \gg \frac{3}{2} \frac{k_z^2 v_e^2 \omega_{pe}^2}{\omega^4} \quad (2.2a)$$

$$1 - \omega_{pi}^2/\omega^2 + \omega_{pe}^2/\omega_{ce}^2 \gg \frac{3}{2} k_x^2 \frac{v_i^2 \omega_{pi}^2}{\omega^4} + \frac{v_e^2 \omega_{pe}^2}{4\omega_{ce}^4} \quad (2.2b)$$

which are assumed to be valid if our small temperature approximation $k_z^2 v_e^2/\omega^2 \ll 1$ is valid, for frequencies in the range

$$3\omega_{\ell h}^2(x) \lesssim \omega^2 \lesssim \omega_{pe}^2(x)/2$$

i.e., for cold plasma cone angles $\theta_c \approx \tan^{-1} \left[\frac{\omega^2 - \omega_{\ell h}^2}{\omega_p^2 - \omega^2} \right]^{1/2}$ in the range

$$\left[\frac{2m_e}{m_i} \right]^{1/2} \lesssim \theta_c \lesssim \pi/4 \quad (2.4)$$

We will also assume that the imaginary parts of K_{\parallel} and K_{\perp} are small compared with their real parts, i.e., that damping is small. The general criterion for this approximation is that the damping length of the waves that we are studying is much longer than the wavelength.

2.2 Equation for Potential

We are characterizing the plasma by a warm plasma dielectric tensor expanded to first order in the thermal terms $k_z^2 v_{\alpha}^2/\omega^2$ and $k_x^2 v_{\alpha}^2/\omega^2$ given by Eqs. (1.16) and (1.18). We want the form of Poisson's equation for the warm plasma for $\phi(x,z)$. Such an equation can be obtained by use of a nonlocal dielectric tensor,

$\bar{K}(x, z, -i \frac{\partial}{\partial x}, -i \frac{\partial}{\partial z})$ which is an operator Fourier transform of the usual k -space representation, obtained by replacing k_α by $-i \frac{\partial}{\partial x_\alpha}$ as discussed in Chapter I. (Thermal effects make the dielectric tensor in \vec{r} -space nonlocal). Thus the equation we want is of the form

$$\left\{ -\frac{\partial}{\partial x} [K_{\perp}(x, -i \frac{\partial}{\partial x}) \frac{\partial}{\partial x}] + \frac{\partial}{\partial z} [K_{\parallel}(x, -i \frac{\partial}{\partial z}) \frac{\partial}{\partial z}] \right\} \phi(x, z) = 0 \quad (2.5a)$$

Letting

$$\phi(x, z) = \int_{-\infty}^{\infty} \tilde{\phi}(x, k_z) e^{ik_z z} \frac{dk_z}{2\pi} \quad (2.6)$$

we obtain [see Eq. (1.21)]:

$$\left(\frac{\partial}{\partial x} \{K_{\perp 0}(x) + \frac{\partial}{\partial x} [\beta(x) \frac{\partial}{\partial x}]\} - k_z^2 K_{\parallel}(x, k_z) \right) \tilde{\phi}(x, k_z) = 0 \quad (2.5b)$$

where $K_{\perp 0}$ is the cold plasma part of K_{\perp} . For the homogeneous plasma K_{\parallel} and $K_{\perp 0}$ are independent of x , and the $K_{\perp 0}$ and β slip outside the partials.

The dispersion relation obtained from Poisson's equation is

$$\beta k_x^4 + K_{\perp 0} k_x^2 - k_z^2 K_{\parallel}(x, k_z) = 0 \quad (2.7)$$

This equation has a large and a small root k_x^2 . The large root is an ion thermal (acoustic) mode, and is not generally coupled for the condition we are presently considering. The correct inclusion of this mode would require an extra boundary condition. (This point will be discussed in more detail in Chapter III, where we include this mode.) Thus, in this chapter we will ignore the ion thermal mode and consider

only the small k_x^2 (X-mode) root.

Write the value of k_x for the X-mode in the form

$$k_x = \pm \alpha(k_z) |k_z| \quad (2.8)$$

where α is complex with the inclusion of damping. In the cold, collisionless plasma case

$$\alpha \rightarrow (-K_{\parallel}/K_{\perp})^{1/2} = [\tan \theta_c]^{-1}$$

For the warm plasma we want an expansion of α to first order in the thermal (and damping) terms in order to get an expression for $\phi(x,z)$. The ion cyclotron harmonic damping is ordinarily negligible for the electron frequency range given in Eq. (2.1) and will be neglected. To first order in thermal and imaginary terms

$$\alpha = \left(1 - \frac{\omega_{lh}^2}{\omega^2}\right)^{-1/2} \left\{ \left[\frac{\omega_p^2}{\omega^2} - 1 + \frac{3}{2} k_z^2 \left[\frac{v_e^2 \omega_{pe}^2}{\omega^4} + \left(\frac{\omega_p^2 - \omega^2}{\omega^2 - \omega_{lh}^2} \right) \left(\frac{v_i^2 \omega_{pi}^2}{\omega^4} + \frac{v_e^2 \omega_{pe}^2}{4\omega_{ce}^4} \right) \right] \right]^{1/2} \right. \\ \left. - \frac{i\sqrt{\pi} \left(\frac{\omega_p^2 \omega}{k_z^3 v_e^3} \right) \exp(-\omega^2/k_z^2 v_e^2) + \frac{i v}{2\omega^3} [\omega^2 - \omega_{pi}^2 \left(\frac{\omega_p^2 - \omega^2}{\omega^2 - \omega_{lh}^2} \right)]}{\left(\frac{\omega_p^2}{\omega^2} - 1 \right)^{1/2}} \right\}. \quad (2.9)$$

Here the assumptions $\frac{3}{2} k_z^2 v_e^2 \omega_{pe}^2 / \omega^4 \ll \omega_p^2 / \omega^2 - 1$ and $\frac{3}{2} k_x^2 \left(\frac{v_i^2 \omega_{pi}^2}{\omega^4} + \frac{v_e^2 \omega_{pe}^2}{4\omega_{ce}^4} \right) \ll 1 - \omega_{lh}^2 / \omega^2$ were utilized, and the thermal terms in the

imaginary part of α were neglected, since they are second order. Split α into its real and imaginary parts: $\alpha = \alpha_r + i\alpha_i$. Then, upon further expansion of α_r , we obtain

$$\alpha_r = D + Ek_z^2 \quad (2.10)$$

where

$$D = \left(\frac{\omega_p^2 - \omega^2}{\omega^2 - \omega_{lh}^2} \right)^{1/2} = [\tan \theta_c]^{-1} \quad (2.11a)$$

$$E = \frac{3[\omega_{pe}^2 v_e^2 + \left(\frac{\omega_p^2 - \omega^2}{\omega^2 - \omega_{lh}^2} \right)^2 (\omega_{pi}^2 v_i^2 + \frac{\omega_{pe}^2 v_e^2 \omega^4}{4\omega_{ce}^4})]}{4\omega^2 (\omega_p^2 - \omega^2)^{1/2} (\omega^2 - \omega_{lh}^2)^{1/2}}, \quad (2.11b)$$

and

$$\alpha_i = \frac{-\sqrt{\pi} \omega_p^2 \left(\frac{\omega}{k_z v_e} \right)^3 \exp(-\omega^2/k_z^2 v_e^2) - \frac{v}{2\omega} \left[\omega_p^2 - \omega_{pi}^2 \left(\frac{\omega_p^2 - \omega^2}{\omega^2 - \omega_{lh}^2} \right) \right]}{(\omega_p^2 - \omega^2)^{1/2} (\omega^2 - \omega_{lh}^2)^{1/2}}. \quad (2.12)$$

A solution to Eq. (2.8) which fits the boundary condition $\tilde{\phi}(x=a) = 0$ and is causal (produces proper exponential decay away from the source for $\alpha_i < 0$) is

$$\tilde{\phi}(x, k_z) = \tilde{\phi}(0, k_z) \left(\frac{\exp(-i\alpha|k_z|x) - \exp[i\alpha|k_z|(x-2a)]}{1 - \exp(-2i\alpha|k_z|a)} \right) \quad (2.13)$$

2.3 Guided Wave Solutions

We may obtain the potential as a sum of guided modes by utilizing the poles of $\tilde{\phi}(x, k_z)$ in doing the inverse Fourier transform. These are given by

$$|k_z| \alpha(k_z) a = n\pi \quad (2.14)$$

where n is any non-negative integer. Thus the poles are the roots of an algebraic equation which can be found approximately as the roots of a cubic equation by utilizing our first order expansion of α and ignoring the imaginary parts:

$$|k_z| (D + Ek_z^2) \approx n\pi \quad (2.15)$$

This equation admits only two real roots for each value of n . The presence of a nonzero imaginary component of α puts the roots in the complex plane. Since $\alpha_i < 0$, then $\text{Im } k_z > 0$ for $\text{Re } k_z > 0$ and $\text{Im } k_z < 0$ for $\text{Re } k_z < 0$. Denote the two poles for each value of n by $k_z = \epsilon k_n$, where the real part of k_n is slightly less than its cold plasma value $\text{Re } k_n = n\pi/D$, and $\epsilon = \pm 1$. Since we must close the contour for the Fourier transform of $\tilde{\phi}(x, k_z)$ in $\text{Im } k_z < 0$ for $z < 0$, and in $\text{Im } k_z > 0$ for $z > 0$, then we pick up the poles $k_z = k_n$ for $z > 0$ and $k_z = -k_n$ for $z < 0$ (see Fig. 2.1).

$$\phi(x, z) = i \sum_{n=0}^{\infty} \text{Res}[\tilde{\phi}(x, k_z) e^{ik_z z}] \Big|_{k_z = (\text{sgn } z) k_n} \quad (2.16)$$

Evaluating the residues gives

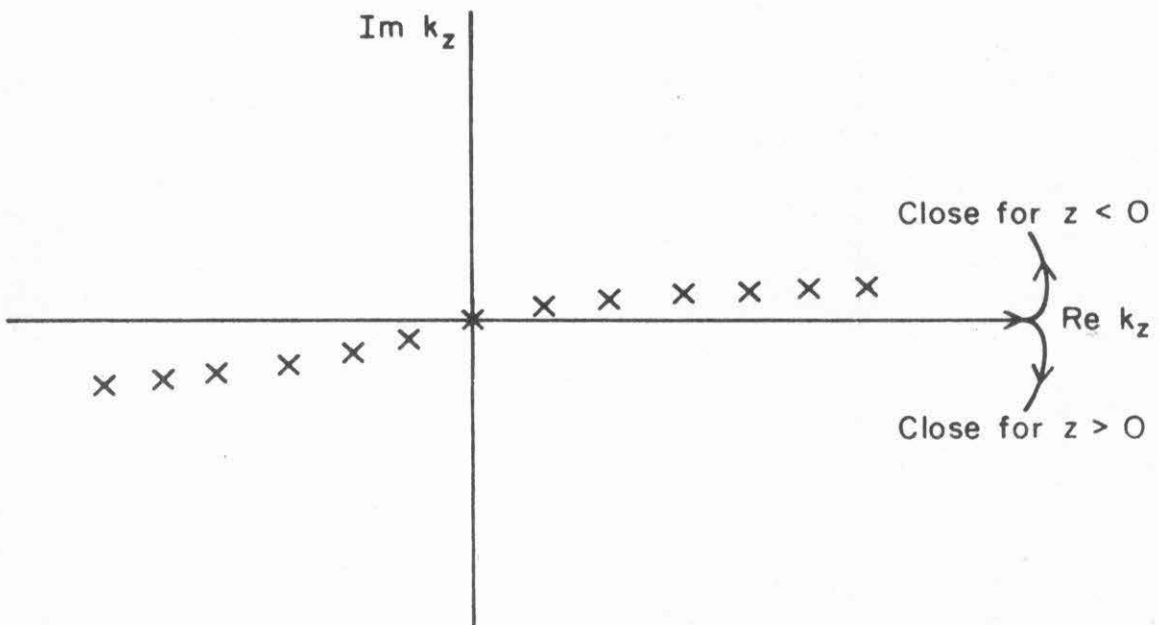


Fig. 2.1 Poles of $\tilde{\phi}(x, k_z)$ and contours for inverse Fourier transform

$$\phi(x, z) = -i \sum_{n=0}^{\infty} \frac{\tilde{\phi}(0, k_n) \sin(n\pi x/a) e^{i k_n |z|}}{\alpha(k_n) + k_n \alpha'(k_n)} \quad (2.17)$$

for the gap source $\tilde{\phi}(0, k_n) = 1$, and the denominator is given approximately by $D + 3Ek_n^2$.

The presence of damping causes the waves to decay in the z direction through an imaginary component of k_n given by (for $\alpha_i \ll \alpha_r$)

$$\text{Im } k_n \simeq \frac{-n\pi \alpha_i(k_n)}{\alpha_r^2(k_n)} \quad (2.18)$$

Thus the higher the order n of the mode, the faster it damps away as it propagates away from the source. For small z , i.e., for near fields, we must consider a very large number of modes, but for sufficiently large z , i.e., in the very far field, all but the lowest order modes have decayed away to negligible amplitude. Thus the guided mode solution is the most useful for determining the field in the far field region, but is not as useful in the near field, where the quasistatic approximation is best. Finally, it should be noted that each of the guided modes are nonlocal, i.e., they are nonzero over a very large region, except for the sufficiently large n modes that die away very rapidly in z . This will be contrasted with the local nature of the resonance cones in the next section.

2.4 Resonance Cone Solutions and Properties

To get the form of the resonance cones we must expand the denominator of $\phi(x, z)$ before Fourier transforming it:

$$[1 - \exp(-2i\alpha|k_z|a)]^{-1} = \sum_{n=0}^{\infty} \exp(-2i\alpha|k_z|n) \quad (2.19)$$

This converges since $\alpha_j < 0$. Then

$$\begin{aligned} \phi(x,z) = & \sum_{n=0}^{\infty} \left(\int_0^{\infty} \tilde{\phi}(0,k_z) \exp(ik_z z) \{ \exp(-i\alpha|k_z|x) - \exp[i\alpha|k_z|(x-2a)] \} \right. \\ & \times \exp(-2in\alpha|k_z|a) \frac{dk_z}{2\pi} - \int_{-\infty}^0 \tilde{\phi}(0,k_z) \exp(ik_z z) \\ & \left. \times \{ \exp[-i\alpha|k_z|(x-2a)] - \exp(i\alpha|k_z|x) \} \exp(-2ni\alpha|k_z|a) \frac{dk_z}{2\pi} \right) \end{aligned} \quad (2.20)$$

It should be noted that the upper and lower limits of the integrals in Eq. (2.20) lie outside the range of k_z for which our electrostatic and small thermal velocity approximations are valid, so the integral forms are valid only when the k_z lying outside this range make a negligible contribution to the total integral. (This point will be examined in more detail later.)

For a point gap excitation the second boundary condition is of the form $\phi(x=0,z) = \delta(z)$. Then, $\tilde{\phi}(0,k_z) = 1$ and

$$\phi(x,z) = - \sum_{n=0}^{\infty} \sum_{\delta=\pm 1} \sum_{\epsilon=\pm 1} \epsilon f[\delta z + \epsilon\alpha(a-x) + (2n+1)\alpha] \quad (2.21)$$

where

$$f(\xi) = \int_0^{\infty} \exp[-ik_z \xi(k_z)] \frac{dk_z}{2\pi} . \quad (2.22)$$

We want to evaluate the integral $f(\xi)$ for $\xi(k_z) = \delta z + \epsilon \alpha(a-x) + (2n+1)n\alpha$. Assume $\alpha \approx \alpha_r$ as a first approximation, since $\alpha_i \ll \alpha_r$ from previous assumptions. This will give us the undamped solution. We will include the effects of α_i by a perturbation on the undamped solution to take the effect of Landau and collisional damping into account. We may thus write $\xi = \xi_0 + i\xi_i$ where ξ_0 and ξ_i are the real and imaginary parts of ξ , and $\xi \approx \xi_0$ is the first approximation. Then

$$\xi_0(k_z) = \mu_n(\delta z, x, \epsilon) + \nu_n(x, \epsilon) k_z^2 \quad (2.23)$$

where

$$\begin{aligned} \mu_n(\delta z, x, \epsilon) &= \delta z + [(2n+1+\epsilon)a - \epsilon x] D \\ \nu_n(x, \epsilon) &= [(2n+1+\epsilon) - \epsilon x] E \end{aligned} \quad (2.24)$$

We have

$$\phi(x, z) = - \sum_{n=0}^{\infty} \sum_{\epsilon=\pm 1} \sum_{\delta=\pm 1} \epsilon \int_0^{\infty} \exp[-i(\mu_n k_z + \nu_n k_z^3)] \frac{dk_z}{2\pi} \quad (2.25)$$

From the Airy integral forms²⁴

$$Ai(\eta) = \frac{1}{\pi} \int_0^{\infty} \cos(v\eta + \frac{v^3}{3}) dv \quad (2.26a)$$

$$Gi(\eta) = \frac{1}{\pi} \int_0^{\infty} \sin(v\eta + \frac{v^3}{3}) dv \quad (2.26b)$$

we obtain

$$\phi(x, z) = - \sum_{n=0}^{\infty} \sum_{\epsilon=\pm 1} \sum_{\delta=\pm 1} \frac{\epsilon}{(3\nu_n)^{1/3}} F\left[\frac{\mu_n}{(3\nu_n)^{1/3}}\right], \quad (2.27)$$

where $F(\xi) = Ai(\xi) - iGi(\xi)$. This is the form of the potential, neglecting damping. The corresponding field components are

$$E_z = - \frac{\partial \phi}{\partial z} = \sum_{n=0}^{\infty} \sum_{\epsilon=\pm 1} \sum_{\delta=\pm 1} \left[\frac{\delta \epsilon}{(3\nu_n)^{2/3}} F'\left(\frac{\mu_n}{(3\nu_n)^{1/3}}\right) \right] \quad (2.28a)$$

$$E_x = - \frac{\partial \phi}{\partial x} = \sum_{n=0}^{\infty} \sum_{\epsilon=\pm 1} \sum_{\delta=\pm 1} \frac{1}{(3\nu_n)^{4/3}} \left[EF\left(\frac{\mu_n}{(3\nu_n)^{1/3}}\right) + \frac{E\mu_n - 3D\nu_n}{(3\nu_n)^{1/3}} F'\left(\frac{\mu_n}{(3\nu_n)^{1/3}}\right) \right]. \quad (2.28b)$$

There are several observations that can be made from the form of the potential in Eq. (2.27). First, as $T_e \rightarrow 0$, then $E \rightarrow 0$ so $\nu_n \rightarrow 0$ for all n , and

$$(3\nu_n)^{-1/3} Ai\left(\frac{\mu_n}{(3\nu_n)^{1/3}}\right) \rightarrow \delta(\mu_n) \quad (2.29a)$$

$$(3\nu_n)^{-1/3} Gi\left(\frac{\mu_n}{(3\nu_n)^{1/3}}\right) \rightarrow \frac{1}{\pi\mu_n} \quad (2.29b)$$

Thus

$$\phi(x, z) \rightarrow - \sum_n \sum_{\epsilon, \delta} \epsilon \left[\frac{-i}{\pi\mu_n} + \delta(\mu_n) \right] \quad (2.30)$$

and we recover the cold bounded plasma resonance cones given by Gould.²⁸ In this limit it is easy to identify each term with a given n , ϵ , and δ with an individual member of the multiply-reflected resonance cones which in cold plasma theory is singular for $\mu_n(\delta z, x, \epsilon) = 0$. The cones in $z > 0$ have $\delta = -1$, and those in $z < 0$ have $\delta = +1$. The cones reflected off the $x = a$ boundary have $\epsilon = +1$, and the ones originating from or reflected off the $x = 0$ boundary have $\epsilon = -1$ (see Fig. 2.2).

The effect of the temperature is the shifting of the maximum of the potential of a given cone (which is no longer singular) to a smaller angle and the appearance of an interference structure (secondary maxima) inside the cone as was first noted by Fisher and Gould.² This is illustrated by the graph of the magnitude of the "cone function" $F(\zeta)$ in Fig. 2.3. The graph can be considered to be a cross-sectional cut of the cone, e.g., the cone field structure as a function of z for a fixed x , where $\zeta = 0$ is the position of the cold plasma cone trajectory, with the warm plasma cone maximum at $\zeta = -1.83$ and subsequent maxima at $\zeta = -5.4, -7.9, \dots$. The warm plasma cone structure is caused by interference between the cold plasma cone and a warm plasma wave, as can be seen by taking the asymptotic limit of Eq. 2.27 (valid for very small T_e away from the cold plasma cone line). For $\mu_n/(3\nu_n)^{1/3} \gg 1$,²⁵

$$\phi \sim - \sum_{n=0}^{\infty} \sum_{\epsilon=\pm 1} \sum_{\delta=\pm 1} \epsilon \left[\frac{-i}{\pi \mu_n} + \frac{1}{2\sqrt{\pi}(3\nu_n)^{1/4} \mu_n^{1/4}} \exp\left(-\frac{2\mu_n^{3/2}}{3(3\nu_n)^{1/2}}\right) \right] \quad (2.31a)$$

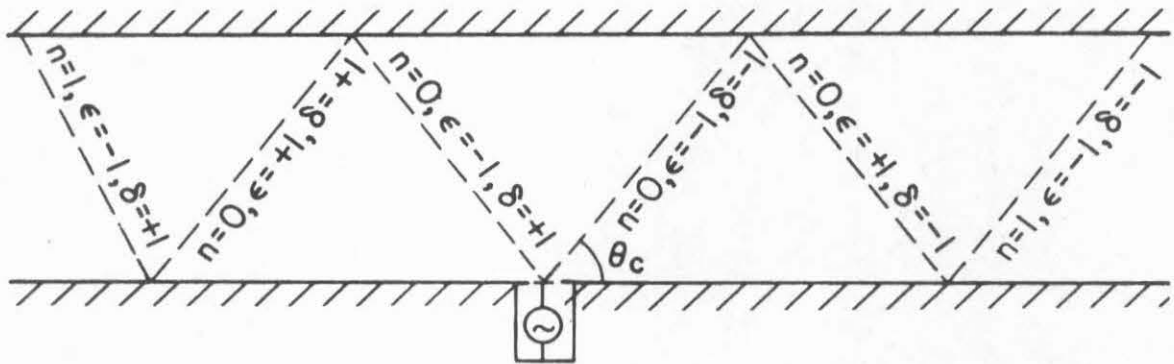


Fig. 2.2 Surfaces of singularity (dotted lines) of the cold plasma resonance cones, labeled by the cone which is singular there in cold plasma theory. θ_c is the cone angle.

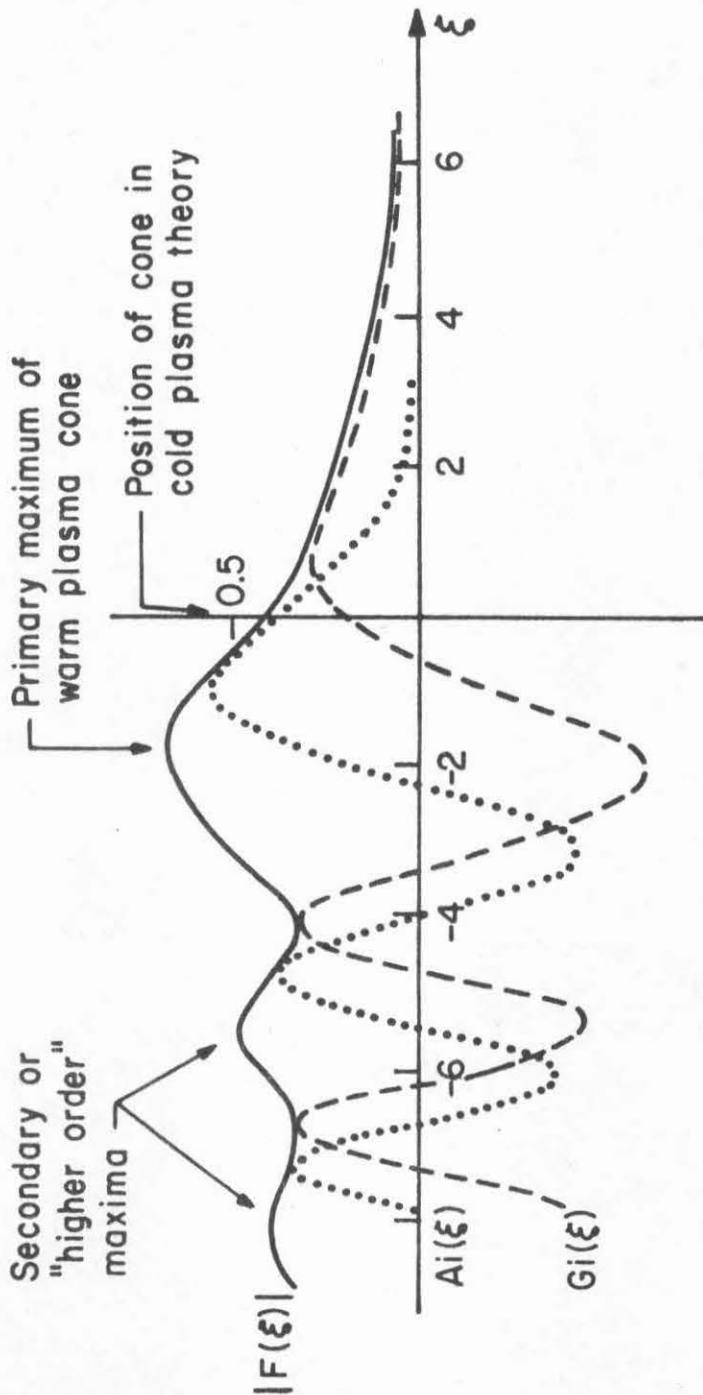


Fig. 2.3 Cross section of the cone magnitude $\sim |F(\xi)|$, and graph of the Airy functions making up $F(\xi)$

and for $\mu_n/(3v_n)^{1/3} \ll -1$

$$\phi \sim - \sum_{n=0}^{\infty} \sum_{\epsilon=\pm 1} \sum_{\delta=\pm 1} \epsilon \left\{ \frac{-i}{\pi\mu_n} + \frac{1}{\sqrt{\pi}(-\mu_n)^{1/4}(3v_n)^{1/4}} \exp\left[\frac{-2i(-\mu_n)^{3/2}}{3(3v_n)^{1/12}} - \frac{\pi}{4}\right] \right\}$$

(2.31b)

The first term of the potential for each multiply-reflected cone (each value of n , ϵ , and δ in the sum) goes like μ_n^{-1} (i.e., Coulomb-like) and may be identified with the cold plasma wave cone. The second term goes like $\mu_n^{-1/4}$ and may be identified with the thermal wave which produces the interference structure. The thermal wave is propagating on the $\mu_n < 0$ side of the cold plasma cone line, and evanescent on the $\mu_n > 0$ side. The thermal wave contribution to ϕ falls off much more slowly with μ_n than the cold plasma contribution for $\mu_n < 0$, giving rise to a long tail on the cone and a considerable broadening of the cone from the cold plasma case. When asymptotic forms are valid, the primary contribution to each cone in the sum comes from k_z lying close to the saddle point of the integral in Eq. (2.22).

$$k_z = \pm \left[\frac{-\mu_n}{3v_n} \right]^{1/2} \quad (2.32)$$

and the magnitude of this saddle point increases the distance from the cold plasma cone line $\mu_n = 0$. This explains why as we go from the primary maximum to the higher order secondary maxima for $\mu_n < 0$, the narrower the peaks or spatial oscillations become; these peaks are caused by successively higher values of k_z .

The width of the peaks and spatial oscillations associated with each cone spreads out in a uniform fashion away from the source, while their amplitude correspondingly decreases as $(3\nu_n)^{-1/3}$. Let

$$\Delta z = z - z_c(x, \delta, \epsilon) \quad (2.33)$$

be the vertical distance from the cold plasma cone (a function of z for a given x) for a given cone labelled by n , δ , and ϵ , where z_c is the value of z at which the cold plasma cone singularity occurs for the given x and given cone. Also, let

$$x_n = [(2n+1+\epsilon)a - \epsilon x] \quad (2.34)$$

which acts like a total vertical distance from the source for the given cone (i.e., is x for the cone coming directly from the source, $2a-x$ for the first cone reflected off the $x=a$ boundary, $2a+x$ for the cone reflected off the $x=0$ boundary, etc.) Then the argument of F is

$$\mu_n / (3\nu_n)^{1/3} = \frac{-\delta \Delta z}{[3x_n(\epsilon)E]^{1/3}} \sim \Delta z x_n^{-1/3} T_e^{-1/3} \quad (2.35)$$

Thus we see that for a given peak [fixed $\mu_n / (3\nu_n)^{1/3}$] the width of the peak and its distance from the cold plasma cone line increases as the cube root of the vertical distance from the source and of the temperature. This shows that the cones spread out away from the source, and become wide and more nonlocal as the temperature is increased. The corresponding angular shift of the maximum of the potential due to thermal effects goes like

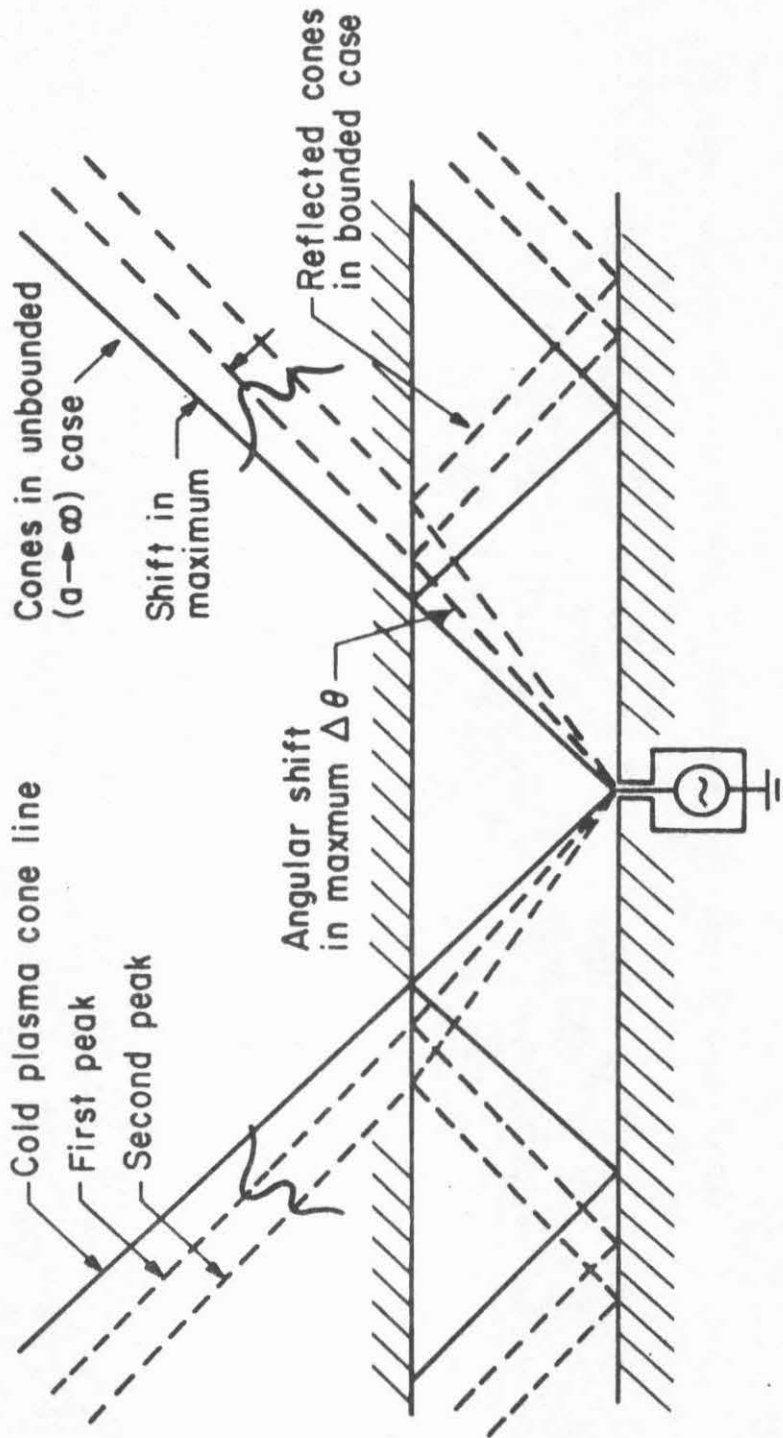


Fig. 2.4 Cone trajectories for warm plasma, compared with unbounded plasma limit

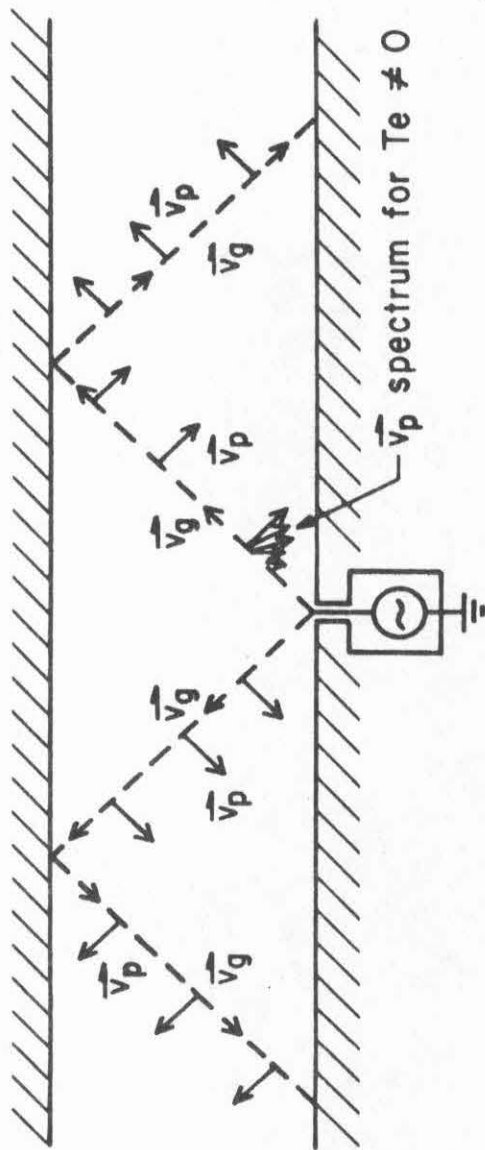


Fig. 2.5 Phase and group velocities for cold plasma theory, and phase velocity spectrum for warm plasma

$$\Delta\theta \sim \Delta z/x_n \sim x_n^{-2/3} T_e^{1/3} \quad (2.36)$$

for $\Delta\theta \ll 1$ (valid everywhere except very near the source). We see then that not only does the angular shift increase with temperature, but it decreases with effective vertical distance from the source, i.e., the trajectory of the cone maxima becomes more and more parallel to the corresponding cold plasma cone line as it moves away from the source.

We can similarly analyze the primary (saddle point) k_z contributions along the $\mu_n < 0$ side of the cones in terms of the above introduced parameters. From Eq.(2.32)

$$k_z = \pm \left[\frac{\Delta z}{3x_n E} \right]^{1/2} \sim x_n^{-1/3} T_e^{-1/3} \quad (2.37)$$

Thus we see that for a peak in the asymptotic region of the cone, not only does the primary set of k_z making up that peak increase with the square root of the distance of the peak from the cold plasma cone line for a given x , but it decreases as the cube root of the effective vertical distance of the cone from the source, as well as the temperature. This explains the spreading of the cones from the source and their increase in width with increase in temperature.

The solution for an unbounded plasma is obtained by letting $a \rightarrow \infty$. (This gives us the solution for a half-space plasma with a conductor at $x = 0$.) Then only the $n = 0, \epsilon = -1$ terms survive. Thus, the form of the potential for the unbounded case is the same as the $n, \epsilon = -1$ term of the potential for the bounded case for $2n < x < 2n+1$, and the same as the negative of the $n, \epsilon = +1$ term of the bounded case potential for $2n+1 < x < 2n+2$. The individual terms in $\psi(x, z)$ therefore correspond to

perfect repeated multiple reflection of the unbounded form of the potential with the conducting boundaries acting as mirrors. That is, the resonance cones reflect off the boundaries, changing sign upon each reflection, and each (reflected) cone with a given (η, ϵ, δ) has the same shape (up to a -1 factor) as a successive segment of the corresponding unbounded cone (see Fig. 2.4). However, in the unbounded case, more than one term in the sum may contribute to the potential at a given point in space, hence, there is interference between nearby reflected cones because of the nonlocality (spreading away from the source). Thus, the effect of boundaries is to produce interference between the cone coming into a boundary and the one reflected off of that boundary. Indeed, adjacent cones come together (interfere perfectly) at the boundary to give $\phi = 0$ there (the boundary condition produces the reflected cone), so interference is most important near the boundary. The higher T_e the greater the width of the region near the boundary in which interference of adjacent cones is important, and the greater the importance of interference. Also, the higher the driving frequency, ω , the larger the cold plasma cone angle θ_c , and hence the greater the importance of interference.

The cones are localized structures, particularly near the source, although they spread out and become less localized as they move away from the source. Thus in the region relatively near the source (the near field), where the fields are largest and where the quasistatic approximation is best, only a very few (two or three) cone terms contribute to the total field (the few multiply-reflected cones that interfere with each other at that point), with this number increasing as we go to the far field. This is in contrast to the guided mode form

of the fields, in which a very large number of modes contribute to the field in the near-field, but a smaller number in the far-field. Thus the two views are complementary, with the resonance cone form being the most useful for the near field region, which is of most interest, but with the guided waveform being of possibly greater use for the far field. The low order guided modes are nonlocal, with the higher order modes becoming increasingly localized, due to damping, whereas the low order resonance cones are localized, with the higher order modes becoming increasingly delocalized due to spreading of the cones. (As shall be seen in the next section, damping has the effect of increasing the locality of the cones, with severity increasing with cone order, but this is more than offset by the cone spreading in most circumstances.)

As seen in Eq. (2.20), the cones in the $z > 0$ half of the plane are produced by the $k_z > 0$ components from the source, while the $z < 0$ cones are produced by the $k_z < 0$ components. However, it is clear from the form of $\tilde{\phi}(x, k_z)$ in Eq. (2.13) that the x component of the phase velocity is always opposite to that of the direction of decay of the wave, which is the x -component of the group velocity \vec{v}_g or of the direction of cone propagation. Thus the wave is "backward" along x , but is forward along z . This causes the group velocity \vec{v}_g and the phase velocity \vec{v}_p to be perpendicular along the resonance cones in cold plasma theory. Indeed the cold plasma forms for the phase and group velocity directions for the cones in our model are

$$\begin{aligned}\hat{v}_g &\sim -\delta\hat{z} - \epsilon\hat{x}/D \\ \hat{v}_p &\sim \hat{k} \sim -\delta\hat{z} + \epsilon D\hat{x}\end{aligned}\tag{2.38}$$

where $\delta = -1$ for the $z > 0$ cones and $+1$ for the $z < 0$ cones, $\epsilon = -1$ for the cones coming from the $x = 0$ boundary and $+1$ for the cones coming from the $x = a$ boundary, and D is related to the cone angle by Eq. (2.11a) (see Fig. 2.5). The effect of finite temperature is to replace D by $D + Ek_z^2$, which will give the phase velocity of a given k_z component and the group velocity of a narrow spectrum of waves centered around that component. (The latter is well defined only in the asymptotic region of the cone, where the local cone field is produced by a narrow spectrum of k_z centered around the saddle point.) Thus thermal effects cause the phase velocity to be a function of k_z , so that the phase velocity angle increases with k_z (i.e., v_p is greater and lies increasingly more along x with increasing k_z). This results in constructive and destructive interference between the various k_z components and produces the interference structure inside the cone.

2.5 Damping of the Resonance Cones

We now include Landau and collisional damping. Go back to the integral in Eq. (2.21). We have $\xi(k_z) = \xi_0(k_z) + i\xi_i(k_z)$ where $\xi_i(k_z) = \alpha_i[(2n+1+\epsilon)a - \epsilon x]$ was previously neglected. The integral

$$f(\xi_0) = \int_0^{\infty} \exp[-ik_z \xi_0(k_z)] \frac{dk_z}{2\pi} \text{ may be solved by saddle point integra-}$$

tion, and if we so solved it we would get an asymptotic form of the exact solution $f(\xi_0) \propto \text{Ai}(\xi_0) - i\text{Gi}(\xi_0)$. Thus, treating the α_i term as a perturbation,

$$f(\xi) = \int_0^{\infty} \exp[-ik_z \xi(k_z)] \frac{dk_z}{2\pi} \approx \exp\{k_0[(2n+1+\epsilon)a - \epsilon x] \alpha_i(k_0)\} \quad (2.39)$$

$$\times \int_0^{\infty} \exp[ik_z \xi(k_z)] \frac{dk_z}{2\pi} = \exp\{k_0[(2n+1+\epsilon)a - \epsilon x] \alpha_i(k_0)\} F(\xi_0),$$

where k_0 is the appropriate saddle point of $f(\xi_0)$. Since $k_z \xi_0(k_z) = \mu_n k_z + \nu_n k_z^3$, then $k_0 = \pm \left[\frac{-\mu_n}{3\nu_n}\right]^{1/2}$. Since $\alpha_i < 0$, we must choose the plus sign in the saddle point because the negative sign violates causality. We thus obtain

$$\phi(x, z) = \sum_{n=0}^{\infty} \sum_{\epsilon, \delta=\pm 1} \left\{ \frac{-\epsilon}{(3\nu_n)^{1/3}} F\left[\frac{\mu_n}{(3\nu_n)^{1/3}}\right] \exp[-\Gamma_n(\delta, \epsilon)] \right\} \quad (2.40)$$

where

$$\Gamma_n(\delta, \epsilon) = \frac{\left[\frac{-\mu_n}{3\nu_n}\right]^{1/2} [(2n+1+\epsilon)a - \epsilon x]}{(\omega_p^2 - \omega^2)^{1/2} (\omega^2 - \omega_{1h}^2)^{1/2}} \left\{ \sqrt{\pi} \omega_p^2 \left(\frac{-3\nu_n \omega^2}{\mu_n \nu_e^2}\right)^{3/2} \exp(3\nu_n \omega^2 / \mu_n \nu_e^2) + \frac{\nu}{2\omega} [\omega_p^2 - \omega_{pi}^2 \left(\frac{\omega_p^2 - \omega^2}{\omega^2 - \omega_{1h}^2}\right)] \right\} \quad (2.41)$$

This form of the damping is quantitatively correct only when the asymptotic form of F is valid, i.e., for argument $|\mu_n / (3\nu_n)^{1/3}| \gg 1$. However, for smaller arguments it should give a qualitative indication of the nature of the damping.

One interesting observation is that the Landau damping factor is exponentially decaying away from the source for $\mu_n < 0$ (inside the cone), but introduces a spatially-dependent phase for $\mu_n > 0$ (outside the cone). This phase does not influence the magnitude of the potential at points where only one cone contributes significantly to it, but at points where two or more cones are interfering this phase is important in determining the way the two contributions add, hence may have an influence on the potential.

For a given cone the damping exponent goes like

$$|\Gamma_n(\epsilon, \delta)| \sim \left(\frac{\delta z + x_n D}{3Ex_n} \right)^{1/2} x_n \sim |\Delta z|^{1/2} x_n^{1/2} \quad (2.42)$$

This means, for example, that the parts of the thermal interference structure inside a given cone which are the farthest from the cold plasma cone line are the most highly damped, and thus become negligible the fastest as one goes away from the source. Damping thus reduces the importance of interference between nearby cones. It is to be noted that the higher T_e is, the greater the Landau damping contribution to Γ_n , but the less the collisional damping contribution.

There is a clear reason for the increase in the damping with the distance from the cold plasma cold line. As already pointed out, the primary k_z contributing to the cone structure at a given point on the cone is the saddle point value given by Eq. (2.37), and the magnitude of this increases with the distance from the cold plasma cold line. But the higher the k_z , the greater the damping of that component because of its greater interaction with the particles. Hence the observed nature

of the damping.

It can be seen from Eq. (2.31) that the thermal wave contribution to a given cone falls off much more slowly with increasing distance $|\mu_n|$ from the cold plasma cone line than the cold plasma cone contribution, for $\mu_n < 0$. Thus the thermal wave gives rise to a long slowly dying tail, which is spatially oscillatory due to its interference with the residual cold plasma contribution. This long tail will interfere with nearby cones, and the saddle point k_z making up this thermal tail increases with the distance $|\mu_n|$ from the cold plasma cone line. If finite sources are used, the amplitude with which each k_z component is excited will tend to fall off with increasing k_z , so there will be an eventual cutoff and elimination of the higher k_z 's excited by the source. Thus a finite source will tend to cause the thermal tail of the cone to have a more rapid falloff with μ_n than $(-\mu_n)^{-1/4}$; and thus cut off the tail at some large μ_n , although it would also be expected to broaden and flatten the cold plasma contribution to the cone structure. A Gaussian source spectrum

$$\tilde{\phi}(0, k_z) = \sqrt{\frac{\alpha}{\pi}} e^{-\alpha k_z^2} \quad (2.43a)$$

will be assumed as a typical finite source. This is for a Gaussian source in real space

$$\phi(0, z) = \frac{1}{\sqrt{\pi\alpha}} e^{-z^2/\alpha} \quad (2.43b)$$

With this Gaussian form of the source, the very large k_z components that violate the small thermal velocity approximation are suppressed. The cone field function for the source in the expansion of $\phi(x, z)$ as a sum

of cones in Eqs. (2.21-25) is

$$f(\mu_n + \nu_n k_z^2) \approx \sqrt{\frac{\alpha}{\pi}} \int_0^{\infty} \exp[-i(\mu_n k_z + \nu_n k_z^3) - \alpha k_z^2] \frac{dk_z}{2\pi} \quad (2.44)$$

In the asymptotic region of the cone, for $\alpha \ll (3\mu_n \nu_n)^{1/2}$, we have

$$\phi(x, z) \sim \frac{\alpha \ll (3\mu_n \nu_n)^{1/2}}{\mu_n \gg (3\nu_n)^{1/3}} \sum_n \sum_{\epsilon, \delta} \exp\left[\frac{\alpha \mu_n}{3\nu_n}\right] F[(2n+1+\epsilon)a - \epsilon x] \quad (2.45)$$

where the asymptotic form of F is valid. Thus we see that out away from the cold plasma cone line $\mu_n = 0$, the effect of $\alpha \neq 0$ is to cause an exponential decay of the cone field with increasing distance from the cold plasma cone line compared to the point source case. The source will also broaden the cold plasma cone contribution near $\mu_n = 0$, as it does for the $T_e = 0$ case, but in the $\mu_n > \alpha^2/3\nu_n$ region the finite source effect on the thermal tail dominates over its effect on the cold plasma cone contribution, so that the finite source cone has a more rapid falloff in the thermal tail. A narrower cone structure results from the finite source effects if α is sufficiently small.

In Fig. 2.6 the form of ϕ is shown for $\omega = \omega_{pe}/4$, or cone angle $\theta_c = 14.5^\circ$, and thermal velocity $v_e = .005 a\omega$. The source is the finite Gaussian profile discussed above, and Landau damping is included, but $\nu = 0$. Only the $z > 0$ portion is shown, since ϕ is symmetrical about $z = 0$. There are four cones present in the region shown, and these are labeled. The thermal interference structure associated with each cone is sometimes visible, particularly so for the $(\eta=0, \epsilon=-1, \delta=-1)$ cone becomes more pronounced in the region near the $(\eta=0, \epsilon=1, \delta=-1)$ cone, and

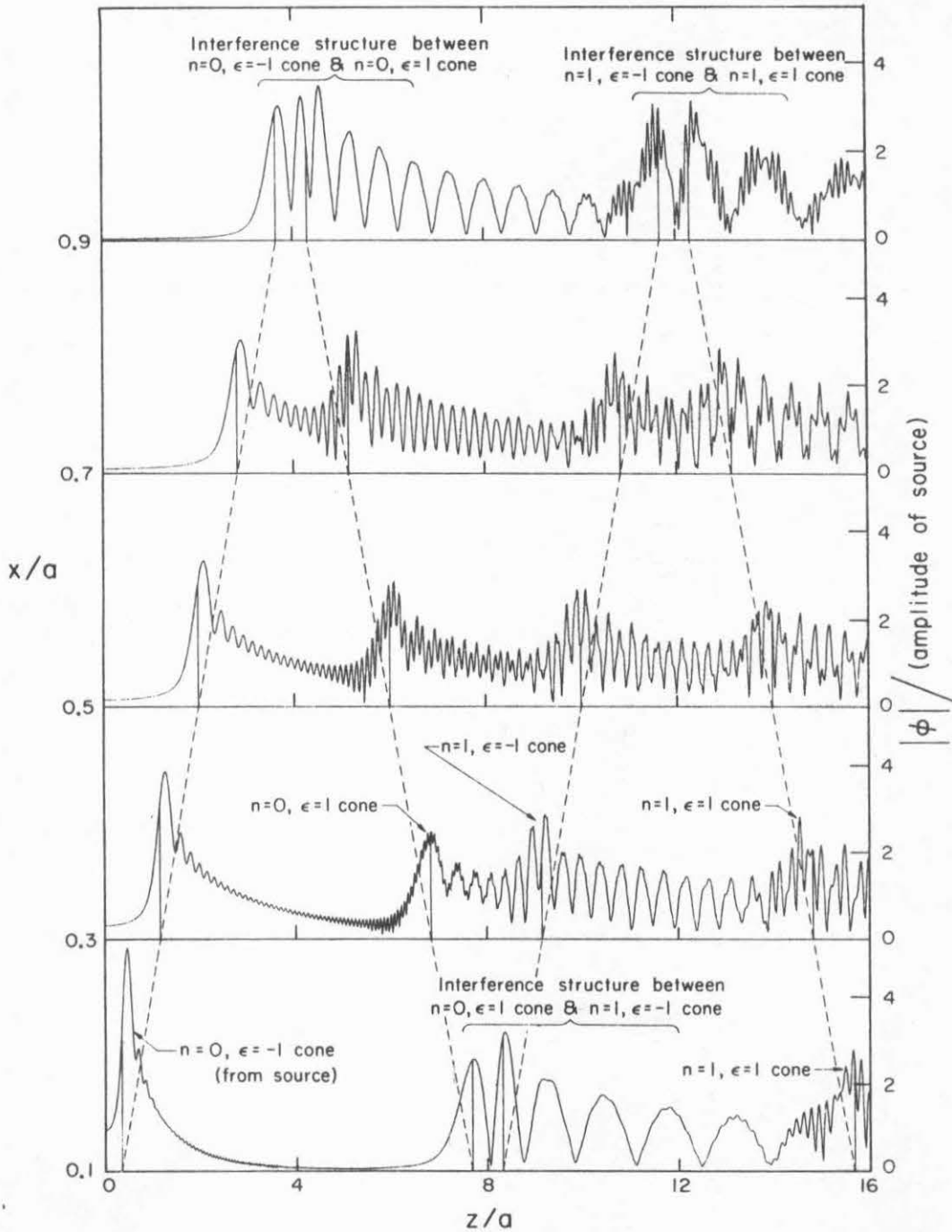


Fig. 2.6 Plots of $|\phi|$ vs z for various x , for $\omega_{pe} = 4\omega$, $v_e = .005 a\omega$, $\theta_c = 14.5^\circ$. The dotted lines correspond to cold plasma cone position as in Fig. 2.2. The potential for $z < 0$ is a mirror image of that shown for $z > 0$. Individual resonance cones are indicated.

modulates the main peak of that cone. This can be interpreted as follows. The interference structure of the $\epsilon = -1$ cone is caused by an interference between the cold plasma and thermal waves of that cone, but at a large distance μ_0 from the cone line, the cold plasma contribution $\sim |\mu_0|^{-1}$ has become rather small compared to the thermal contribution $\sim |\mu_n|^{-1/4}$, so the interference structure dies down for large $|\mu_0|$. But, near the region of the $\epsilon = 1$ cone, the thermal wave of the $\epsilon = -1$ cone interferes with the cold plasma wave of the $\epsilon = 1$ cone, and the interference structure immediately becomes more pronounced.

The interference structure between two adjacent cones takes on a different character when the two come together near the boundary, and the individual cones making up the field there cannot be distinguished. The interference structures are shown in the graph for each adjacent pair. Figures 2.7-8 show the cone structure for higher temperatures and larger cone angles. In those graphs the interference between nearby cones is greater, and the individual resonance cones harder to distinguish or identify. A conclusion that might be drawn is that for quite large temperatures and cone angles the resonance cone picture is no longer as useful for interpreting the structure of the potential in this geometry, although it is still quite useful as a method for calculating that potential. Typical low density plasma parameters which might apply to the graphs are $\omega = 200$ MHz and $a = 10$ cm. Then Fig. 2.6 would correspond to $T_e = 1.1$ eV, and Fig. 2.7 to $T_e = 4.4$ eV.

For higher driving frequency ω , the graphs would correspond to much higher temperatures. For smaller ω/ω_{pe} , the cone angle is smaller and interference is less, and as ω approaches ω_{lh} , the interference becomes

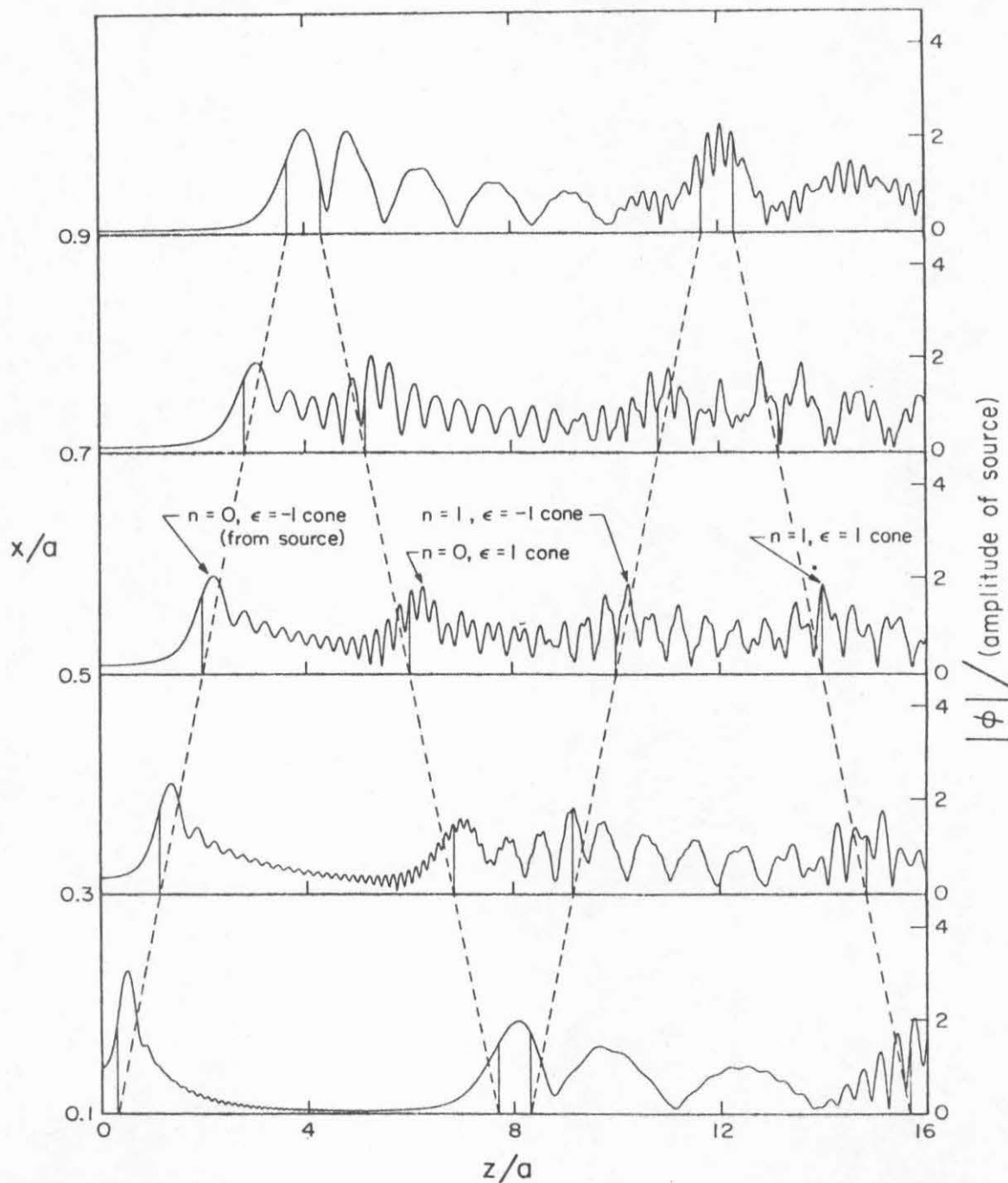


Fig. 2.7 Same as Fig. 2.6 for $v_e = .01 \text{ aw}$

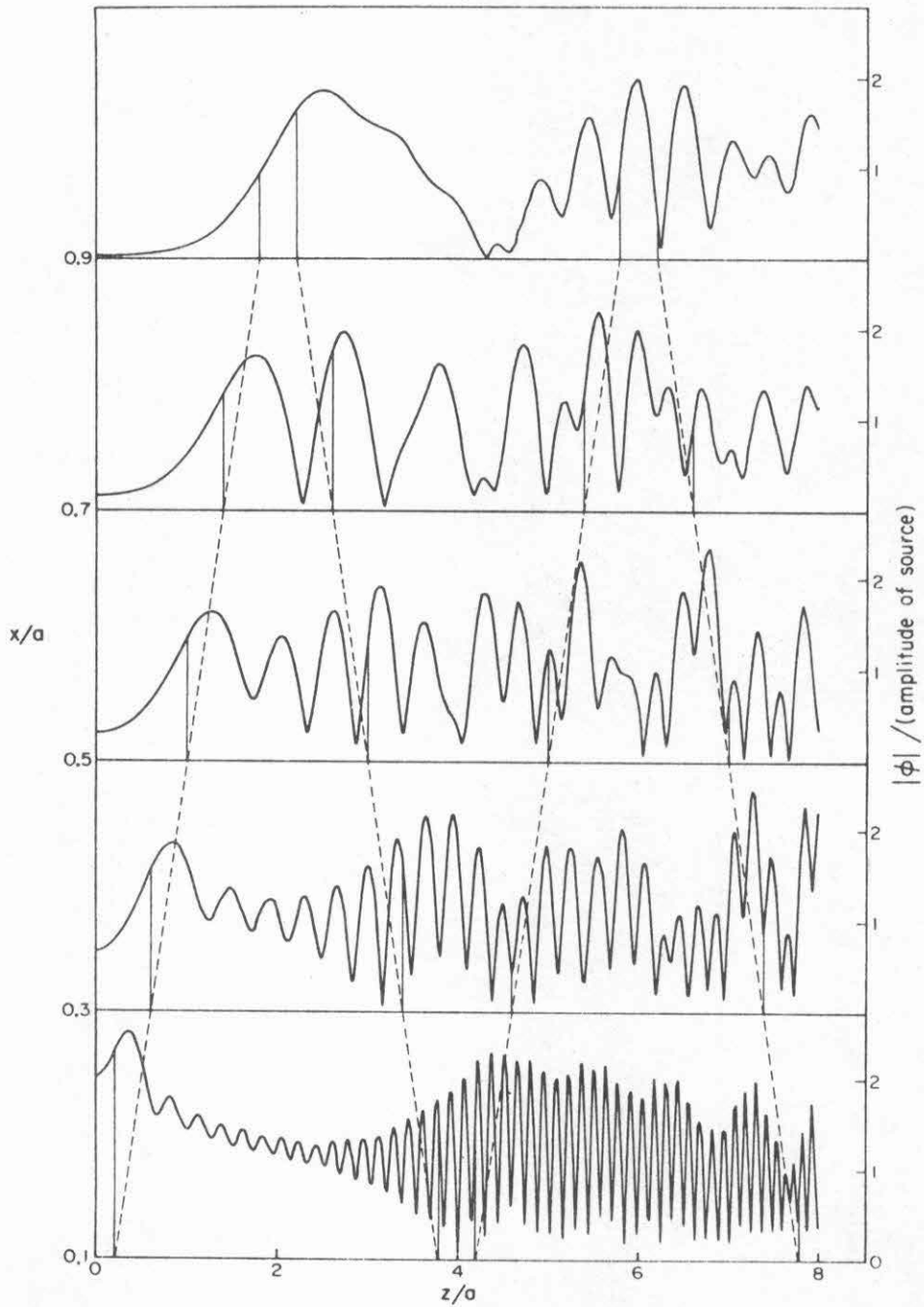


Fig. 2.8 Same as Fig. 2.6 for $v_e = .02 a\omega$ and $\omega_{pe} = 2\omega$ (cone angle = 30°). The individual resonance cones are hard to identify for this case.

almost nonexistent (except on the boundary). Also, the high frequency spatial oscillations (for large z and small x in the graphs) will be more subdued or suppressed for larger finite sources (for which our point source solution acts as a Green's function), so the interference will not be as pronounced for finite sources as is indicated by the point source solution.

2.6 Analysis of Assumptions

A few words are in order on the validity of the electrostatic and small thermal velocity approximations. The criterion for the validity of the former may be written

$$k_z^2 \gg \frac{\omega^2 |K_{ij}|}{c^2 (1 - K_{\parallel}/K_{\perp})}$$

where

$$\frac{\omega^2 |K_{ij}|}{c^2 (1 - K_{\parallel}/K_{\perp})} \leq \frac{(\omega^2 - \omega_{\ell h}^2) \max[(\omega^2 - \omega_{\ell h}^2), (\omega_p^2 - \omega^2)]}{c^2 (\omega_p^2 - \omega_{\ell h}^2)} < (\omega^2 - \omega_{\ell h}^2)/c^2$$

so both approximations are valid for k_z in the range

$$(\omega^2 - \omega_{\ell h}^2)/c^2 \ll k_z^2 \ll \omega^2/v_e^2 \quad (2.46)$$

The very large k_z are severely Landau damped, and k_z greater than $k_{\max} \sim 1/L$, where L represents the characteristic size of the source, are never excited in a real plasma. These facts help assure that our approximations are valid in an actual plasma. But the limits on the integral $F[\mu_n/(3v_n)^{1/3}]$ in (2.27) are for k_z outside the range given by (2.42), so our form of the potential is only valid if the k_z outside the range in

(2.42) make a negligible contribution to the total integral. More precisely, there must be some $k_{\min}(\mu_n, \nu_n) \gtrsim 3(\omega^2 - \omega_{\ell h}^2)^{1/2}/c$ and some $k_{\max}(\mu_n, \nu_n) \lesssim \omega/3v_e$ such that for the integral $F[\mu_n/(3\nu_n)^{1/3}]$,

$$\int_0^{k_{\min}} \ll \int_0^{\infty} \text{ and } \int_{k_{\max}}^{\infty} \ll \int_0^{\infty}. \quad \text{In the case that } |\mu_n/(3\nu_n)^{1/3}| \gg 1 \text{ (away from}$$

the corresponding cold plasma resonance cone lines), so that ϕ takes the form in Eq. (2.31), and the damping is correctly given in (2.41), the major contribution to the integral comes from the saddle points $k_z = \pm (-\mu_n/3\nu_n)^{1/2}$. We thus have a criterion for where in r -space the approximation is satisfied in that case for the (n, ϵ, δ) term:

$$(\omega^2 - \omega_{\ell h}^2)/c^2 \ll \frac{|\delta z + [(2n+1+\epsilon)a - \epsilon x]D|}{3[(2n+1+\epsilon)a - \epsilon x]E} \ll \omega^2/v_e^2 \quad (2.47)$$

For a given point (x, z) , this criterion has to be satisfied only for the cone terms (n, ϵ, δ) which make a significant contribution to the net potential at (x, z) , so normally at most two or three terms are involved. Expressed in terms of cone parameters and using $E \sim 3\omega_{pe} v_e^2 / 4\omega^3$ for the higher frequency range of the cone branch ($\omega^2 \gg \omega_{\ell h}^2$), the criterion becomes

$$\omega^2/c^2 \ll \frac{\Delta z \omega^3}{2\omega_{pe} v_e^2 x_n} \ll \omega^2/v_e^2 \quad (2.48)$$

This form shows clearly that the quasistatic approximation is best in the near field (small x_n) and breaks down first far away from the source, while the small thermal velocity approximation becomes better as one moves away from the source (to large x_n), and is least good very near the

source. Also, for a given x the quasistatic approximation breaks down first very near the cold plasma cone line ($\Delta z = 0$), i.e., near the first maximum, whereas the small thermal velocity approximation breaks down first far away from this line (i.e., for the higher order maxima).

We can also study the validity conditions with respect to a given maximum of the resonance cone structure, i.e., for fixed

$$\zeta = \mu_n / (3v_n)^{1/3} = \Delta z / (3x_n E)^{1/3} \quad (2.49)$$

in Fig. 2.3. In terms of this

$$\omega^2 / c^2 \ll \frac{\zeta \omega^2}{(\alpha \omega_{pe} v_e x_n)^{2/3}} \ll \omega^2 / v_e^2 \quad (2.50)$$

The quasistatic approximation breaks down first for the primary peak ($\zeta = 1.8$), so the condition for the validity of the approximation for that peak becomes

$$x_n \ll c^3 / \omega_{pe} v_e^2 \quad (2.51)$$

For example, for the extreme case $\omega_{pe} = 2\omega$ and $v_e = .05 a\omega$ with $a = 10$ cm, $\omega \cong 2\pi \times 10^8$ rad/sec, the right hand side is about 1.2×10^4 a. That means that the quasistatic approximation is good for the resonance cones for a few hundred reflections, i.e., is very good.

The small thermal velocity approximation for a given peak becomes

$$\zeta^{3/2} \ll 2\omega_{pe} x_n / v_e \quad (2.52)$$

This breaks down in our graphs after the first few maxima very close to

the $x=0$ boundary for the cone coming directly from the source, so the high frequency spatial oscillations produced by that cone in that region do not give quantitatively correct fields there. For finite sources this high frequency spatial structure, produced by the high k_z components from the source are more subdued or nonexistent, so the fields produced in that region are more like slowly varying spatial averages of the calculated fields shown. An important point is that our solution is a valid Green's function for the fields produced by any finite source which excites only those k_z that are within the range of Eq. (2.47) everywhere that we are interested in the fields, because the k_z components in the Green's function solution outside of this range are suppressed in the integration of the Green's function over the source. A final point is that a better approximation to the cone fields can be made by modifying the calculated fields outside the range in Eq. (2.48). For those parts of the cone for which the primary k_z [given by Eq. (2.32)] satisfies Eq. (2.48), the form of the field is reasonably accurate. For those parts of the cone created by k_z outside of this range, a finite source is assumed of sufficient size so that these k_z are not excited, and the thermal term in the asymptotic form, Eq. (2.31), is neglected, since that is the term arising from the high k_z components and producing the local spatial oscillations, and only the cold plasma Coulomb-like term $\phi \sim \mu_n^{-1}$ is retained.

2.7 Inhomogeneous Plasma

Having studied the solution for a homogeneous plasma, we are interested in seeing how this is modified by the presence of weak inhomogeneities. Assume the inhomogeneities to be perpendicular to \vec{B}_0 and in

the x direction, since that is the case of interest in most plasmas. Now,

$\omega_{pe} = \omega_{pe}(x)$, $\omega_{pi} = \omega_{pi}(x)$ and $K_{||}$ and K_{\perp} and then the functions of x.

We seek a solution of Poisson's equation, Eq. (2.8) in this case.

In the WKB approximation, solutions which fit the boundary condition at $x = a$ are of the form

$$\tilde{\phi}(x, k_z) = \tilde{\phi}(x=0, k_z) \frac{\left(\frac{\alpha(0)K_{\perp}(0)}{\alpha(x)K_{\perp}(x)} \right)^{1/4} \left(\exp[-i|k_z|\eta(x)] - \exp\{-i|k_z|[2\eta(a)-\eta(x)]\} \right)}{1 - \exp[-2i|k_z|\eta(a)]} \quad (2.53)$$

where $\eta(x) = \int_0^x \alpha(x') dx'$. Then, we may expand the denominator as before.

Letting $g(x) = \int_0^x D(x') dx'$ and $q(x) = \int_0^x E(x') dx'$ we straightforwardly obtain the solution for a point gap excitation:

$$\begin{aligned} \phi(x, z) \approx & - \left(\frac{[\omega_p^2(0) - \omega^2][\omega^2 - \omega_{1h}^2(0)]}{[\omega_p^2(x) - \omega^2][\omega^2 - \omega_{1h}^2(x)]} \right)^{1/4} \\ & \times \sum_{n=0}^{\infty} \sum_{\epsilon, \delta=\pm 1} \frac{\epsilon}{(3N_n)^{1/3}} F[M_n/(3N_n)^{1/3}] \end{aligned} \quad (2.54)$$

where $M_n(\delta z, x, \epsilon) = \delta z + (2n+1+\epsilon)g(a) - \epsilon g(x)$ and $N_n(\delta z, x, \epsilon) = (2n+1+\epsilon)q(a) - \epsilon q(x)$. The cold plasma cone lines satisfy $M_n = 0$, so we see inhomogeneities cause a bending of the cold plasma cone lines and of the maxima of the warm plasma cones. They also cause a spatial modulation of the field amplitudes.

The WKB approximation assumes $dk_x/dx \ll k_x^2$ where k_x is the wave

number in the x direction. From the electrostatic dispersion relation,

$$k_x = \left(-\frac{K_{\parallel}}{K_{\perp}} \right)^{1/2} k_z = \left(\frac{\omega_p^2(x) - \omega^2}{\omega^2 - \omega_{\ell h}^2(x)} \right)^{1/2} k_z \quad (2.55a)$$

The criterion for the validity of the WKB approximation then becomes

$$\frac{\omega^2 d(\omega_{pe}^2)}{dx} \ll 2 [(\omega_p^2 - \omega^2)^3 (\omega^2 - \omega_{\ell h}^2)]^{1/2} k_z \quad (2.55b)$$

The WKB solution breaks down for strong inhomogeneities, for very small

k_z components and as $\omega \rightarrow \omega_p(x)$ or $\omega \rightarrow \omega_{\ell h}(x)$. [By our assumptions $\omega_{\ell h}^2(x) < \omega^2 < \omega_p^2(x)$ for all x.] These two frequencies are turning points:

the plasma frequency cutoff and the low hybrid resonance, respectively.

In the case $\omega = \omega_{\ell h}(x)$ for some x, i.e., for a lower hybrid layer present, $\text{Re } K_{\perp}(x) \rightarrow 0$ in our approximation and thermal terms become dominant in K_{\perp} ,

and mode conversion of the resonance cones may take place. The WKB approximation breaks down near the plasma frequency because the perpendicular wavelength becomes as large as the order of the scale length of

the density variation, but breaks down near the lower hybrid resonance because the perpendicular wavenumber becomes very large so rapidly as the lower hybrid layer is approached. It is to be noted that the WKB approximation breaks down for k_z near 0, so that since we integrate over k_z in

this region when taking the inverse Fourier transform, the validity of the solution depends upon the contribution to the integral from this

region being negligible compared with the total integral. This should be all right for gentle density gradients whenever the quasistatic approxi-

mation is valid, except near the turning points.

mation is valid, except near the turning points.

The damping factor associated with each cone for the inhomogeneous case is just a generalization of that for the homogeneous case and is

$$\Gamma_n(\delta, \epsilon) = \left(\frac{-M_n}{3N_n}\right)^{1/2} [(2n+1+\epsilon)\eta_i(a) - \epsilon\eta_i(x)] \quad (2.56)$$

where

$$\begin{aligned} \eta_i(x) &= \int_0^x \alpha_i(x') dx' \Big|_{k_z=k_0} = \left(\frac{-M_n}{3N_n}\right)^{1/2} \\ &= \left[\sqrt{\pi} \omega_p^2 \left(\frac{-3N_n \omega^2}{M_n v_e^2}\right)^{3/2} \exp(3N_n \omega^2 / M_n v_e^2) \int_0^x \{[\omega_p^2(x') - \omega^2]^{1/2} [\omega^2 - \omega_{1h}^2(x')]^{1/2}\}^{-1} dx' \right. \\ &\quad \left. + \frac{v}{2\omega} \int_0^x \left(\frac{\omega_p^2(x') [\omega^2 - \omega_{1h}^2(x') - \omega_{pi}^2(x')] + \omega^2 \omega_{pi}^2(x')}{[\omega_p^2(x') - \omega^2]^{1/2} [\omega^2 - \omega_{1h}^2(x')]^{3/2}} \right) dx' \right] \quad (2.57) \end{aligned}$$

In Fig. 2.9, the cold plasma cone trajectories are shown for the inhomogeneous plasma, which illustrates that the large cone angle in the low density region near the boundary and the smaller cone angle near the center of the plasma cause the cones to bend in accordance with the local density. The shift in the cone maximum given by Eq. (2.36) due to thermal effects will similarly be controlled by the local density, and this will control the trajectory of the peaks of the warm plasma cones.

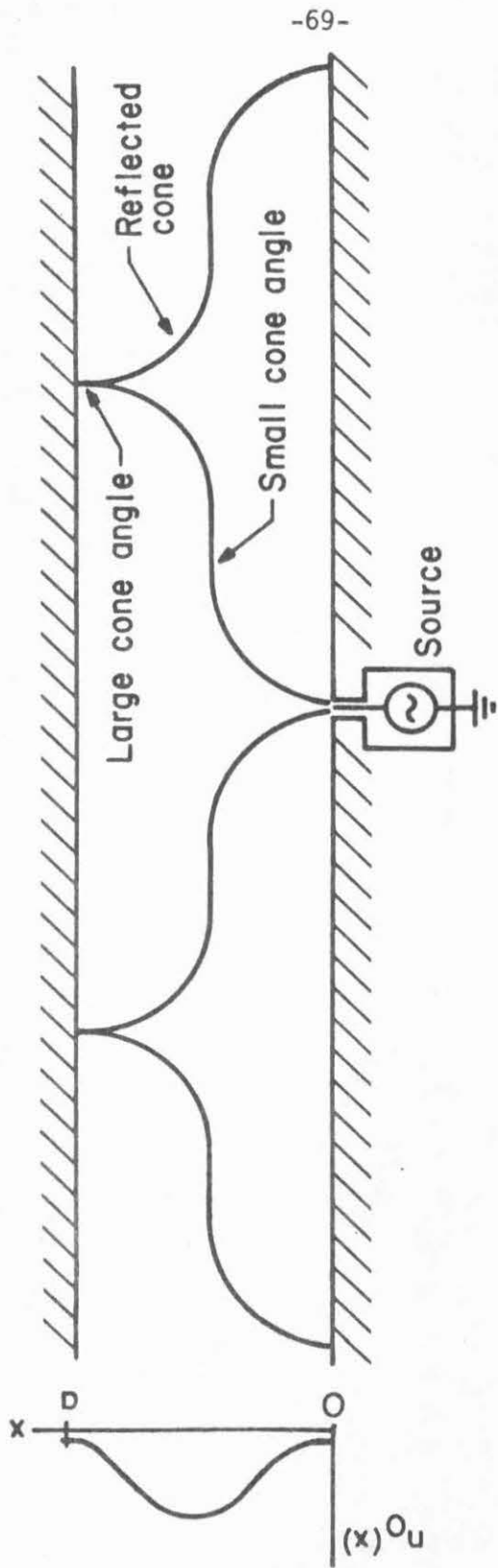


Fig. 2.9 Trajectories of resonance cones in cold plasma limit for inhomogeneous plasma

CHAPTER III: RESONANCE CONES IN INHOMOGENEOUS PLASMA WITH LOWER HYBRID LAYER

3.1 Lower Hybrid Density Model

We now want to investigate the resonance cone structure in our slab plasma model for an inhomogeneous plasma when the low frequency bound of the middle branch of the cones, i.e. the lower hybrid frequency turning point, is present in the plasma. This turning point will modify our cone structure because of the possibility of mode conversion at the hybrid layer, and because of the presence of a region where the waves are evanescent on the high density side of the hybrid layer. What happens to the cones and how their energy is absorbed are important questions to lower hybrid heating that we want to answer.

The density profile is taken to be symmetric about $x=a/2$, with density increasing from the source boundary at $x=0$ to $x=a/2$, and decreasing from $x=a/2$ to $x=a$. Our problem will be formulated and solved for the more general case of a nonsymmetric density profile, then specialized to the symmetric case. The range of frequencies in the plasma will be taken as $\omega_{ci} < \omega_{pi}(x) < \omega_{pe}(x) < \omega_{ce}$ where ω_{ci} and ω_{ce} are the ion and electron cyclotron frequencies, and ω_{pi} and ω_{pe} the ion and electron plasma frequencies. We will also take $\omega_{ci}^2 \ll \omega^2 \ll \omega_{ce}^2$. It is assumed that there are lower hybrid layers present, i.e. values of x for which the source frequency ω is equal to the local hybrid frequency $\omega_{lh}(x)$. We will let the lower hybrid layer nearest the source be at $x=x_{h1}$, so that there is a mirror layer at $x=x_{h2} = a-x_{h1}$ because symmetry, and $\omega = \omega_{lh}(x_{h1}) = \omega_{lh}(x_{h2})$. We will consider propagation of

the extraordinary mode from the source, which is evanescent on the high density side of the hybrid layer, for $\omega < \omega_{\ell h}(x)$. Thus the wave will be evanescent in the region between the hybrid layers, and we will be concerned with the case that this evanescent region is quite small compared to a . (See Fig. 3.1.)

We will calculate the quasistatic fields in this model including first order thermal effects. This will give four wave modes everywhere: the extraordinary wave (which will sometimes be called the cold plasma wave, since it is present in a cold plasma), and the ion thermal (Bernstein) wave (which will sometimes be called the warm plasma wave, since it arises purely from thermal effects), each of which may have components propagating in the direction of increasing x and the direction of decreasing x .

There are three natural regions introduced into the plasma by the hybrid layers: the two regions between the boundaries and the hybrid layers where the waves are propagating, and the region between the hybrid layers where the waves are evanescent. In each of these regions, the fields away from the lower hybrid layers can be obtained in the WKB form for a mildly inhomogeneous plasma, but these break down very near the lower hybrid layers, where a different approach to the solution must be made. Thus to aid in obtaining the fields in this model, we will further subdivide the three regions into regions where the WKB solutions are valid, and hybrid layer regions where they are not. This gives seven regions as shown in Fig. 3.1. Region I is the region near $x=0$ where the waves are propagating and WKB solutions are valid. Regions II and III are on either side of the hybrid layer $x=x_{h1}$ where WKB forms are

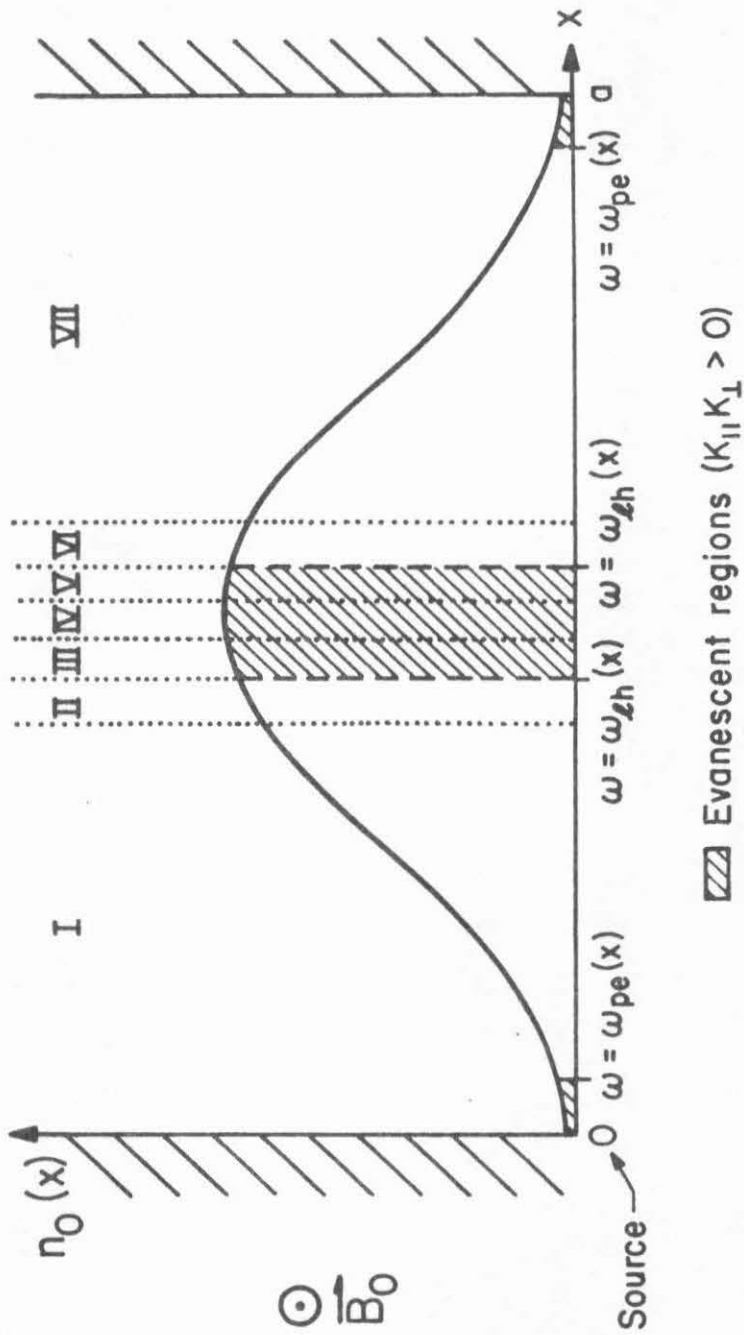


Fig. 3.1 Density profile showing the seven regions, the lower hybrid layers, and the evanescent regions

not valid except at the edge, where the solutions in these regions connect onto the WKB solutions. Region II is on the low density propagating side of $x=x_{h1}$, and region III on the high density evanescent side. Similarly, regions V and VI are the high density evanescent side and the low density propagating side of $x=x_{h2}$, respectively. We may have a region inside the evanescent region where WKB solutions are valid, and this we call region IV. Region IV will not be present in most cases of interest where the evanescent layer is thin so that tunnelling through that layer is important. Finally, region VII will be the region near the $x=a$ boundary where the WKB solution is valid.

In cold plasma theory, the cones can exist, i.e., the fields are singular in regions I and II between $x=0$ and $x=x_{h1}$ since $K_{||} K_{\perp} < 0$ there. In regions III, IV and V between $x=x_{h1}$ and $x=x_{h2}$, $K_{||} K_{\perp} > 0$ and the cones do not exist in cold plasma theory. In regions VI and VII, $K_{||} K_{\perp} < 0$ again, so in principle, cold plasma resonance cone singularities could exist, but will not be present because of the intervening evanescent layer between the regions and the source. However, if the evanescent layer is thin, conelike fields exist in these regions as well as in the evanescent regions. (These facts begin to illustrate the limitations of cold plasma criteria for the existence of resonance cones.)

The method of finding the fields will be to obtain the form of the solutions in each region and then find the coefficients of the linear independent solutions by connection to adjacent regions and use of the boundary conditions. There are two kinds of connections to be done: connections across the lower hybrid turning points at x_{h1} and x_{h2} , and connections between the WKB regions and the hybrid resonance

regions.

Energy is coupled into the plasma at the source at $x=z=0$. To excite the extraordinary mode in the plasma we require the perpendicular component of the wave at the source to have its electric field vector perpendicular to the background magnetic, since the tangential component of the electric field is continuous across the boundary at $x=0$. Since we are thinking primarily of a waveguide source, this means that we want to use the TM mode of the guide. The TE mode couples to the ordinary (electromagnetic) mode in the plasma, which does not experience a resonance at the lower hybrid frequency. For optimum coupling to the plasma, the source impedance should be matched to that of the plasma in the low density region, since that minimized the power that is reflected back into the guide from the boundary.

In the low density region near the source the large k_z 's are evanescent for a small distance if the plasma frequency falls below the source frequency. If the plasma density is zero at $x=0$, the dispersion relation of the electromagnetic wave there is

$$k_x^2 + k_z^2 = \omega^2/c^2 \quad (3.1)$$

and the $k_z > \omega/c$ components are evanescent. Since we are solving for the fields in the quasistatic approximation, which gives the dispersion relation in the zero density region

$$k_x^2 + k_z^2 = 0$$

our solutions will give evanescent waves for all k_z , which is incorrect

for the small k_z , but will give the correct decay rate for $k_z \gg \omega/c$.

Since the decay introduced in the waves in this region is quite small, the inaccuracy for small k_z will have a negligible effect on our results.

We want to solve Poisson's equation for the potential (which is valid in the quasistatic approximation) in k_z space, which takes the form

$$\frac{\partial}{\partial x} \left[K_{\perp}(x, k_z) \frac{\partial \tilde{\phi}(x, k_z)}{\partial x} \right] - k_z^2 K_{\parallel}(x, k_z) \tilde{\phi}(x, k_z) = 0 \quad (3.2)$$

where

$$\phi(x, z) = \int_{-\infty}^{\infty} \tilde{\phi}(x, k_z) e^{i k_z z} \frac{dk_z}{2\pi} \quad (3.3)$$

The form of K_{\perp} as an operator in x , which is obtained by appropriate replacement of the k_x 's in the k -space form of K_{\perp} by partials in x , as in Eq. (1.21), is

$$K_{\perp}(x) = K_{\perp 0}(x) + \frac{\partial}{\partial x} \left[\beta(x) \frac{\partial}{\partial x} \right] \quad (3.4a)$$

where

$$K_{\perp 0}(x) = 1 - \frac{\omega_{pi}^2(x)}{\omega^2} + \frac{\omega_{pe}^2(x)}{\omega_{ce}^2} + i \text{Im} K_{\perp}(x) \quad (3.4b)$$

and

$$\beta(x) = \frac{3}{2} \left[\frac{v_i^2 \omega_{pi}^2(x)}{\omega^4} + \frac{v_e^2 \omega_{pe}^2(x)}{\omega_{ce}^4} \right] \quad (3.4c)$$

is the thermal coefficient in K_{\perp} . As pointed out in Chapter I, the correct position of $\beta(x)$ with respect to the operators is a nontrivial

thing to determine, but the solution for $\tilde{\phi}$ is quite insensitive to that position because the $\beta'(x)$ terms in Poisson's equation are not very important.

The equation for the potential is now

$$\left[\beta(x) \frac{\partial^4}{\partial x^4} + 2\beta'(x) \frac{\partial^3}{\partial x^3} + K_{10}(x) \frac{\partial^2}{\partial x^2} + K_{10}'(x) \frac{\partial}{\partial x} - k_z^2 K_{11}(x, k_z) \right] \tilde{\phi}(x, k_z) = 0 \quad (3.5)$$

It will be useful to split off the first order thermal corrections to K_{\perp} as was done for K_{\parallel} :

$$K_{\parallel}(x, k_z) = K_{\parallel 0}(x, k_z) - \frac{3}{2} \frac{k_z^2 v_0^2 \omega_{p0}^2}{\omega^4} \quad (3.6)$$

The first and third order terms in the potential equation arise from the inhomogeneities of the plasma, with the third order term being the thermal correction to the first order term. The third order term is $\mathcal{O}(\lambda_x/\ell)$ compared with the first order term, where ℓ is the scale length of the density gradient and λ_x is the wavelength associated with the x direction. We are assuming gentle density inhomogeneities everywhere, so $\lambda_x \ll \ell$ except for a thin region near the plasma frequency layer, and the third order term is negligible compared to the first order term. This term arises from the effect of the pressure gradient associated with the gentle inhomogeneity of the background density on the wave field.

We will present solutions in each of the seven regions, with coefficients $a_j^{(i)}$, in the form

$$\gamma^{(i)} = \sum_{j=1}^4 a_j^{(i)} \phi_j^{(i)} \quad (3.7)$$

Here i numbers the region and runs from one to seven, and j numbers the particular solution in the region. Thus $\gamma^{(i)}$ is the general solution in region I , and $\phi_j^{(i)}$ is the j^{th} particular solution in that region. The convention that we will adopt for the j indices is summarized in the following table:

j	Type of Mode	Sign of v_{gx}	Sign of v_{px}
1	Extraordinary	+	-
2	Bernstein	-	-
3	Extraordinary	-	+
4	Bernstein	+	+

Table 1. Labelling of modes and their group and phase velocity directions

3.2 Dispersion Relation near the Lower Hybrid

Before obtaining the solutions to the potential equation, a review of the dispersion relation is in order, since it illustrates the coalescing of the modes necessary for mode conversion. We will consider the dispersion relation in a WKB sense, so that the wave number is a function of the local density, and ignore the effect of inhomogeneities on the dispersion relation. This breaks down near the cutoffs and resonances but illustrates all of the essential features. Fourier transforming Eq. (3.5) without the inhomogeneous terms gives

$$D(\vec{k}, \omega) = \beta k_x^4 - K_{\perp 0}^2 k_x^2 - k_z^2 K_{\parallel}(k_z) = 0 \quad (3.8)$$

The roots are

$$k_x = \pm \left\{ \frac{K_{\perp 0} \pm \left[K_{\perp 0}^2 + 4\beta K_{\parallel} k_z^2 \right]^{1/2}}{2\beta} \right\}^{1/2} \quad (3.9a)$$

Far from the hybrid layer, $K_{\perp 0}^2 \gg 4\beta K_{\parallel} k_z^2$, and the roots are widely separated:

$$k_x = k_{1,2} \approx \pm \left\{ |k_z| \left[-\frac{K_{\perp 0}}{K_{\perp 0}} \right]^{1/2} - \frac{3}{4} \frac{\omega_{pe}^2 v_e^2 |k_z|^3}{\omega^4 \left(-K_{\perp 0} K_{\perp 0} \right)^{1/2}} \right\} \quad (3.9b)$$

$$k_x = k_{3,4} = \pm \left\{ \left[\frac{-K_{\perp 0}^3}{K_{\perp 0}^5} \right]^{1/2} \beta |k_z^3| \right\} + \left\{ \left[\frac{K_{\perp 0}}{2\beta} \right]^{1/2} + \left[\frac{\beta}{2K_{\perp 0}^3} \right]^{1/2} k_z^2 K_{\perp 0} \right\} \quad (3.9c)$$

The roots coalesce at

$$k_z \approx \frac{K_{\perp 0}}{2(-K_{\parallel 0})^{1/2}} \quad (3.10)$$

If one assumes an approximately linear density profile in the thin layer near the lower hybrid, as we will do to obtain the solutions there, so that

$$\text{Re } K_{\perp 0}(x) \approx \gamma(x - x_h) \quad (3.11)$$

where $\gamma = \frac{n'(x_h)}{n(x)}$, then for a fixed k_z it is seen that mode conversion (coalescing of the roots) takes place not at the hybrid layer but at

$$x \approx x_h \pm \frac{2|k_z| (-\beta K_{\parallel})^{1/2}}{\gamma} \quad (3.12)$$

This shows that the higher the k_z , the further the distance from $x = x_h$ at which that particular component of the incoming mode converts into

the outgoing mode.

The dispersion relation, k_x^2 as a function of x , is shown in Fig. 3.2 across the plasma cross section. Between the coalescence of the roots on each side of the hybrid layers, i.e., for

$$x_h - \frac{2|k_z| (-\beta K_{||})^{1/2}}{\gamma} < x < x_h + \frac{2|k_z| (-\beta K_{||})^{1/2}}{\gamma} \quad (3.13)$$

k_x^2 is complex and the roots are complex and conjugate (partially propagating and partially decaying waves). The conjugate solutions connect the propagating solutions on one side of the hybrid layer to the evanescent solutions on the other side of the hybrid layer, and were studied by Moore and Oakes.¹⁶

3.3 WKB Solutions

For slowly varying densities it is valid to use WKB solutions in certain regions of the plasma. Such solutions are valid for²⁹

$$\frac{dk_x(x)}{dx} \ll k_x^2(x) \quad (3.14)$$

From the electrostatic dispersion relation, we may rewrite this criterion as

$$\omega^2 \frac{d[\omega_p^2(x)]}{dx} \ll 2 [(\omega_p^2 - \omega^2) (\omega^2 - \omega_{\ell h}^2)]^{1/2} |k_z| \quad (3.15)$$

for the x-mode. This is not valid near $\omega = \omega_{\ell h}(x_h)$, i.e., near the lower hybrid layers $x = x_{h1}$ and $x = x_{h2}$, and we must use special solutions in those regions. This is also invalid near the plasma frequency region $\omega = \omega_p(x)$ in the low density regions near the edge of the plasma if the density falls off sufficiently so that such layers exist, but it will not be important for this problem to write the explicit solutions

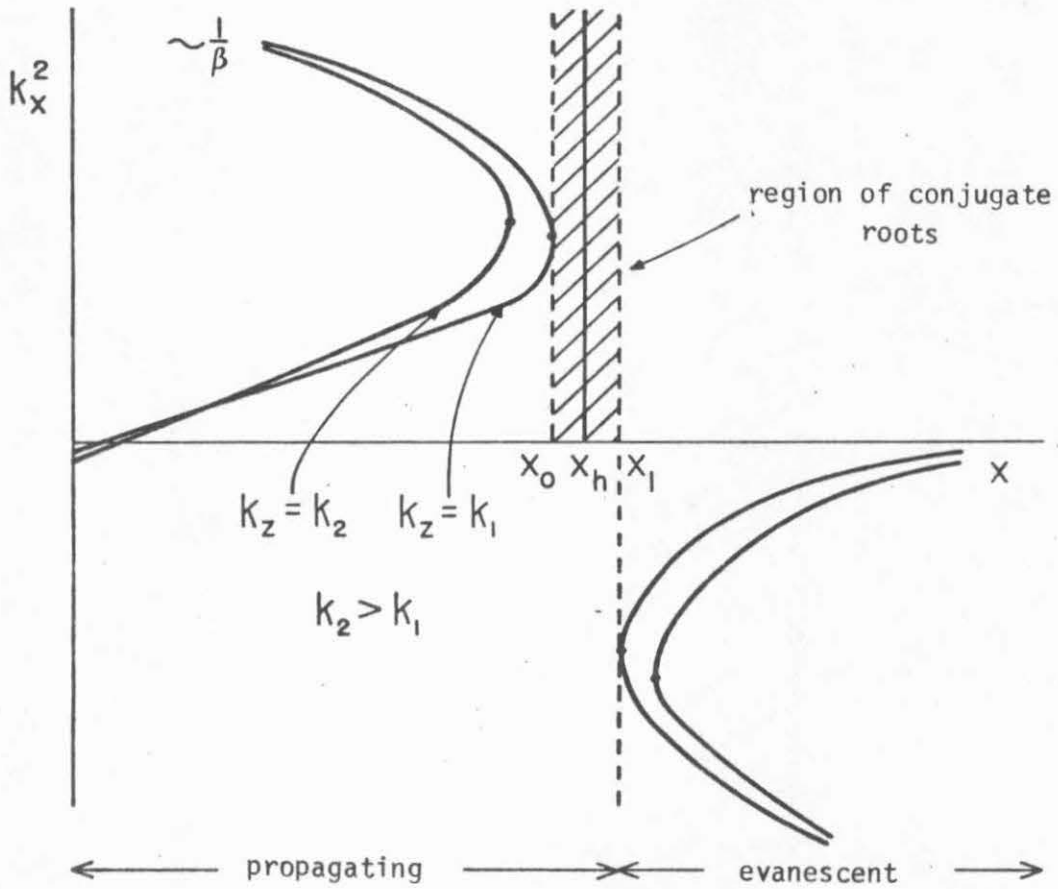


Fig. 3.2. Dispersion relation near the lower hybrid showing the long and short wavelength modes, and their points of confluence x_0 and x_1 . x_h is the lower hybrid layer.

in those regions.

For the ion thermal mode the WKB criterion may be written

$$\frac{d}{dx} [\omega_{pi}^2(x)] \ll (\omega^2 - \omega_{lh}^2)^{3/2} \frac{\omega_{pi}}{v_i \omega} \quad (3.16)$$

Then WKB form for this mode also breaks down near the lower hybrid layer $\omega_{lh}(x) \cong \omega$.

There are four solutions to Eq. (3.4): the two extraordinary modes and the two ion Bernstein modes, corresponding to propagation in the x or the -x directions. For the x-mode, the second order term and the $K_{||0}$ part of the zeroth order term are the most important, whereas the fourth order term and the thermal terms in $K_{||}$ are the first order thermal correction terms to the basic cold plasma x-mode. However, for the ion Bernstein mode, the fourth order and the second order terms are the most important, and the zeroth order term is a correction for a finite component for propagation in the z-direction. [See the value of k_x for the two modes, Eq. (3.9)].

The general form for the WKB solutions can be obtained, for example, from Bellan and Porkolab,¹⁹ but these must be extended slightly by using the expansion for k_x in Eq. (3.9) in the $e^{i \int k_x dx}$ factor in each linear independent solution, adding in damping terms for the four types of damping, and specializing to each region. A discussion of a quick way to obtain these forms from the power flux is given in Appendix B.

In region I, the WKB solutions to Eq. (3.4) takes the form,

$$\tilde{\phi}^{(1)}(x, k_z) = \tilde{\phi}_0 \left\{ A(x) e^{-i|k_z|g_1(x)} + a_2^{(1)} |k_z|^{1/2} B(x) \right. \\ \left. \times e^{-ih_1(x)} + a_3^{(1)} A(x) e^{i|k_z|g_1(x)} + a_4^{(1)} |k_z|^{1/2} B(x) e^{ih_1(x)} \right\} \quad (3.17)$$

where

$$\tilde{\phi}_0 = \left[\frac{\tilde{\phi}^{(1)}(0, k_z)}{(1 + a_3^{(1)}) + (a_2^{(1)} + a_4^{(1)}) |k_z|^{1/2} B(0)} \right] \quad (3.18)$$

$$A(x) = \left[\frac{K_{\parallel 0}(0) K_{\perp 0}(0)}{K_{\parallel 0}(x) K_{\perp 0}(x)} \right]^{1/2} \quad (3.19a)$$

$$B(x) = \left[\frac{-K_{\parallel 0}(0) K_{\perp 0}(0) \beta(x)}{K_{\perp 0}^{(3)}(x)} \right]^{1/2} \quad (3.19b)$$

$$g_1(x) = \int_0^x \left[\frac{-K_{\parallel 0}(x')}{K_{\perp 0}(x')} \right]^{1/2} dx' \quad (3.20a)$$

is the phase of the x-mode, and

$$h_1(x) = \int_0^x \left[\frac{K_{\perp 0}(x')}{\beta(x')} \right]^{1/2} dx' \quad (3.20b)$$

is the phase of the ion thermal mode. These are the WKB forms ignoring the thermal corrections to the X-mode and the finite k_z corrections to the ion Bernstein mode. However, we must include these effects to get the correct (nonsingular) fields in our final result. We can do this by adding their contributions to the phases of each mode:

$$g_1(x) = g_1(x) + |k_z|^2 q_1(x) \\ h_1(x) = h_1(x) + |k_z|^2 p_1(x) \quad (3.21)$$

where

$$g_1(x) = -\frac{1}{2} \int_0^x \left\{ \beta(x') \left[\frac{-K_{110}^3(x')}{K_{10}^3(x')} \right]^{\frac{1}{2}} + \frac{3 v_e^2 \omega_{pe}^2(x')}{2 \omega^4 [-K_{110}(x') K_{10}(x')]^{\frac{1}{2}}} \right\} dx' \quad (3.22a)$$

and

$$h_1(x) = \int_0^x K_{110}(x') \left[\frac{\beta(x')}{K_{10}^3(x')} \right]^{\frac{1}{2}} dx' \quad (3.22b)$$

It should be noted that the Bernstein mode $e^{ih_1(x)}$ travels in the \hat{x} direction and $e^{-ih_1(x)}$ in the $-\hat{x}$ direction, while the x-mode is a backward wave (i.e., the x component of the group velocity is opposite in sign to the same component of the phase velocity), so that $e^{i|k_z|g_1(x)}$ is travelling in the $-\hat{x}$ direction and $e^{-i|k_z|g_1(x)}$ in the \hat{x} direction.

That those are indeed the correct directions of the group velocity can be seen by writing out the imaginary parts of g_1 and h_1 which arise from damping, and seeing the direction in which each of these modes decays, which is the group velocity direction. For a small imaginary part of K_{11} and K_{10} compared to their real part, these are given by

$$\text{Im } g_1(x) \cong \frac{1}{2} \int_0^x \left\{ \left[\frac{-K_{110}}{K_{10}^3} \right]^{\frac{1}{2}} \text{Im } K_{10} + \frac{\text{Im } K_{110}}{(-K_{110} K_{10})^{\frac{1}{2}}} \right\} dx' \quad (3.23a)$$

$$\text{Im } h_1(x) \cong \frac{1}{2} \int_0^x \frac{\text{Im } K_{10} dx'}{(\beta K_{10})^{\frac{1}{2}}} \quad (3.23b)$$

where $\text{Im } K_{11}$ and $\text{Im } K_{10}$ are both positive and given in Eqs. (1.16) and (1.19).

In region IV, the waves are evanescent and K_{11} and K_{10} are of the same sign, so the fields could not be singular here even for a cold collisionless plasma. The solution then takes the form

$$\begin{aligned} \tilde{\phi}^{(4)}(x, k_z) = & \tilde{\phi}_0 \left\{ a_1^{(4)} A(x) e^{-|k_z|g(x)} \right. \\ & \left. + a_2^{(4)} B(x) e^{-g(x)} + a_3^{(4)} A(x) e^{|k_z|g(x)} + a_4^{(4)} B(x) e^{g(x)} \right\} \end{aligned} \quad (3.24)$$

where

$$\mathcal{G}(x) = \int_{x_{h1}}^x \left[\frac{K_{\parallel}(x')}{K_{\perp}(x')} \right] dx' \quad (3.25a)$$

is the exponent of the X-mode and

$$\mathcal{H}(x) = \int_{x_{h1}}^x \left[\frac{-K_{\perp}(x')}{\beta(x')} \right]^{1/2} dx' \quad (3.25b)$$

is the exponent of the Bernstein mode. The higher order corrections to the exponents are obtained by making the replacement

$$\begin{aligned} \mathcal{G}(x) &\rightarrow \mathcal{G}(x) + |k_z|^2 \mathcal{Q}(x) \\ \mathcal{H}(x) &\rightarrow \mathcal{H}(x) + |k_z|^2 \mathcal{P}(x) \end{aligned} \quad (3.26)$$

where

$$\mathcal{Q}(x) = \frac{1}{2} \int_0^x \left\{ \beta(x') \left[\frac{K_{\parallel}^2(x')}{K_{\perp}^5(x')} \right]^{1/2} + \frac{3 v_e^2 \omega_{pe}^2(x')}{\omega^4 [-K_{\parallel 0} K_{\perp 0}]^{1/2}} \right\} dx' \quad (3.27a)$$

and

$$\mathcal{P}(x) = \frac{1}{2} \int_0^x K_{\parallel}(x') \left[\frac{-\beta(x')}{K_{\perp}^3(x')} \right] dx' \quad (3.27b)$$

The imaginary parts are given by

$$\text{Im } \mathcal{G}(x) = \frac{1}{2} \int_{x_{h1}}^x \left\{ \left[\frac{K_{\parallel 0}(x')}{K_{\perp 0}(x')} \right]^{1/2} \text{Im } K_{\perp} + \frac{\text{Im } K_{\parallel}}{[-K_{\parallel 0}(x') K_{\perp 0}(x')]^{1/2}} \right\} dx' \quad (3.28a)$$

$$\text{Im } \mathcal{H}(x) = \frac{1}{2} \int_{x_{h1}}^x \frac{\text{Im } K_{\perp 0} dx'}{[-\beta(x') K_{\perp 0}(x')]^{1/2}} \quad (3.28b)$$

In region VII, the wave is propagating again and $K_{\parallel} K_{\perp} < 0$. Although singular cones could in principle exist in this region if a cold, collisionless plasma is assumed, they will not be present in this model even under such assumptions because the source is on the other side of

the evanescent layer, and the cones are made nonsingular upon passing through the evanescent layer. The solution takes a form similar to that of region I.

$$\begin{aligned} \tilde{\phi}^{(7)}(x, k_z) = & \tilde{\phi}_0 \left\{ a_1 A(x) e^{-i|k_z| g_2(x)} \right. \\ & + a_2^{(7)} |k_z|^{1/2} B(x) e^{-i h_2(x)} + a_3^{(7)} A(x) e^{i|k_z| g_2(x)} \\ & \left. + a_4^{(7)} |k_z|^{1/2} B(x) e^{i h_2(x)} \right\} \end{aligned} \quad (3.29)$$

The higher order corrections are given by

$$\begin{aligned} g_2(x) & \rightarrow g_2(x) + |k_z| g_2(x) \\ h_2(x) & \rightarrow h_2(x) + |k_z|^2 p_2(x) \end{aligned} \quad (3.30)$$

where

$$g_2(x) = -\frac{1}{2} \int_{x_{h1}}^x \left\{ \beta(x') \left[\frac{-K_{110}^3(x')}{K_{10}^5(x')} \right]^{1/2} + \frac{3}{2} \frac{v_e^2 \omega_{pe}^2(x')}{\omega^4 [-K_{110} K_{10}]^{1/2}} \right\} dx' \quad (3.31a)$$

$$p_2(x) = \frac{1}{2} \int_{x_{h2}}^x K_{11}(x') \left[\frac{\beta(x')}{K_{10}^3(x')} \right]^{1/2} dx' \quad (3.31b)$$

The imaginary parts of the phases which are involved with damping are

$$\text{Im } g_2(x) \cong -\frac{1}{2} \int_{x_{h2}}^x \left\{ \left[\frac{-K_{110}}{K_{10}^3} \right]^{1/2} \text{Im } K_1 + \frac{\text{Im } K_{11}}{(-K_{110} K_{10})^{1/2}} \right\} dx' \quad (3.32a)$$

$$\text{Im } h_2(x) = \frac{1}{2} \int_{x_{h2}}^x \frac{\text{Im } K_{10}(x') dx'}{(\beta K_{10})^{1/2}} \quad (3.32b)$$

3.4 Resonance Region Solutions

Near the hybrid layers, $\text{Re } K_{\perp} \rightarrow 0$, and the fourth-order term in Eq. (3.4) becomes all important in preventing the differential equation from becoming singular since the second-order term has such a small coefficient. We will be primarily concerned with the asymptotic forms of the solution in these regions, so we will solve the differential equation by saddle point methods.

We assume the density to be approximately linear in the small region about the hybrid layers. We will define the inverse scale length of the density gradient at the hybrid layers to be

$$\gamma = \frac{n'(x_{h1})}{n(x_{h1})} = - \frac{n'(x_{h2})}{n(x_{h2})} \quad (3.33)$$

where the equality of the two forms comes from the symmetry of the density profiles. The real part of $K_{\perp 0}(x)$ goes to zero at the hybrid resonances. Near $x = x_{h1}$ we have

$$K_{\perp 0}(x) \cong \gamma (x - x_{h1}) + \mathcal{O}[(x - x_{h1})^2] \quad (3.34)$$

and near $x = x_{h2}$

$$K_{\perp 0}(x) \cong \gamma (x_{h2} - x) + \mathcal{O}[(x - x_{h2})^2] \quad (3.35)$$

Define

$$\begin{aligned} u_1 &= (\gamma/\beta)^{1/3} (x_{h1} - x) \\ u_2 &= (\gamma/\beta)^{1/3} (x - x_{h2}) \end{aligned} \quad (3.36)$$

Then we may rewrite the differential equation, Eq. (3.4) in the form

$$\left[\partial_u^4 + (u + i\varepsilon) \partial_u^2 + 2u + \mu \right] \tilde{\phi}(u) = 0 \quad (3.37)$$

where u is u_1 near $x = x_{h1}$ and u_2 near $x = x_{h2}$, and

$$\varepsilon = (\gamma^2 \beta)^{-1/3} \left\{ \frac{\nu_i \omega_{pi}^2}{\omega^3} + \frac{2 \omega_{pi}^2 \omega_{ci}^2}{\omega k_z k_{x0}^3} e^{-\omega^2 / k_{x0}^2 \nu_i^2} \sum_{n=-\infty}^{\infty} n^2 e^{-\frac{(\omega - n \omega_{ci})^2}{k_z^2 \nu_i^2}} \right\} \quad (3.38a)$$

$$\mu = - \left(\frac{\beta}{\gamma^4} \right)^{1/3} k_z^2 K_{||}(x, k_z) \quad (3.38b)$$

(Here μ includes the thermal terms in $K_{||}$.) $k_{x0} \approx k_z \left[-K_{||0}/K_{\perp 0} \right]^{1/2}$ when ε appears in the X-mode, and $k_{x0} \approx \left[K_{\perp 0}(x)/\beta(x) \right]^{1/2}$ when it appears in the ion thermal mode [it acts like an operator on $\tilde{\phi}(u)$].

The theory of mode conversion near the lower hybrid has been investigated by several researchers by doing a linearization as in Eqs. (3.34), obtaining an equation similar to Eq. (3.37), and investigating asymptotic solutions to it. T. Stix¹² first considered the problem and predicted that an incoming "cold" (X-mode) wave would convert into an outgoing "hot" (ion thermal) wave. Similarly, Moore and Oakes¹⁶ investigated the asymptotic solutions to the same equation, including ion damping effects [$\varepsilon \neq 0$ in Eq. (3.37)]. The form of the solutions between the point of confluence of the mode on each side of the hybrid layer studied and an estimate of mode conversion efficiency was made. These calculations were done for a single fixed k_z for the incoming wave.

For sources that currently appear to be most useful for lower hybrid heating experiments, a whole spectrum of k_z is excited, and it was shown that for such sources the waves may come into the lower hybrid concentrated along cones.⁵ It was shown by a numerical solution by

M. Simonutti¹⁸ that the whole cone undergoes mode conversion. This was confirmed by Bellan and Porkolab¹⁹ who found the resonance cone fields for some finite sources. They pointed out that the $\partial_u^{\gamma} \phi$ term, arising from plasma inhomogeneities is an important term previously neglected. This term changes the rate of swelling of the fields near the hybrid layer.

The results of the above work are not adequate for our purposes. These analyses were for the single case of an X-mode incoming into the hybrid layer, which is physically the most interesting case. However, we have four modes in each region, either one of which may come into a given hybrid layer from either the propagating or evanescent side and undergo mode coupling and conversion. Thus we want the complete set of connections across the hybrid layer, which we will apply to each hybrid layer in our model. We also want to consider the detailed nature of all types of damping on the modes. Moore and Oakes¹⁶ considered the effect of an $\epsilon \neq 0$ on mode conversion efficiency of the incoming mode, and Bellan and Porkolab¹⁹ considered the effects of collisional damping on the incoming mode, but there has been no complete study of the effect of both the collisional and collisionless forms of damping on both the incoming and outgoing modes. We will review the method of solution by transforming Eq. (3.37) to reduce it to a solvable first order equation and using saddle point integration.

We will be concerned with the case $|\epsilon| \ll |u|$, so will drop ϵ in Eq. (3.37), and include it as a perturbation to the $\epsilon = 0$ solution later by lumping its effect into a slowly varying amplitude factor of the Laplace transform.

The Laplace transform form of $\tilde{\phi}$ is

$$\tilde{\phi}(u) = \int_{\Gamma} y(s) e^{su} ds \quad (3.39a)$$

where $y(s)$ is the Laplace transform of $\tilde{\phi}(u)$. By substituting Eq. (3.39a) into Eq. (3.27) and integrating by parts twice, we obtain a first order differential equation for $y(s)$, which is readily solved to give

$$y(s) = \frac{A(s) e^{s^3/3} - \mu/s}{s} \quad (3.39b)$$

As a solution to the Laplace transform of Eq. (3.37) with $\epsilon = 0$, A is a constant, but we allow A to be a slowly varying function of s as it will be for the inclusion of the following small effects:

1. Damping, with $\epsilon \neq 0$ and $\text{Im } \mu \neq 0$.
2. The third order term $\sim (\gamma^2 \beta)^{1/3} \partial_u \tilde{\phi}$ in Eq. (3.37)
3. The inclusion of the nonlinear ponderomotive force, which might be expected to be an important correction to K_{\perp} as $u \rightarrow 0$. The study of these effects will be deferred to later.

Our integral expression to evaluate is

$$\tilde{\phi}(u) = \int_{\Gamma} A(s) e^{s^3/3 - \mu/s + us} \frac{ds}{s} \quad (3.39c)$$

We want the asymptotic forms of this integral for $|u| \gg 2\sqrt{\mu}$, which we will do by deforming the contours Γ over the saddle points of the integrand. The condition that the "surface terms" in the integration by parts to obtain $y(s)$ disappear is that $y(s)e^{isu}$ goes to zero at the endpoints of the contour. There are four linearly independent solutions to Eq. (3.39), which will be obtained by choosing four linearly independent contours Γ over which to evaluate the integrals, with endpoints such that

the integrand goes to zero. Each contour will be deformed over a single saddle point, so that the contribution from the integration over each saddle point will give a linearly independent solution.

The four saddle points of Eq. (3.39) are given by

$$s_{1,2} \approx \pm \left[-u + \mu/u \right]^{1/2} \quad s_{3,4} \approx \pm \left[-\mu/u \right]^{1/2} \quad (3.40)$$

The saddle points lie on the real axis in the s -plane for $u < 0$ (evanescent side of the hybrid layer), and on the imaginary axis for $u > 0$ (propagating side of the hybrid layer). Saddle points s_1 and s_2 are much further from the origin, and give rise to the ion thermal mode solutions, while s_3 and s_4 give rise to the extraordinary modes. The paths of steepest descent near these saddle points are found by expanding the exponent $f(s) = s^3/3 - \mu/s + us$ in the integrand about each saddle point s_0 and choosing the directions that make this integrand decrease the most rapidly:

$$f(s) \approx f(s_0) + \frac{f''(s_0)}{2} (s - s_0)^2 + \mathcal{O}[(s - s_0)^3] \quad (3.41)$$

and require $f''(s_0) (s - s_0)^2 = -\tau$ for τ real and > 0 for s on the path of steepest descent. This gives the angles for the paths across the saddle points summarized in the following table:

Saddle Point	Arg (s - s ₀)	
s ₁	- π/4	3π/4
s ₂	-3π/4	π/4
s ₃	-3π/4	π/4
s ₄	- π/4	3π/4

Table 2. Paths of steepest descent angles at saddle points.

The endpoints must lie in regions for which $\text{Re } f(s) \rightarrow -\infty$. As $|s| \rightarrow \infty$, $s^3/3$ becomes the leading term in $f(s)$, so the endpoint regions then are

$$\begin{aligned} \pi/6 < \arg s < \pi \\ 5\pi/6 < \arg s < 7\pi/6 \\ 3\pi/2 < \arg s < 11\pi/6, \end{aligned} \tag{3.42a}$$

whereas as $|s| \rightarrow 0$, $-\mu/s$ dominates and an endpoint may lie along

$$-\pi/2 < \arg s < \pi/2. \tag{3.42b}$$

The linearly independent contours we choose are shown in the s -plane in Figs. 3.3 and 3.4 with the saddle points for $|u| > 2\sqrt{\mu}$ indicated and the endpoint regions shaded. We have a different set of contours for $u > 0$ (Fig. 3.3) than for $u < 0$ (Fig. 3.4) because the saddle points are different. There is a pole at the origin, which makes it possible to choose a contour which both begins and ends there. We label the contours for $u > 0$ by I_i , and $u < 0$ by J_i , where i runs 1 to 4. By seeing how the I 's deform into the J 's, one may obtain the connection between the $u > 0$ region and the $u < 0$ region.

Each contour Γ , having been deformed over a single saddle point s_0 , gives

$$\int_{\Gamma} A(s) e^{s^3/3 - \mu/s + us} \frac{ds}{s} \sim \left[\frac{-2\pi}{f''(s_0)} \right]^{1/2} \frac{A(s_0) e^{f(s_0)}}{s_0} \tag{3.43}$$

The form this takes to lowest order for the various paths is summarized in the following table:

Γ	$\int_{\Gamma} e^{f(s)} \frac{ds}{s}$	Mode	Direction of \vec{v}_g
I_1	$(\mu u)^{-1/4} \exp[2i(\mu u)^{1/2} + \frac{\pi i}{4}]$	Extraordinary	Ingoing to hybrid layer
I_2	$u^{-3/4} \exp[\frac{2i}{3} u^{3/2} - \frac{\pi i}{4}]$	Bernstein	Outgoing
I_3	$(\mu u)^{-1/4} \exp[-2i(\mu u)^{1/2} - \frac{\pi i}{4}]$	Extraordinary	Outgoing
I_4	$u^{-3/4} \exp[-\frac{2i}{3} u^{3/2} + \frac{\pi i}{4}]$	Bernstein	Ingoing
J_1	$(-\mu u)^{-1/4} \exp[-2(-\mu u)^{1/4}]$	Extraordinary	Decaying away from hybrid layer
J_2	$i(-u)^{-3/4} \exp[-\frac{2}{3}(-u)^{3/2}]$	Bernstein	Decaying
J_3	$i(-\mu u)^{-1/4} \exp[2(-\mu u)^{1/2}]$	Extraordinary	Growing
J_4	$(-u)^{-3/4} \exp[\frac{2}{3}(-u)^{3/2}]$	Bernstein	Growing

Table 3. Linearly independent asymptotic solutions obtained by integrating over contours Γ .

These are the forms of $\int_{\Gamma} e^{f(s)} \frac{ds}{s}$ including only the leading order term in the exponential. We must include the next order terms to get the correct cone fields, as we did in the WKB regions. There are also damping corrections, not shown, which were lumped into $A(s)$. These may be included by letting

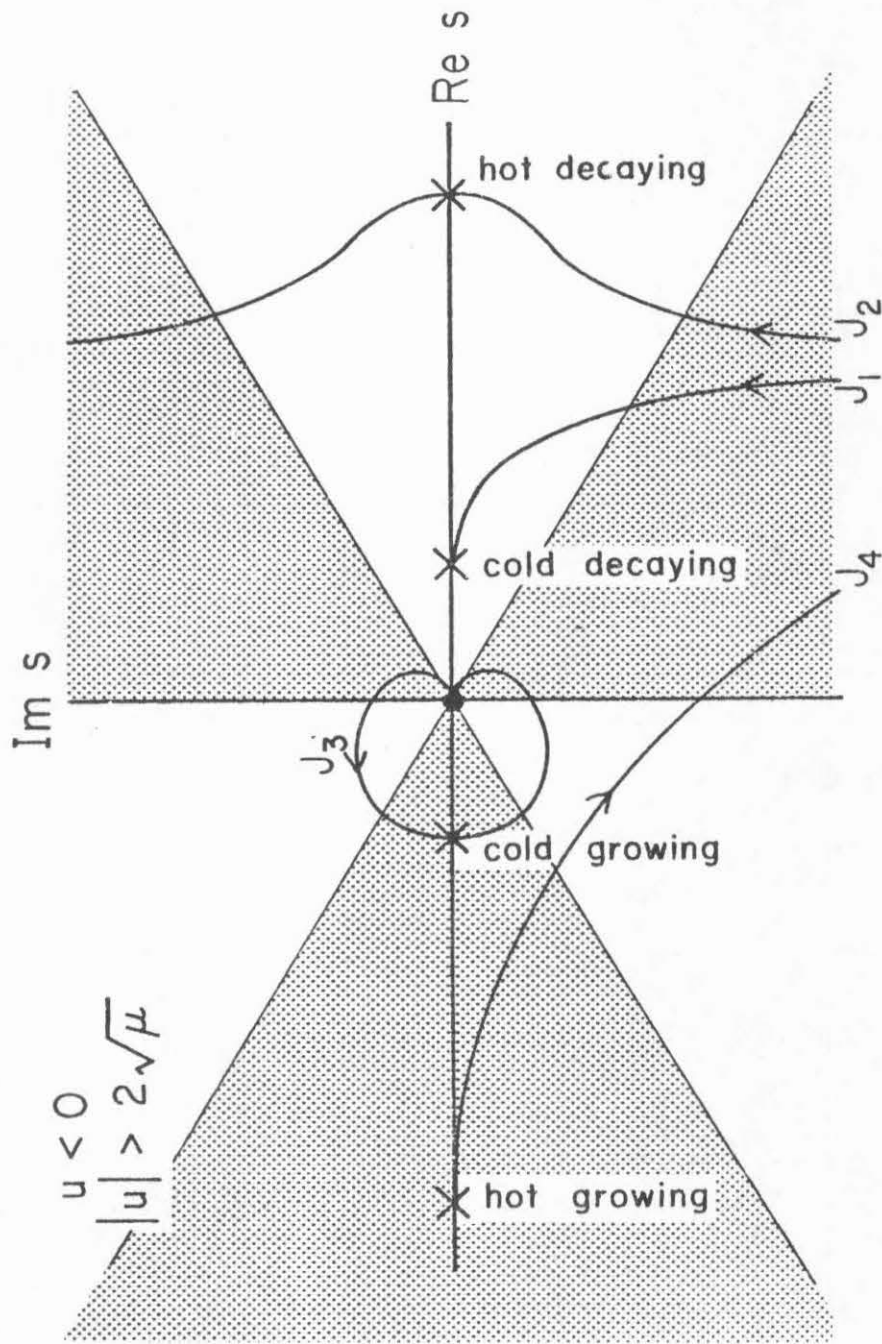


Fig. 3.4 Same as Fig. 3.3, for $u < 0$

$$2(\mu u)^{1/2} \rightarrow 2(\mu u)^{1/2} + |k_z|^3 \left\{ \frac{3V_e^2 \omega_{pe}^2}{2\sqrt{-K_{110}}} \left(\frac{\beta}{\gamma}\right)^{1/6} u^{1/2} \right. \quad (3.44a)$$

$$\left. - \left(\frac{\beta}{\gamma}\right)^{1/2} \frac{(-K_{110})^{3/2}}{3} u^{-3/2} + i \left\{ \left(\frac{u}{\mu}\right)^{1/2} \text{Im} \mu + \left(\frac{\mu}{u}\right)^{1/3} \varepsilon \right\} \right.$$

$$\frac{2}{3} u^{3/2} \rightarrow \frac{2}{3} u^{3/2} + 2\mu u^{-1/2} + i\varepsilon u^{1/2} \quad (3.44b)$$

where ε is given by Eq. (3.38). These extra terms will be left implicit in the forms given in the table.

The paths for $u > 0$ may be expressed as linear combinations of the $u < 0$ paths. Each path has been assigned a direction as indicated by the arrows in Figs. 3.3-4. Then

$$\begin{aligned} I_1 &= J_1 - J_3 + J_4 \\ I_2 &= J_2 - J_3 + J_4 \\ I_3 &= J_1 + J_4 \\ I_4 &= J_4 \end{aligned} \quad (3.45)$$

Let us write the solutions on the $u > 0$ side as

$$\tilde{\phi}(u) = \sum_i a_i I_i \quad (3.46a)$$

and on the $u < 0$ side as

$$\tilde{\phi}(u) = \sum_i b_i J_i \quad (3.46b)$$

Thus Eq. (3.46) gives the connection between the sets of coefficients a_i and b_i

$$\begin{aligned}
 a_1 &= -b_2 - b_3 & b_1 &= a_1 + a_3 \\
 a_2 &= b_2 & b_2 &= a_2 \\
 a_3 &= b_1 + b_2 + b_3 & b_3 &= a_1 - a_2 \\
 a_4 &= b_1 - b_2 + b_4 & b_4 &= a_1 + a_2 + a_2 + a_4
 \end{aligned}
 \tag{3.47}$$

This set of relations shows how the waves transform at the hybrid layer. The interpretation is summarized in Fig. 3.5 in four independent cases (solutions) which cover all possible cases.

The first case is the well known mode conversion solution considered by Stix and several subsequent authors. The other three cases may also be important in our model, hence were also obtained.

It should be noted that the problem of mode conversion at the lower hybrid is quite similar to that of the upper hybrid mode conversion problem considered by a number of authors. The upper hybrid case has a propagation X-mode on the high density side of the hybrid layer which converts $\omega_{\ell h}(x) = \omega$ at the hybrid layer into an ion Bernstein mode propagating into the low density side of the hybrid layer or vice versa. The differential equation describing it differs principally from that of Eq. (3.37) in that u and μ have a different sign, although there are other minor differences. This problem was examined by Kuehl, O'Brien and Stewart,³¹ by Tang³² and by Gorman³³, among others. Also Buchsbaum and Hasegawa³⁴ examined the problem in connection with resources set up between the hybrid layer and the boundary.

We apply these results specifically to each of the hybrid layers $x = x_{h1}$ and $x = x_{h2}$. Near $x = x_{h1}$ the $u_1 > 0$ side is region II and $u_1 < 0$ is region III. Near $x = x_{h2}$, the $u_2 < 0$ side is region V and the $u_2 > 0$

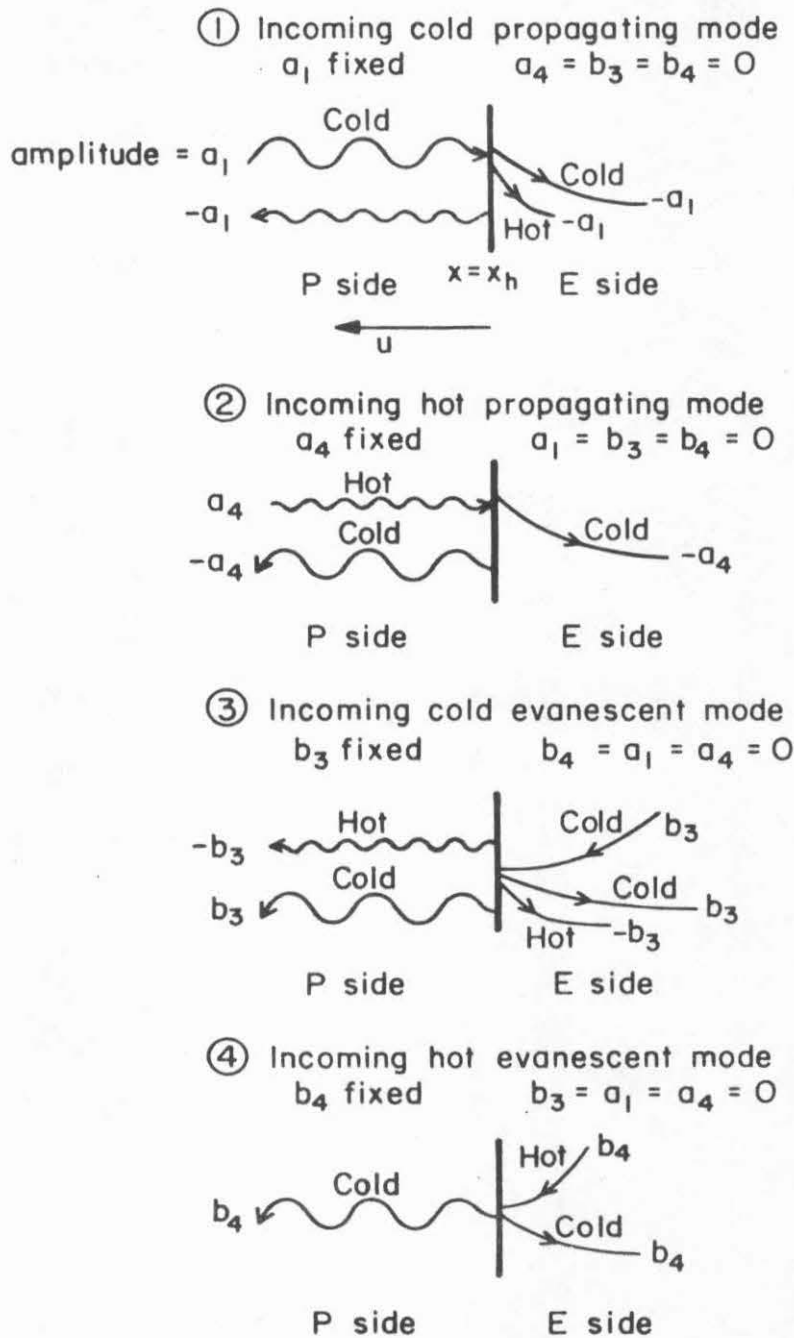


Fig. 3.5 Summary of possible mode conversion processes as four linearly independent cases (solutions)

side is region VI. We may then translate the connection of the a_i 's and b_i 's may be translated into the connection between the $a_i^{(2)}$'s and the $a_i^{(3)}$'s, and between the $a_i^{(5)}$'s and the $a_i^{(6)}$'s. (It should be noted that the convention for the i 's above is not always the same as that adopted for our solutions in each region in Table 1.)

$$\begin{aligned}
 a_1^{(3)} &= a_1^{(2)} + a_3^{(2)} & a_1^{(6)} &= a_1^{(5)} + a_3^{(5)} + a_4^{(5)} \\
 a_2^{(3)} &= a_2^{(2)} & a_2^{(6)} &= a_2^{(5)} - a_3^{(5)} - a_4^{(5)} \\
 a_3^{(3)} &= a_1^{(2)} - a_2^{(2)} & a_3^{(6)} &= a_1^{(5)} - a_4^{(5)} & (3.48) \\
 a_4^{(3)} &= a_1^{(2)} + a_2^{(2)} + a_3^{(2)} + a_4^{(2)} & a_4^{(6)} &= a_4^{(5)}
 \end{aligned}$$

We will define a set of transfer matrices $\bar{M}^{(J)}$ which connect the coefficients in adjacent regions by

$$a_i^{(J+1)} = \sum_j M_{ij}^{(J)} a_j^{(J)} \quad (3.49)$$

Thus we have found two of these matrices

$$\bar{M}_2 = \begin{bmatrix} 1 & 0 & 1 & 0 \\ 0 & 1 & 0 & 0 \\ -1 & -1 & 0 & 0 \\ 1 & 1 & 1 & 1 \end{bmatrix} \quad \bar{M}^{(5)} = \begin{bmatrix} 1 & 0 & 1 & 1 \\ 0 & 1 & -1 & -1 \\ -1 & 0 & 0 & -1 \\ 0 & 0 & 0 & 1 \end{bmatrix} \quad (3.50)$$

The solution in region II is of the form

$$\begin{aligned}
 \tilde{\Phi}^{(2)}(u) &= \tilde{\Phi}_0 \left\{ (\mu u)^{-1/4} \left[a_1^{(2)} e^{2i(\mu u_1)^{1/2}} + a_3^{(2)} \right. \right. \\
 &\quad \times e^{-2i(\mu u)^{1/2}} \left. \right] + u_1^{-3/4} \left[a_2^{(2)} e^{\frac{2i}{3} u_1^{3/2}} \right. \\
 &\quad \left. \left. + a_4^{(2)} e^{-\frac{2i}{3} u_1^{3/2}} \right] \right\} \quad (3.51)
 \end{aligned}$$

In region III,

$$\begin{aligned} \tilde{\Phi}^{(3)}(u) = & \tilde{\Phi}_0 \left\{ (\mu u_1)^{-1/4} \left[a_1^{(3)} e^{-2(-\mu u_1)^{1/2}} \right. \right. \\ & + a_3^{(3)} e^{2(-\mu u_1)^{1/2}} \left. \right] + (-u_1)^{-3/4} \\ & \times \left[a_2^{(3)} e^{-2/3(-u_1)^{3/2}} + a_4^{(3)} e^{2/3(-u_1)^{3/2}} \right] \left. \right\} \end{aligned} \quad (3.52)$$

In region V,

$$\begin{aligned} \tilde{\Phi}^{(5)}(u) = & \tilde{\Phi}_0 \left\{ (\mu u_2)^{-1/4} \left[a_1^{(3)} e^{-2(-\mu u_1)^{1/2}} + a_3^{(3)} e^{2(-\mu u_1)^{1/2}} \right] \right. \\ & \left. + (-u_1)^{-3/4} \left[a_2^{(3)} e^{-2/3(-u_1)^{3/2}} + a_4^{(3)} e^{2/3(-u_1)^{3/2}} \right] \right\} \end{aligned} \quad (3.53)$$

In region VI,

$$\begin{aligned} \tilde{\Phi}^{(6)}(u) = & \tilde{\Phi}_0 \left\{ (\mu u_2)^{-1/4} \left[a_1^{(6)} e^{-2i(\mu u_2)^{1/2}} \right. \right. \\ & + a_3^{(6)} e^{2i(\mu u_2)^{1/2}} \left. \right] + u_2^{-3/4} \left[a_2^{(6)} e^{-2i/3 u_2^{3/2}} \right. \\ & \left. + a_4^{(6)} e^{2i/3 u_2^{3/2}} \right] \left. \right\} \end{aligned} \quad (3.54)$$

3.5 Connections Between WKB and Hybrid Layer Solutions

We will expand the WKB solutions near the hybrid layers $x = x_{h1}$ and $x = x_{h2}$ and match them to the asymptotic hybrid layer solutions. This will give us the transfer matrices which relate the coefficients in each of the two regions. We will do the connections between regions I and II as an example, then summarize the transfer matrices which are the result of the connections between the rest of the regions.

Expand $g_1(x)$ and $h_1(x)$ near $x = x_{h1}$:

$$\begin{aligned}
 g_1(x) &= g_1(x_{h1}) - [-K_{110}(x_{h1})/\gamma]^{1/2} \int_x^{x_{h1}} (x_{h1}-x')^{1/2} dx' \\
 &= g_1(x_{h1}) - 2[-K_{110}(x_{h1})/\gamma]^{1/2} (x_{h1}-x)^{1/2}
 \end{aligned}
 \tag{3.55}$$

$$\begin{aligned}
 h_1(x) &= h_1(x_{h1}) - (\gamma/\beta)^{1/2} \int_x^{x_{h1}} (x_{h1}-x')^{1/2} dx' \\
 &= h_1(x_{h1}) - \frac{2}{3} (\gamma/\beta)^{1/2} (x_{h1}-x)^{3/2}
 \end{aligned}$$

Similarly expanding A(x) and B(x):

$$A(x) \cong \left[\frac{K_{110}(0) K_{10}(0)}{K_{110}(x_{h1}) \gamma} \right]^{1/4} (x_{h1}-x)^{-1/4}
 \tag{3.56}$$

$$B(x) \cong \left[\frac{-K_{110}(0) K_{10}(0) \beta(x_{h1})}{\gamma^3} \right] (x_{h1}-x)^{-3/4}$$

One can see that when Eqs. (3.55) and (3.56) are substituted into Eq.

(3.17) for $\tilde{\phi}^{(i)}(x, k_z)$, one gets the same functional form as Eq. (3.51) for $\tilde{\phi}^{(ii)}(x, k_z)$, where $u_1^{3/2} = (\gamma/\beta)^{1/2} (x_{h1} - x)^{3/2}$ and

$$(\mu u_1)^{1/2} = |k_z| \sqrt{-K_{11}} (x_{h1} - x)^{1/2} / \gamma$$

Thus the two solutions overlap in a common region, and we have the relation between the coefficients:

$$\begin{aligned}
 a_1^{(2)} &= Ce^{-i|k_z|g_1(x_{h1})} a_1^{(1)} \\
 a_2^{(2)} &= iCe^{-ih_1(x_{h1})} a_2^{(1)} \\
 a_3^{(2)} &= iCe^{i|k_z|g_1(x_{h1})} a_3^{(1)} \\
 a_4^{(2)} &= Ce^{ih_1(x_{h1})} a_4^{(1)}
 \end{aligned}
 \tag{3.57}$$

where

$$c = \left(\frac{k_z}{\gamma} \right)^{1/2} \left[K_{\parallel 0}(0) K_{\perp 0}(0) \right]^{1/4}
 \tag{3.58}$$

The connection between the other regions is similar, and gives the rest of the set of transfer matrices we are seeking. We will introduce a shorthand notation for the exponentials that arise in the coefficients and the transfer matrices that are summarized, along with the physical importance of the quantities, in the following table:

Symbol	Definition	Physical Significance
U	$ k_z g_1(x_{h1})$	Phase of cold wave from 0 to x_{h1}
V	$h_1(x_{h1})$	Phase of warm wave from 0 to x_{h1}
P	$ k_z G(x_{h2})$	Exponent of cold wave from x_{h1} to x_{h2}
Q	$H(x_{h2})$	Exponent of warm wave from x_{h1} to x_{h2}
W	$ k_z g_2(x_{h2})$	Phase of cold wave from x_{h1} to x_{h2}
Y	$h_2(x_{h2})$	Phase of warm wave from x_{h1} to x_{h2}

Table 4. Definition of symbols for phase and exponent factors.

The set of transfer matrices obtained by the WKB to hybrid layer solutions connections are [recall the definition in Eq. (48)]:

$$\bar{M}^{(1)} = c \begin{bmatrix} e^{iU} & 0 & 0 & 0 \\ 0 & ie^{-iV} & 0 & 0 \\ 0 & 0 & ie^{iU} & 0 \\ 0 & 0 & 0 & e^{iV} \end{bmatrix} \quad (3.58a)$$

$$\bar{M}^{(3)} = ic^{-1} \begin{bmatrix} 1 & 0 & 0 & 0 \\ 0 & -i & 0 & 0 \\ 0 & 0 & i & 0 \\ 0 & 0 & 0 & -1 \end{bmatrix} \quad (3.58b)$$

$$\bar{M}^{(4)} = c \begin{bmatrix} e^{-P} & 0 & 0 & 0 \\ 0 & -e^{-Q} & 0 & 0 \\ 0 & 0 & ie^P & 0 \\ 0 & 0 & 0 & ie^Q \end{bmatrix} \quad (3.58c)$$

$$\bar{M}^{(6)} = ic^{-1} \begin{bmatrix} 1 & 0 & 0 & 0 \\ 0 & i & 0 & 0 \\ 0 & 0 & i & 0 \\ 0 & 0 & 0 & 1 \end{bmatrix} \quad (3.58d)$$

These matrices, when combined with the boundary conditions, give a sufficient set of equations to solve for the coefficients.

3.6 Calculation of Coefficients

To aid in the calculation of the coefficients, we will use two approximations which should be valid for almost all cases of interest. These approximations involve the ion thermal mode in the evanescent layer and near the boundary. First, the ion thermal mode in the evanescent layer decays much more rapidly than the X-mode, so that in the asymptotic region $u \gg 2\sqrt{\mu}$ we have

$$u^{-3/4} e^{-\frac{2}{3}(-u)^{3/2}} \ll (\mu u)^{-1/4} e^{-2(-\mu u)^{1/2}} \quad (3.60)$$

i.e., the magnitude of the ion thermal mode is negligible compared to the X-mode. In fact, the size of this mode is on the order of the error in the use of the saddle point method to get the asymptotic form of the X-mode in the evanescent layer, as can be seen from the contours for those two modes in Fig. 3.4. J_1 can be deformed in addition to the deformation over saddle point s_1 shown, into the path shown in Fig. 8. The latter deformation picks up contributions from both s_1 and s_2 . Since either deformation gives an approximate form of the asymptotic X-mode solution and since the two forms differ by the contribution of saddle point s_2 , which is just equal to the ion thermal mode and much less than the contribution from saddle point s_1 , then there is an ambiguity or error in the asymptotic form of the X-mode which is on the order of the asymptotic ion thermal mode magnitude. Thus, we will neglect the decaying ion thermal mode compared to the decaying X-mode in the evanescent region.

Secondly, the amplitude of the ion thermal modes near the boundary should be very small compared to the X-mode amplitude. This is because a source designed to couple to an X-mode will couple very inefficiently to

the ion thermal mode, so that there is no substantial excitation of this mode by the source. Thus, the mode can only be excited when the X-mode couples to it near the lower hybrid layer. But the excited outgoing mode thus produced is very highly damped, decaying away over a very short distance, so that for a hybrid layer deep in the center of the plasma, this mode will have died away to a very small amplitude by the time it reaches the boundaries. (The damping of this mode will be studied later.)

To see why these facts are so, consider first the coupling at the source. For a given $E_z(x, k_z)$, the value of $E_x(x, k_z)$ of the ion thermal mode is given by [see Eq. (3.17)]

$$E_x(x, k_z) = \frac{1}{|k_z|} \left[\frac{K_{\perp}(x)}{\beta(x)} \right]^{1/2} E_z(x, k_z) \gg E_z(x, k_z) \quad (3.61a)$$

whereas for the X-mode this is

$$E_x(x, k_z) = \left[\frac{-K_{\parallel}}{K_{\perp}} \right]^{1/2} E_z(x, k_z) \quad (3.61b)$$

Thus if the source is in the vacuum, $\beta(x) \rightarrow 0$ and if the ion thermal mode is to exist, it must have $E_z(0, k_z) = 0$ in order for $E_x(0, k_z)$ to be finite, and the source cannot excite this mode at all. In fact, this mode has $\lambda = 0$ in the vacuum, so no source can couple to it there. Even if the source is in a low non-zero density region, the amount of this mode excited will be very small, since E_x is so much larger than E_z at the source for this mode, while the field produced by the source will have $E_x \sim E_z$, which is the case for X-mode, and D_x and E_z are continuous at the source.

Next, consider the ion thermal mode coming out of the $x = x_{n1}$

lower hybrid layer. The decay factor of the wave may be given by $e^{-\Gamma}$ where

$$\Gamma(x) \approx \text{Im} [h_1(x_{h1}) - h(x)] = \frac{1}{2} \int_x^{x_{h1}} \frac{\text{Im} K(x') dx'}{[\beta(x') K_{\perp 0}(x')]^{1/2}} \quad (3.62)$$

[from Eq. (3.20)]. $\text{Im} K_{\perp}(x, k_z)$ is given by Eq. (1.19), and includes contribution from ion collisional and ion cyclotron damping. The latter gets quite large as the ion thermal mode propagates away from the lower hybrid layer. Consider for simplicity only ion collisional damping, so $\text{Im} K_{\perp 0} = \nu \omega_{pi}^2(x) / \omega^3$. Let

$$\beta(x) = \frac{3}{2} \frac{v_i^2 \omega_{pi}^2(x)}{\omega^4} + \frac{v_e^2 \omega_{pe}^2(x)}{\omega_{ce}^4} \equiv \frac{\alpha_0 v_i^2 \omega_{pi}^2(x)}{\omega^4}$$

where α_0 is a constant of order one. Then

$$\Gamma(x) \sim \int_x^{x_h} \frac{\nu \omega_{pi}(x') dx'}{v_i [\omega^2 - \omega_{pi}^2(x')]^{1/2}} \sim \int_x^{x_h} \frac{\nu dx'}{\lambda_{Di}(x') [\omega^2 - \omega_{pi}^2(x')]^{1/2}} \quad (3.63)$$

Evaluating this, for example, for a linear density profile for $x = 0$ gives

$$\Gamma(0) \sim \frac{\nu x_h}{v_i} \quad (3.64)$$

and $\Gamma(0) \gg 1$, i.e., the ion thermal wave has virtually all decayed away by the time it reaches the boundary, if $x_h \gg v_i/\nu$. This is satisfied in typical collisional plasmas, for example, if $\nu = 0.1\omega$. For less collisional plasmas, cyclotron damping, which gives an important contribution to the decay of this wave, will be responsible for much of the absorption.

The approximations on the ion thermal mode at the boundary means

the boundary conditions only effect the X-mode, and so the usual boundary conditions of electromagnetic theory are sufficient to determine the fields. (If the ion thermal mode were important at the boundary, then we would need one more boundary condition in addition to the electromagnetic ones.) Thus the boundary conditions on $\tilde{\phi}(x, k_z)$ are

$$\begin{aligned} \tilde{\phi}(0, k_z) &= 1 \\ \tilde{\phi}(a, k_z) &\approx \frac{a_1^{(7)} e^{-i|k_z|g_2(a)} + a_3^{(7)} e^{i|k_z|g_2(a)}}{1 + a_3^{(1)}} \end{aligned} \quad (3.65)$$

so

$$a_3^{(7)} = -a_1^{(7)} e^{-2iW} \quad (3.66)$$

The relation between the coefficients in region I and those of region VII is

$$\bar{a}^{(7)} = \bar{M}^{(6)} \bar{M}^{(5)} \bar{M}^{(4)} \bar{M}^{(3)} \bar{M}^{(2)} \bar{M}^{(1)} \bar{a}^{(1)} \quad (3.67)$$

The product matrix

$$\bar{T} = \bar{M}^{(6)} \bar{M}^{(5)} \bar{M}^{(4)} \bar{M}^{(3)} \bar{M}^{(2)} \bar{M}^{(1)} \quad (3.68)$$

is given in Table 5. It should be noted that many cancellations in the matrix multiplication cause this matrix to reduce down to a relatively simple form. This illustrates the usefulness and efficiency of the coefficient transfer matrices in solving for the coefficients.

$-e^{-iU}(e^{-P}+e^P+e^Q)$	$-e^{-iV}(e^{-+e^Q})$	$-ie^{-iU}(e^{-P}+e^Q)$	ie^{iV+Q}
$-e^{-iU}(e^P+e^Q)$	$-e^{-iV}(e^{-Q}+e^P+e^Q)$	$-ie^{iU+Q}$	ie^{iV+Q}
$ie^{-iU}(e^{-P}+e^Q)$	ie^{-iV+Q}	$-ie^{iU}(e^Q+e^{-P})$	e^{iV+Q}
$-ie^{-iU+Q}$	$-ie^{-iV+Q}$	e^{iU+Q}	$-e^{iV+Q}$

Table 5. The product matrix \bar{T} given by Eq. (3.68).

Our assumption about the ion thermal mode near the boundary and in in evanescent layer can be summarized as

$$\begin{aligned}
 e^{-Q} &\ll e^{-P} < 1 \\
 |e^{+iV}| &\ll 1 \\
 |e^{+iY}| &\ll 1
 \end{aligned}
 \tag{3.69}$$

where it is the large imaginary part of V and Y that give the last two relations. We want relations between $\bar{a}^{(1)}$ and $\bar{a}^{(7)}$, which take the form

$$\bar{a}^{(1)} = \begin{bmatrix} 1 \\ a_2^{(1)} \\ a_3^{(1)} \\ \sim 0 \end{bmatrix} \quad \bar{a}^{(7)} = \begin{bmatrix} a_1^{(7)} \\ \sim 0 \\ -a_1^{(7)}e^{-2iW} \\ a_4^{(7)} \end{bmatrix}
 \tag{3.70}$$

The terms $a_4^{(1)}$ and $a_2^{(7)}$, which represent the ion thermal mode reflected off of the boundaries and which were assumed to be small, are set to 0 because their inclusion would give rise to terms in the Eqs. (3.67) con-

necting $\bar{a}^{(1)}$ and $\bar{a}^{(7)}$ which are (e^{2iV}) and (e^{2iY}) smaller than the other terms in these equations, and thus are ignorable by Eq. (3.69).

The solution to the set of linear equations obtained by substituting Eq. (3.70) into (3.67) after neglecting terms that are negligible according to Eq. (3.69) are

$$\begin{aligned}
 a_2^{(1)} &= e^{i(V-U)}/D \\
 a_3^{(1)} &= ie^{-2iU}(1+ie^{-2iW})/D \\
 a_1^{(7)} &= -ie^{-iU-P}/D \\
 a_3^{(7)} &= e^{-iU-2iW}/D \\
 a_4^{(7)} &= ie^{-iU-P}(1+ie^{-2iW})/D
 \end{aligned} \tag{3.71}$$

where

$$D = 1 = e^{-2P}(1+ie^{-2iW}) \tag{3.72}$$

We can summarize the seven sets of coefficients obtained from Eqs. (3.49 , (3.50), and (3.59) for the transfer matrices.

$$\bar{a}^{(1)} = D^{-1} \begin{bmatrix} D \\ -e^{i(V-U)} \\ ie^{-2iU-2P}(1+ie^{-2iW}) \\ 0 \end{bmatrix} \tag{3.73a}$$

$$\bar{a}(2) = \left(\frac{|k_z|}{\gamma}\right)^{1/2} \frac{[K_{110}(0)K_{\perp}(0)]^{1/4}}{D} \begin{bmatrix} De^{-iU} \\ -e^{-iU} \\ ie^{-iU-2P}(1+ie^{-2iW}) \\ \sim 0 \end{bmatrix} \quad (3.73b)$$

$$\bar{a}(3) = \left(\frac{|k_z|}{\gamma}\right)^{1/2} \frac{[K_{110}(0)K_{\perp}(0)]^{1/4}}{D} \begin{bmatrix} e^{-iU} \\ -e^{-iU} \\ -e^{-2P}(1+ie^{-2iW})e^{-iU} \\ e^{-P}(1+ie^{-2iW}) \end{bmatrix} \quad (3.73c)$$

$$\bar{a}(4) = \frac{e^{-iU - \frac{\pi i}{4}}}{D} \begin{bmatrix} -i \\ 1 \\ -e^{-2P}(1+ie^{-2iW}) \\ -e^{-P-Q}(1+ie^{-2iW}) \end{bmatrix} \quad (3.73d)$$

$$\bar{a}^{(5)} = \left(\frac{|k_z|}{\gamma}\right)^{1/2} \frac{[K_{110}(0)K_{10}(0)]^{1/4}}{D} \begin{bmatrix} -ie^{-P} \\ -ie^{-Q} \\ -ie^{-P}(1+ie^{-2iW}) \\ e^{-P}(1+ie^{-2iW}) \end{bmatrix} \quad (3.73e)$$

$$\bar{a}^{(6)} = \left(\frac{|k_z|}{\gamma}\right)^{1/2} \frac{[K_{110}(0)K_{10}(0)]^{1/4} e^{-iU}}{D} \begin{bmatrix} -e^{-P} \\ \sim 0 \\ -e^{-P} - 2iW \\ e^{-P}(1+ie^{-2iW}) \end{bmatrix} \quad (3.73f)$$

$$\bar{a}^{(7)} = \frac{e^{-iU}}{D} \begin{bmatrix} -e^{-P} \\ \sim 0 \\ -e^{-P} - 2iW \\ ie^{-P}(1+ie^{-2iW}) \end{bmatrix} \quad (3.73g)$$

Using this set of coefficients in the expressions for $\tilde{\phi}$ in each region, we have the solutions in k_z -space. By doing the Fourier transform into configuration space, we will have the desired solution as a function of x and z .

3.7 Expansion into Resonance Cone Form

To expand in the resonance cone form when doing the Fourier transform, note that the denominator of the solution in each region can be found by looking at the factor common to each solution

$$\tilde{\phi}_0 \sim [a_1^{(1)} + a_3^{(1)}]^{-1} = \frac{D}{[1 + e^{-2P} (1 + ie^{-2iU})(1 + ie^{-2iW})]} \quad (3.74)$$

The D factor here cancels the same in the denominator of the coefficients, so that the denominator of $\tilde{\phi}$ just becomes for all regions

$$\tilde{\phi} \sim [1 + e^{-2P} (1 + ie^{-2iU})(1 + ie^{-2iW})]^{-1} \quad (3.75)$$

Now, to get $\tilde{\phi}$ in the form of a sum of guided wave modes, we would utilize the poles in $\tilde{\phi}$, which are the solutions of a set of transcendental equations, and can only be found numerically. However, one can get the solutions analytically in a more physically useful form by expanding the denominator

$$\begin{aligned} \tilde{\phi} &\sim \sum_{n=0}^{\infty} (-1)^n e^{-2nP} (1 + ie^{-2iU})^n (1 + ie^{-2iW})^n \\ &= 1 - e^{-2P} (1 + ie^{-2iU} + ie^{-2iW} - e^{-2iU-2iW}) + \mathcal{O}(e^{-4P}) \end{aligned} \quad (3.76)$$

As we shall see, the e^{-2P} terms give rise to cones which have tunneled through the evanescent layer twice, and in general the e^{-2nP} terms involve cones which have tunneled $2n$ times. These factors ensure very rapid convergence of the sum in Eq. (3.76), and as indicated we will presently ignore all terms for $n \geq 2$, since they are negligible for all but very thin evanescent layers.

It is interesting to note that for values of k_z such that

$$U = |k_z|g_1(x_{h1}) = -\pi/2 + 2n\pi \quad (3.77a)$$

$$W = |k_z|g_2(a) = -\pi/2 + 2n\pi$$

where n is any positive integer, the denominator in Eq. (3.75) is one, so that there is no tunnelling of the wave component with that $|k_z|$. Under our symmetric density profile assumption $g_1(x_{h1}) = g_2(a)$, so that both forms express the same condition. Similarly, there are values of $|k_z|$ for which the tunnelling is maximum, namely

$$U = W = 2n\pi \quad (3.77b)$$

The latter is the case of optimum impedance matching at the hybrid layer, while the former represents optimum impedance mismatch. The conditions given in Eq. (3.77) are fulfilled only if the imaginary part of g_1 and g_2 , containing the damping is neglected. The presence of damping in those quantities means there is no perfect matching or mismatch, and that some small portion of the wave tunnels through for all k_z , but if one is working with a source that excites a single k_z , that k_z may be chosen for maximum or minimum tunnelling by choosing the real part of g_1 and g_2 to satisfy either Eq. (3.77a) or (3.77b) as is appropriate.

With the expansion in Eq. (3.76) one can evaluate the inverse Fourier transform to get the solutions of ϕ as a sum of resonance cones. We need first to discuss the resonance cone forms and to introduce a more convenient notation before writing out these solutions. The X-mode cones

cones take the form

$$\phi_c \sim [3q(x)]^{-1/3} F \left\{ \frac{\pm z - g(x)}{[3q(x)]^{1/3}} \right\} \quad (3.78)$$

where $F(\zeta) = Ai(\zeta) - iGi(\zeta)$ is a combination of the homogeneous and inhomogeneous Airy functions, and $q(x)$ represents the thermal correction to $g(x)$. The upper sign gives the $z > 0$ cones, and the lower sign the $z < 0$ cone. The integral form of $F(\zeta)$ is¹⁸

$$F(\zeta) = \frac{1}{\pi} \int_0^{\infty} e^{-i[\zeta v + \frac{v^3}{3}]} dv \quad (3.79)$$

A graph of $|F(\zeta)|$ is shown in Fig. 3.7, which illustrates the cross section of the X-mode resonance cone for a warm plasma. The argument of F is zero for $\pm z = \text{Re } g(x)$, which describes the curve along which the cone is singular in cold plasma theory, i.e., when $q(x) \rightarrow 0$.

Similarly, the ion thermal cone takes the form

$$\phi_c \sim \frac{e^{i[h(x_h) - h(x)] - i[g(x_h) \mp z]^2 / 8 s(x)}}{2[2\pi i s(x)]^{1/2}} \times D_{-1/2} \left[\frac{\pm z - g(x_h)}{\sqrt{2i s(x)}} \right] \quad (3.80)$$

where x_h is the hybrid layer from which the ion thermal cone originates, $g(x_h)$ is the phase of the X-mode cone producing it, $s(x)$ is the thermal correction to $h(x_h) - h(x)$, and $D_{-1/2}(\zeta)$ is the Whittaker's function equal to the parabolic cylinder function normally denoted $U(0, \zeta)$.^{20,24}

The parabolic cylinder functions are defined by the integral form

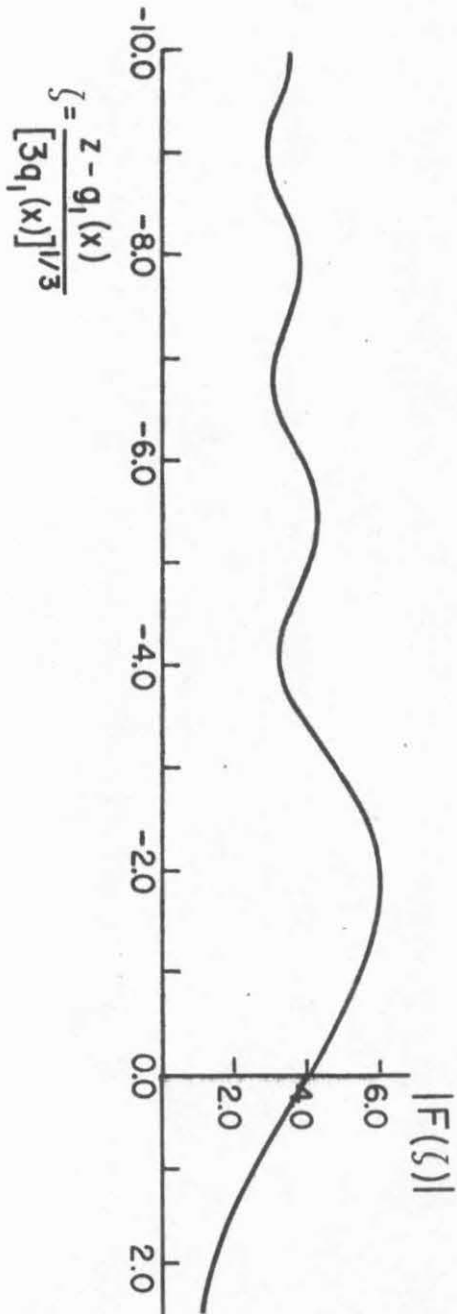


Fig. 3.7 Cross-sectional structure of the X-mode cone (as in Fig. 2.3)

$$U(a, \zeta) = \frac{e^{-\zeta^2/4}}{\Gamma(a + \frac{1}{2})} \int_0^\infty e^{-\zeta s - s^2/2} s^{a - \frac{1}{2}} ds \quad (3.81)$$

A graph of $D_{-1/2}(\zeta)$ is shown in Fig. 3.8 which illustrates the cross section of the cone structure of the thermal cone. The structure of this cone was first obtained by K. Ko and H. Kuehl.²⁰ (We are obtaining a more general form; as we will see, evanescent layers and damping will cause the argument of the Whittaker's function to be complex, and this more general form will describe all the ion thermal cones, and not just the one coming from direct mode conversion of the source wave.) The argument of this function is zero along $z = \text{Re } g(x_h)$, which describes the line along which the cone is singular in the lowest order ("cold plasma") theory, i.e., for $p(x) \rightarrow 0$. In that limit the cone moves along a constant z , or perpendicular to the magnetic field.

Combine the $z > 0$ cone and the $z < 0$ cone into a single term by

$$\begin{aligned} \mathcal{F}[z, g(x), q(x)] &= [3q(x)]^{-1/3} \\ &\times \left\{ F\left[\frac{z - g(x)}{[3q(x)]^{1/3}}\right] + F\left[\frac{z + g(x)}{[3q(x)]^{1/3}}\right] \right\} \\ \mathcal{D}[z, g(x), s(x)] &= [8\pi i s(x)]^{-1/2} \\ &\times \left\{ e^{-i[z - g(x)]^2/8s(x)} D_{-1/2}\left[\frac{z - g(x)}{\sqrt{2is(x)}}\right] \right. \\ &\left. + e^{-i[z + g(x)]^2/8s(x)} D_{-1/2}\left[\frac{z + g(x)}{\sqrt{2is(x)}}\right] \right\} \end{aligned} \quad (3.82)$$

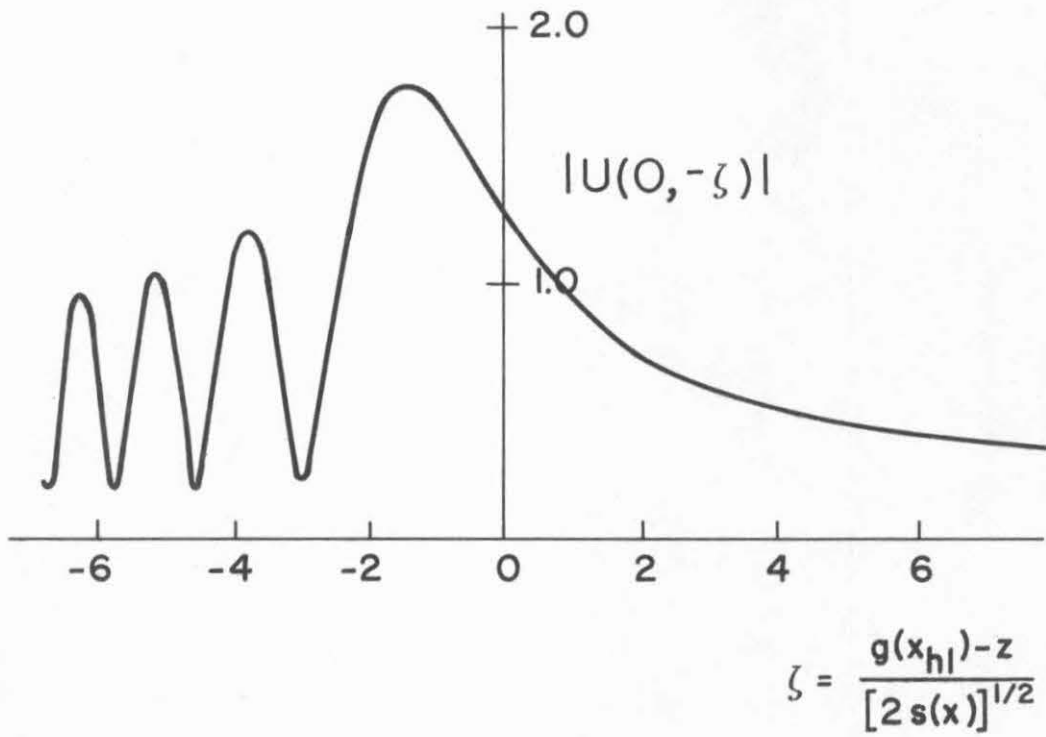


Fig. 3.8 Cross-sectional structure of the ion thermal cone²⁰

Since there is practically no overlap of the $z < 0$ and $z > 0$ cones, we may take the \mathcal{D} 's and the \mathcal{F} 's to be equal to the $z < 0$ cones in $z < 0$, and the $z > 0$ cones in $z > 0$. Note that $q(x)$ is completely determined when $g(x)$ is specified, so that the q 's will normally be suppressed, since they are already implicitly known.

With this notation we can write $\phi(x, z)$ in its resonance cone form. The regions whose solutions are of most interest are regions I and VII. To first order these are:

$$\begin{aligned}
 \phi^{(1)}(x, z) = & \frac{A(x)}{2} \left\{ \mathcal{F}[z, g(x)] + i \mathcal{F}[z, -g_1(x)] \right. \\
 & + 2g_1(x_{h1}) - 2i \mathcal{D}(x_{h2}) \left. \right] - \mathcal{F}[z, -g_1(x) + 2g_1(x_{h1}) \\
 & + 2g_2(\omega) - 2i \mathcal{D}(x_{h2}) \left. \right] - i \mathcal{F}[z, g_1(x) + 2g_1(x_{h1}) \\
 & - 2i \mathcal{D}(x_{h2}) \left. \right] + \mathcal{F}[z, g_1(x) + 2g_1(x_{h1}) + 2g_2(\omega) \\
 & - 2i \mathcal{D}(x_{h2}) \left. \right] \left. \right\} \\
 & - \frac{B(x)}{2} e^{i[h(x_{h1}) - h(x)]} \left\{ \mathcal{D}[z, g_1(x_{h1}), p(x_{h1}) - p(x)] \right. \\
 & - \mathcal{D}[z, g_1(x) - 2i \mathcal{D}(x_{h2}), p(x_{h1}) - p(x)] \\
 & - i \mathcal{D}[z, 3g_1(x_{h1}) - 2i \mathcal{D}(x_{h2}), p(x_{h1}) - p(x)] \\
 & - i \mathcal{D}[z, g_1(x_{h1}) + 2g_2(\omega) - 2i \mathcal{D}(x_{h2}), p(x_{h1}) - p(x)] \\
 & + \mathcal{D}[z, 3g_1(x_{h1}) + 2g_2(\omega) - 2i \mathcal{D}(x_{h2}), p(x_{h1}) - p(x)] \left. \right\} \\
 & + \dots
 \end{aligned} \tag{3.83}$$

$$\begin{aligned}
 \phi^{(7)}(x, z) = & -\frac{A(x)}{2} \left\{ \mathcal{F} [z, g_2(a) + g_1(x_{h1}) - i\mathcal{D}(x_{h2})] \right. \\
 & + \mathcal{F} [z, -g_2(a) + g_1(x_{h1}) + 2g_2(a) - i\mathcal{D}(x_{h2})] \\
 & + 8 \text{ terms involving } 3i\mathcal{D}(x_{h1}) + \dots \left. \right\} \quad (3.84) \\
 & + \frac{B(x)}{2} e^{i h_2(x)} \left\{ \mathcal{D} [z, g_1(x_{h1}) - i\mathcal{D}(x_{h2}), p_2(x)] \right. \\
 & + i \mathcal{D} [z, g_2(x_{h2}) + 2g_2(a) - i\mathcal{D}(x_{h1}), p_2(x)] \\
 & + 8 \text{ terms involving } 3i\mathcal{D}(x_{h2}) + \dots \left. \right\}
 \end{aligned}$$

The solution in region I contains terms representing cones coming directly from the source and terms with $-2i\mathcal{D}(x_{h2})$ in the argument which represent cones that have tunneled through the central evanescent layer to the other side, been reflected and tunneled back. Higher order terms involve four or more tunnelling through the evanescent layer and were neglected. The solution in region VII contains the cones that have tunneled directly through from the source side, and cones involving three or more tunnelling, which are ignored.

We can give a physical interpretation to each cone term that appears in $\phi^{(1)}$ and $\phi^{(7)}$, which will be done with the aid of a schematic diagram scheme. We will use lines to indicate propagating cones and dots to indicate "scattering points", i.e., the boundaries and lower hybrid layers at which the waves can reflect or transform. The symbols to be used in the diagrams are summarized in the following table:

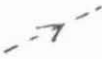
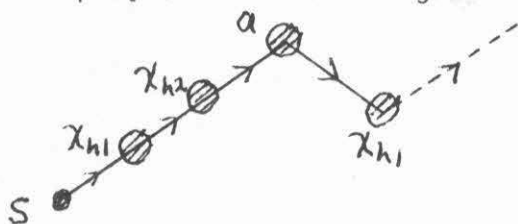
Symbol	Meaning
	X-mode cone with \vec{v}_g in x-direction
	X-mode cone with \vec{v}_g in -x direction
	Ion thermal cone with \vec{v}_g in x direction
	Ion thermal cone with \vec{v}_g in -x direction
s ●	The source, used to indicate origin of all the cones
0 ⊙	The $x = 0$ boundary "scattering point"
x_{h1} ⊙	The $x = x_{h1}$ layer
x_{h2} ⊙	The $x = x_{h2}$ layer
a ⊙	The $x = a$ boundary

Table 6. Symbols to be used in the schematic diagrams for the resonance cones.

As an example, consider the diagram



This represents a warm plasma cone which travelled from the source all of the way to the $x = a$ boundary in the X-mode, reflected at the $x = a$ boundary back to the $x = x_{h2}$ hybrid layer, and mode converted into an ion thermal cone propagating back toward the $x = a$ boundary.

Each cone term in the ϕ 's can be represented by a diagram in the way just introduced. We thus summarize the solutions ϕ_I and ϕ_{VII} in terms of the interpretative diagrams identifying the physical origin of each cone term. These are given in Tables 6 and 7. It should be noticed that these solutions can be almost trivially generalized to include other cones that we have neglected by our approximations, by just writing out the diagrams that would appear according to the transformation rules at the hybrid layer given in Fig. 3.5. Thus, for example, the ion thermal mode that tunnels through the evanescent layer would give rise to extra X-mode cones in regions I and VII, and we could write down the functional form that each one of these cone terms contributes to $\phi^{(1)}$ and $\phi^{(7)}$. Similarly, if we assumed simple perfect reflection of the ion thermal cone at the boundary, we could write down the cone terms resulting from this reflection.

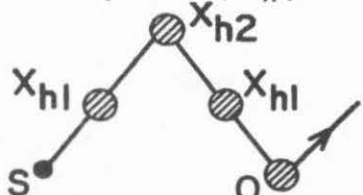
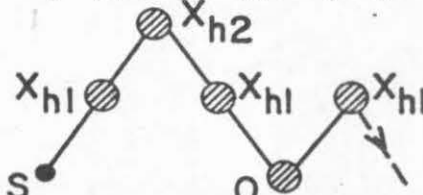
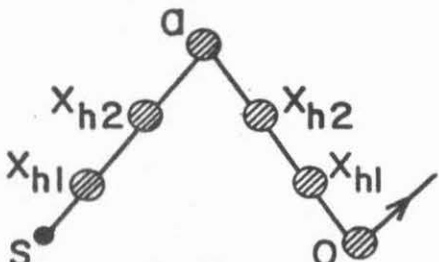
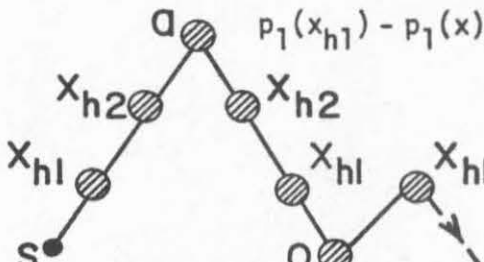
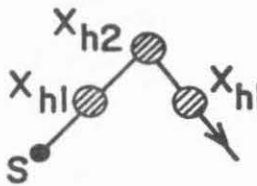
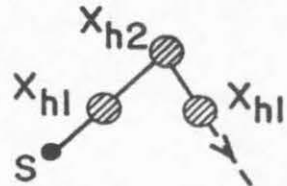
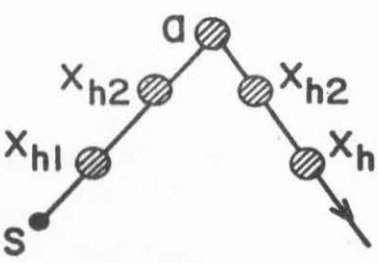
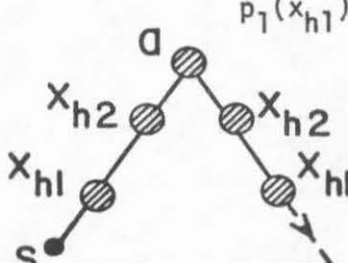
X-MODE CONES	ION THERMAL CONES
$\mathcal{F}[z, g_1(x)]$ 	$\mathcal{D}[z, g_1(x_{h1}), p(x_{h1}) - p(x)]$ 
$\mathcal{F}[z, g_1(x) + 2g_1(x_{h1}) - 2ig(x_{h2})]$ 	$\mathcal{D}[z, 3g_1(x_{h1}) - 2ig(x_{h1}), p_1(x_h) - p_1(x)]$ 
$\mathcal{F}[z, g_1(x) + 2g_1(x_{h1}) + 2g_2(z) - 2ig(x_{h2})]$ 	$\mathcal{D}[z, 3g_1(x_{h1}) + 2g_2(a) - 2ig(x_{h2}), p_1(x_{h1}) - p_1(x)]$ 
$\mathcal{F}[z, -g_1(x) + 2g_1(x_{h1}) - 2ig(x_{h2})]$ 	$\mathcal{D}[z, g_1(x_{h1}) - 2ig(x_{h2}), p_1(x_{h1}) - p_1(x)]$ 
$\mathcal{F}[z, -g_1(x) + 2g_1(x_{h1}) + 2g_2(a) - 2ig(x_{h2})]$ 	$\mathcal{D}[z, g_1(x_{h1}) + 2g_2(a) - 2ig(x_{h2}), p_1(x_{h1}) - p_1(x)]$ 

Table 7. Diagrammatic representation of the cone terms whose sum gives $\phi^{(1)}(x, z)$ to first order

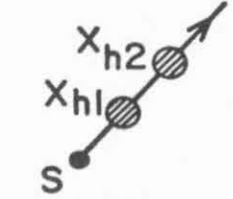
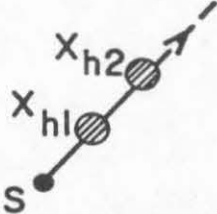
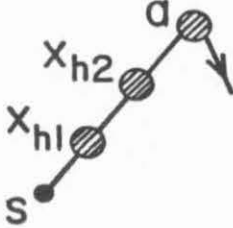
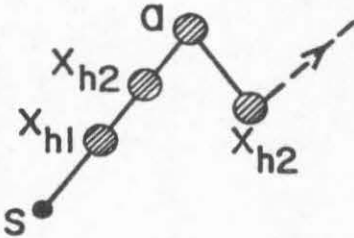
X-MODE CONES	ION THERMAL CONES
$\mathcal{F}[z, g_2(x) + g_1(x_{h1}) - i g(x_{h2})]$ 	$\mathcal{D}[z, g_1(x_{h1}) - i g(x_{h2}), p_2(x)]$ 
$\mathcal{F}[z, -g_2(x) + g_1(x_{h1}) + 2g_2(a) - i g(x_{h2})]$ 	$\mathcal{D}[z, g_1(x_{h1}) + 2g_2(a) - i g(x_{h2}), p_2(x)]$ 

Table 8 Diagrammatic representation of the cone terms whose sum gives $\phi^{(7)}(x, z)$ to lowest order

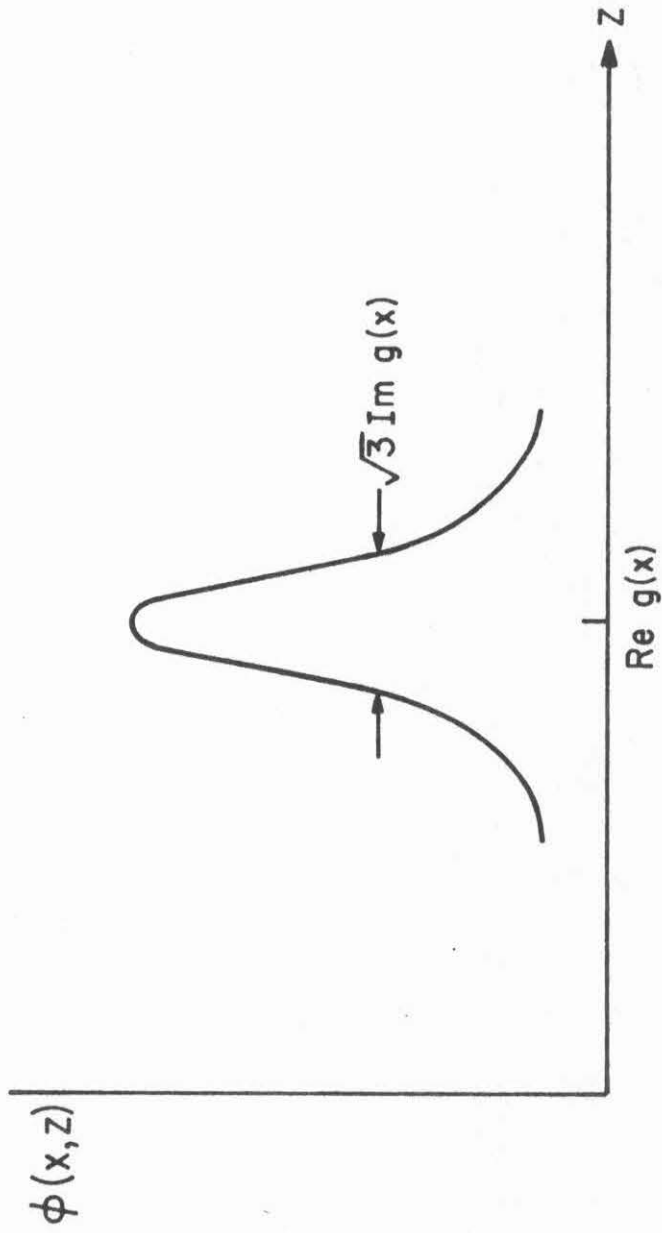


Fig. 3.9 Cross-section of X-mode cone in cold plasma limit with damping, or after passage through evanescent layer

3. Discussion and Illustration of Resonance Cone Solutions

To study and illustrate the cone solutions, we want to first identify the "cold plasma" or singular cone trajectories. This may be done by ignoring the first order thermal corrections to the phase of the waves in k_z space. This gives an idealized (non-physical) approximation to the physical (finite) fields which is useful for very low temperatures. This may be done by letting

$$\begin{aligned}
 q_1(x) &\rightarrow 0 & p_1(x) &\rightarrow 0 \\
 Q(x) &\rightarrow 0 & \underline{p}(x) &\rightarrow 0 \\
 q_2(x) &\rightarrow 0 & p_2(x) &\rightarrow 0
 \end{aligned}
 \tag{3.85}$$

This is like a zero temperature limit of the cones, but not rigorously so, since in a rigorous limit the ion thermal mode is not present; in the zero temperature limit its wavelength $\lambda \rightarrow 0$.

In this limit, the general form of the X mode cones becomes

$$\mathcal{F} \left[z, g(x) + 2ni \mathcal{Y}(xh_2) \right] \rightarrow$$

$$\begin{aligned}
 & - \frac{i}{z - g(x) - 2ni \mathcal{Y}(xh_2)} \\
 & - \frac{i}{z + g(x) + 2ni \mathcal{Y}(xh_2)}
 \end{aligned}
 \tag{3.86}$$

where n is a negative integer, and $g(x)$ some combination of the g_1 's and g_2 's. Similarly, the general form of the ion thermal cone becomes

$$D[z, g(x_h) + 2ni \mathcal{H}(x_{h2}), S(x)] \rightarrow \left\{ \frac{-i}{z - g(x_h) - 2ni \mathcal{H}(x_{h2})} - \frac{i}{z + g(x_h) + 2ni \mathcal{H}(x_{h2})} \right\} \quad (3.87)$$

where x_h is the point (lower hybrid layer) of origin of the cone.

It is important to notice that when either $n \neq 0$ or $\text{Im } g \neq 0$, then the argument of the \mathcal{F} 's and \mathcal{D} 's are complex, so the cones are no longer singular, even in this cold plasma limit. The case $\text{Im } g \neq 0$ is clear: damping will limit the field amplitude of the cones to finite values even when thermal effects are ignored, and cause the cone field profile to assume a Lorentzian shape [see Fig. 3.9]. The case $n \neq 0$ means that the cone is one that has tunneled through the central evanescent layer at least once, so the passing of the cone through the evanescent layer has an effect on limiting the cone field very much like damping; a Lorentzian profile for the cone fields is produced. This fact is related to the criterion for the existence of resonance cones in cold, collisionless plasma theory: the resonance cones exist, i.e., the singularities occur in the fields from a point source in cold collisionless plasmas when $K_{\parallel}(x) K_{\perp} < 0$, and not when $K_{\parallel}(x) K_{\perp} > 0$. In the evanescent layer $K_{\parallel} K_{\perp} > 0$, and so the singular cones do not exist. However, the cones which have tunneled through the evanescent layer are not singular in the propagating regions where $K_{\parallel} K_{\perp} < 0$, either. However, in the physically meaningful sense, the fields are sharply peaked when the evanescent layer is thin, just as they are otherwise when the damping, source size and

temperature is small, and hence it is still meaningful to call them resonance cones; the criterion $K_{\parallel}K_{\perp} < 0$ has only limited usefulness as a criterion for the existence of the cones.

The limiting forms (2.85-2.86) immediately give the "cold plasma" cone trajectories of the cones contributing to $\phi(x,z)$, i.e., the trajectories of the cone maxima. They are $z = \text{Re } \pm g(x)$ for the form of the cone in Eq. (2.85), and $z = \text{Re } \pm g(x_h)$ in Eq. (2.86). The latter ion thermal cone trajectories are perpendicular to \vec{B}_0 . These cone trajectories are shown in Fig. 3.10, which is a generalization of Figs. 2.1 and 2.9, which show the cold plasma cone trajectories in a homogeneous plasma.

The "cold plasma" cone trajectories illustrate some important points about how the cones move from the source and throughout the plasma model, but we now want more detail about the structure of the finite temperature cones and their features as they propagate through the plasma regions. We will concentrate on the $z > 0$ cones, since the cone structure for $z < 0$ is just a mirror image of the $z > 0$ structure by symmetry. First, when $q(x) \neq 0$ and $p(x) \neq 0$, there is the well-known thermal interference structure near the cold plasma cone lines that is exhibited in the structure of the Airy function combination F and the Whittaker's function $D_{-1/2}$ which represent the cone field amplitudes as shown in Figs. 3.7-3.8.

A study of the functional form of the cone coming directly from the source shows the thermal structure of the cone is on the right-hand side with respect to the group velocity of the cone as it goes into the first hybrid layer, as it comes out of that layer as an ion thermal cone, and as it comes out after tunnelling at the second hybrid layer as either the

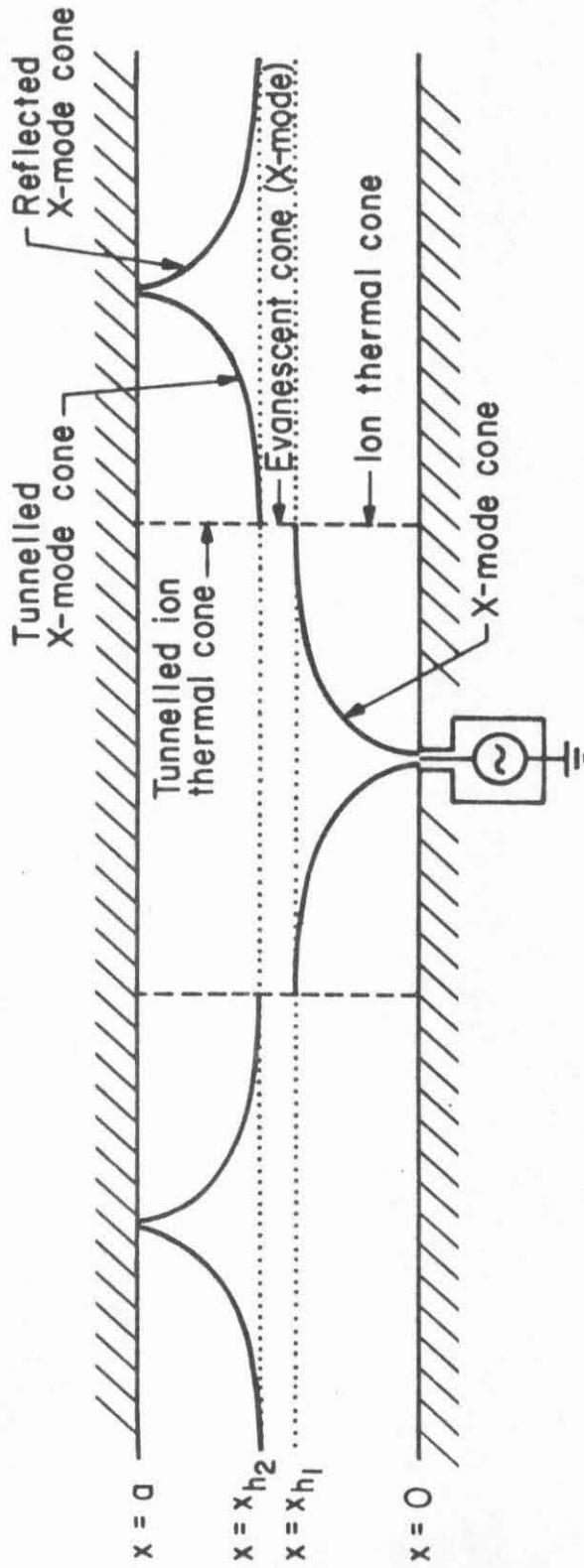


Fig. 3.10 Resonance cone trajectories near lower hybrid in $T_{\alpha} \rightarrow 0$ limit. The evanescent and tunnelled cones are finite even in the cold collisionless limit.

X-mode cone or converted into the ion thermal cone. Similarly, the thermal structure of the cone as it moves in the evanescent layer is on the right-hand side with respect to the direction of decay of the cone (see Fig. 3.11). Once the cone has reflected off the boundary, the thermal structure of it and of all cones produced by mode conversion from it are on the left side of the cone with respect to its direction of motion. Each subsequent reflection again changes the side of the thermal structure, i.e., changes the "parity" of the cone structure.

The cone from the source comes in from the boundary initially perpendicular to the magnetic field, but turns and approaches the lower hybrid layer almost along the field, i.e., at a very small cone angle given by

$$\tan \theta_c \sim \theta_c \sim \frac{\omega[\omega^2 - \omega_{lh}^2(x)]^{1/2}}{\omega_{pe}(x)} \quad (3.88)$$

As the cone comes in from the boundary, for a given x the width of the cone structure in the z direction goes as $[3q(x)]^{1/3}$, i.e., the cone spreads out in the x direction as $q(x)^{1/3}$. However, as the cone approaches the lower hybrid, so that the cones move almost along z , it is more useful to look at the cross sectional structure along x for a given z . It is seen that near the hybrid layer the cone structure does not appreciably widen as it moves asymptotically into the layer.

Near the lower hybrid layer the incoming cone bifurcates into an ion thermal cone which comes out almost perpendicular to \vec{B}_0 , and another X-mode cone which continues into the evanescent layer, also almost perpendicular to \vec{B}_0 . The cone coming out on the propagating side spreads

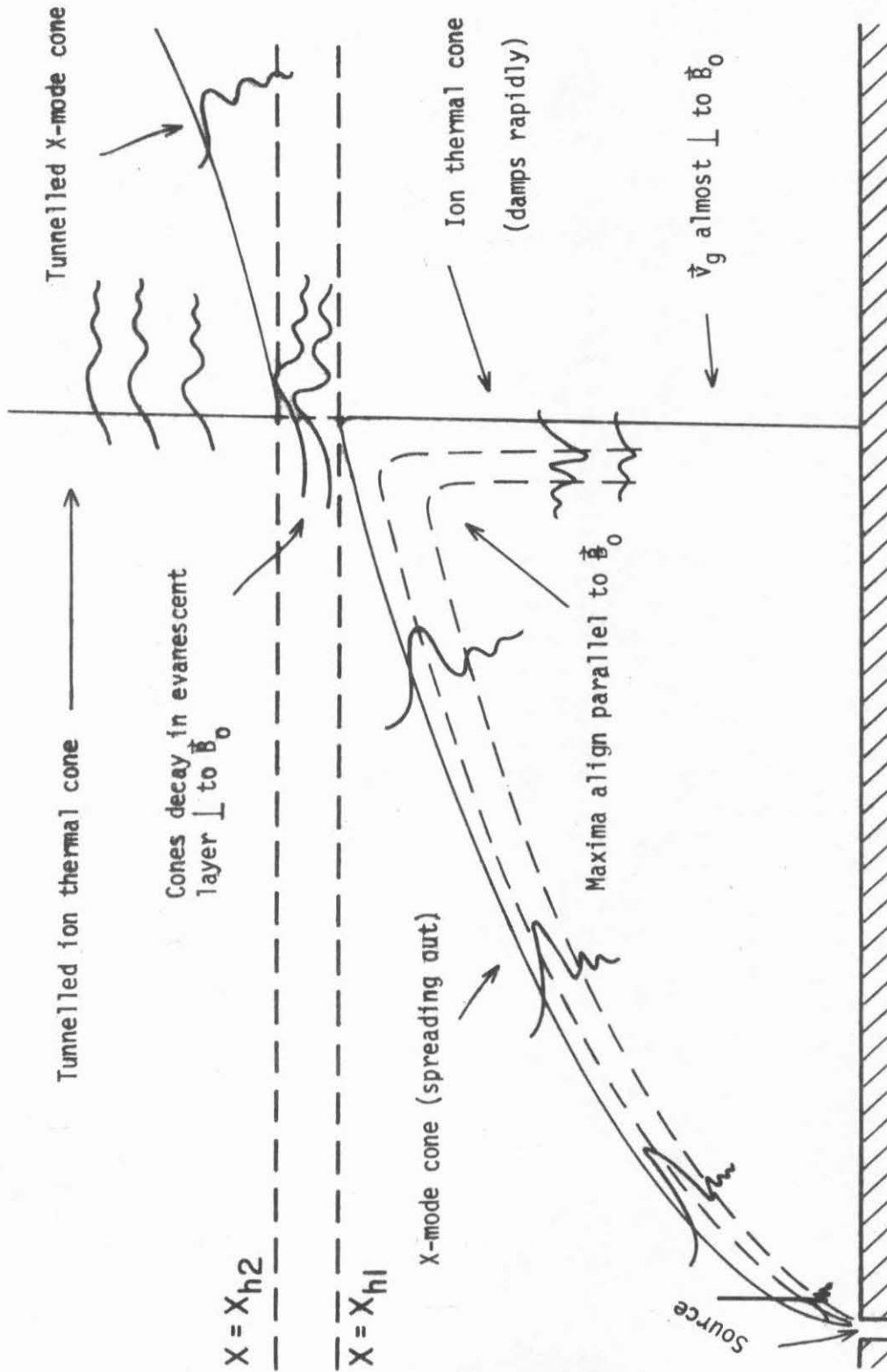


Fig. 3.11 Diagram showing the way the resonance cones propagate into the hybrid layer and through the evanescent layer. Solid lines indicate cold plasma cone lines, and dotted lines the trajectories of the peaks.

out like $[p(x_{h1}) - p(x)]^{1/2}$, but as we will see later, it also decays away very rapidly due to damping. The cone that goes into the evanescent layer decays away until it reaches the second hybrid layer, whereupon it bifurcates into an X-mode cone which propagates out almost parallel to the field, and an ion thermal cone (by mode conversion), which propagates out almost perpendicular to the field, each of which continues to spread out in the manner appropriate for the X mode and ion thermal cone: the former as $[q_2(x)]^{1/3}$ and latter as $[p_2(x)]^{1/2}$. These features are illustrated in Fig. 3.11.

It will be instructive to examine the nature of the decay of the X-mode in the evanescent layer. The functional form of the $z > 0$ cone field in that region is

$$\phi_c \sim F\left(\frac{z - q_1(x_{h1}) - iQ(x)}{\{3[q_1(x_{h1}) + iQ(x)]\}^{1/3}}\right) \equiv F(f) \quad (3.89)$$

Now $Q(x) \ll q_1(x_{h1})$ since the evanescent layer is taken to be moderately thin, and we may expand the denominator

$$[q_1(x_{h1}) + iQ(x)]^{-1/3} \approx [q_1(x_{h1})]^{-1/3} - \frac{iQ(x)}{3[q_1(x_{h1})]^{4/3}} \quad (3.90)$$

Thus the effect of the cone propagating a distance $x - x_{h1}$ into the evanescent layer is to add an imaginary part to the cone potential argument

$$\text{Im } f \approx -[3q_1(x)]^{-1/3} \left\{ Q(x) + \frac{Q(x)}{q_1(x_{h1})} [z - q_1(x_{h1})] \right\} \quad (3.91)$$

Let us examine the asymptotic region of the cone, $|\zeta| \gg 1$ or $|-z + g_1(x_{h1})| \gg [3q_1(x)]^{1/3}$, with $\text{Im } \zeta \ll \text{Re } \zeta$. For $z < g_1(x_{h1})$, where the maximum and cone interference structure is

$$F(\rho) \sim \frac{(-\rho)^{-1/4}}{\sqrt{\pi}} \exp \left\{ i \left[\frac{2}{3} (-\rho)^{3/2} + \pi/4 \right] \right\} - \frac{i}{\rho} \quad (3.92)$$

Let $\zeta = \zeta_r + i\zeta_i$. Then

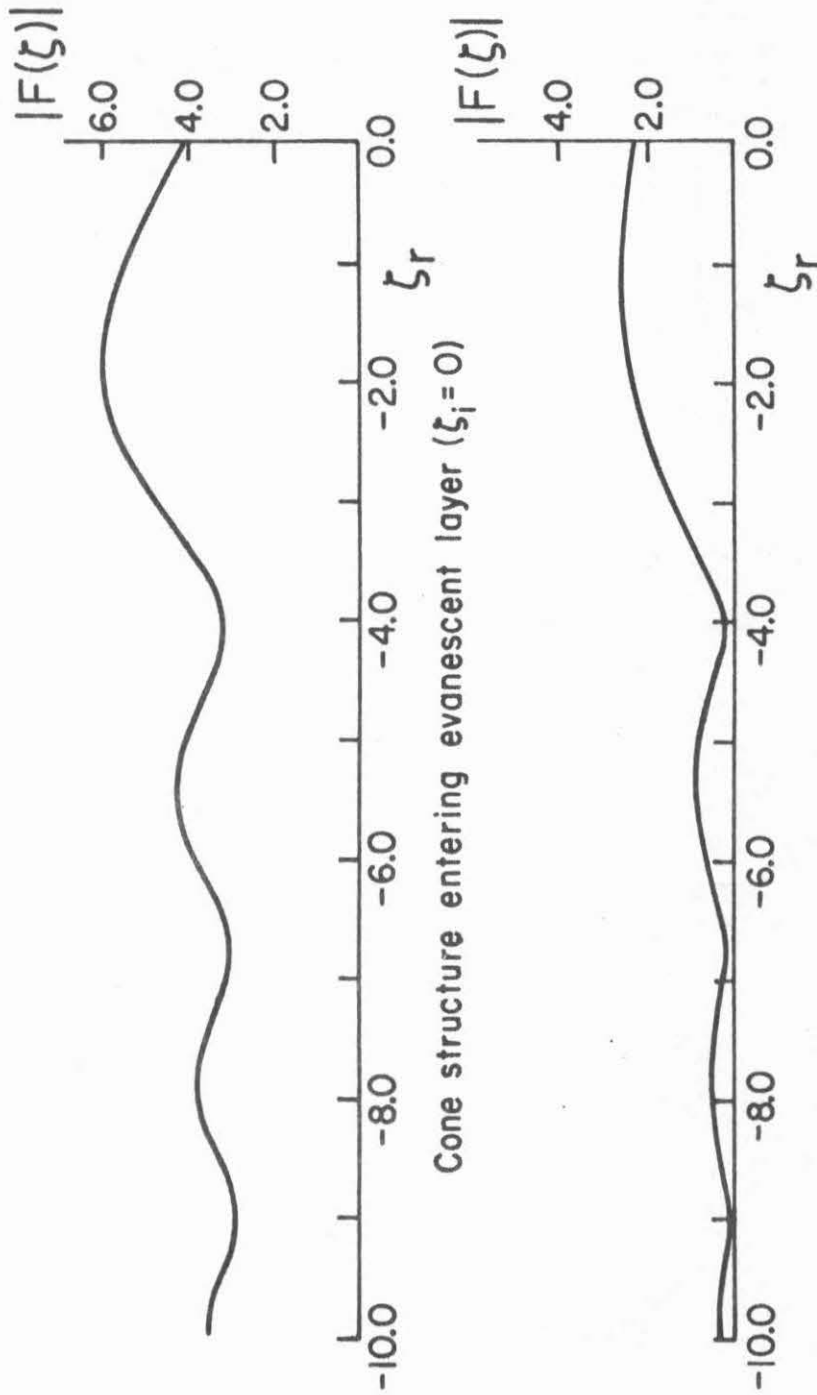
$$(-\rho)^{3/2} \approx (-\rho_r)^{3/2} - \frac{3}{2} i \zeta_i (-\rho_r)^{1/2} \quad (3.93)$$

The leading term in $F(\zeta)$ then decays as

$$\phi_c \sim \exp \left(\frac{-\frac{3}{2} \left\{ \mathcal{H}(x) [z - g_1(x)]^{1/2} + \frac{Q(x)}{q_1(x_{h1})} [z - g_1(x_{h1})] \right\}}{[3q_1(x_{h1})]^{1/2}} \right) \quad (3.94)$$

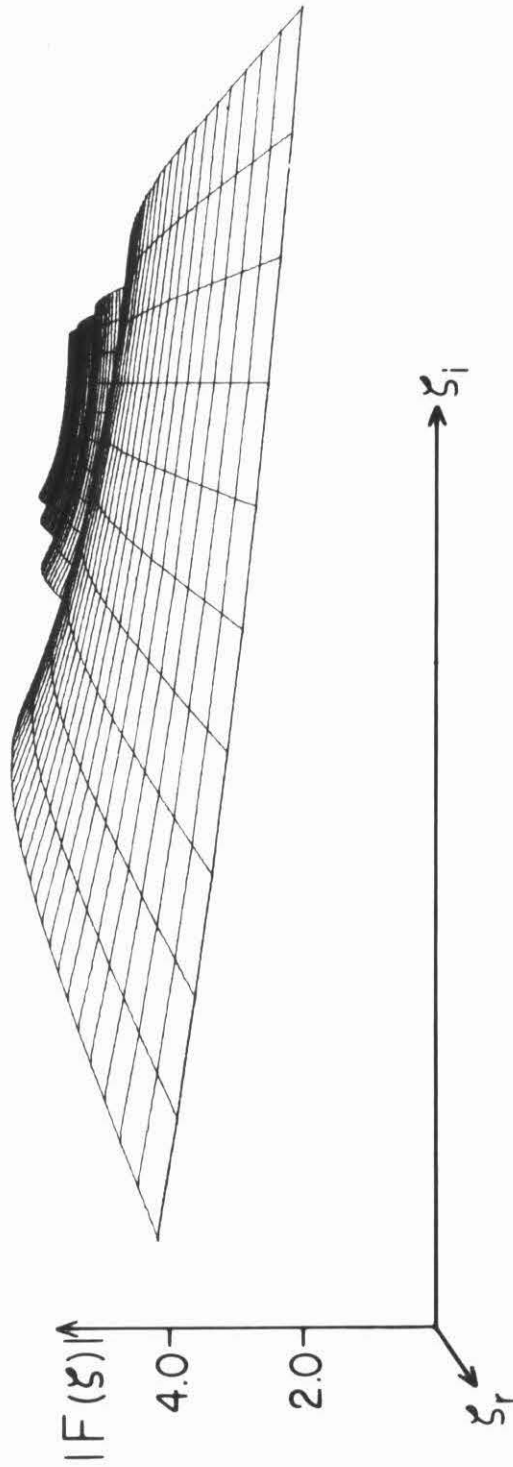
This form clearly shows that the parts of the thermal interference structure that are farthest from the cold plasma cone trajectory $z = g_1(x_{h1})$ decay away the most rapidly as x increases. This form of the decay rate is not valid for the primary maximum of the cone, but is useful for the second and higher maximum.

Plots of the decay of the cone in the evanescent layer are shown in Figs. 3.12 and 3.13, which illustrate the cone structure as a function of ζ_r for various fixed ζ_i . As seen from the diagrams, the whole cone decays but the widths of the maxima are virtually unchanged for the thin layer considered.



Cone structure after tunnelling through evanescent layer ($\xi_i = 1.0$)

Fig. 3.12 Comparison of X-mode cone cross-sectional structure before and after passing through an evanescent layer of thickness $g(x) \approx [3q_1(x_{h1})]^{1/3}$. The main peak has decreased in amplitude by $\sim 50\%$, the second peak by $\sim 80\%$, and the third by $\sim 88\%$, showing that the higher order peaks decay the most rapidly.



EVANESCENT RESONANCE CONES

Fig. 3.13 Three-dimensional perspective of the decaying resonance cones. The main peak is in the foreground, and the secondary peaks in the background.

It is seen that the amplitude of the primary maximum decreases least with the decrease in amplitude of the secondary maxima, increasing in severity with their distance from this primary maximum. Thus, since the effect of the evanescent layer is to make the secondary maxima less important relative to the primary maximum, the cone is as a result a more localized structure than before entering the evanescent layer. It should be noted on the other side of the cold plasma cone trajectory, where the exponential dying tail of the cone is, that there is some decay there also, but this is less than the decay of the maxima on the oscillatory side, and decreases in severity with the distance from the cold plasma cone trajectory, so that in the asymptotic limit there is no decay, but only a phase change as we concluded by asymptotic analysis.

The above analysis of the cone structure produced by the evanescent waves was for a thin layer $Q(x_{h2}) \ll q_1(x_{h1})$, but we can deduce what happens for thicker layers. Our asymptotic analysis showed that evanescence produces a rapid decay of the thermal contribution to the cone structure except very near the cold plasma cone line. This causes the secondary maxima of the cone (caused by the thermal wave) to rapidly disappear, leaving only the main peak. This peak moves closer to the cold plasma cone line, as seen in Fig. 3.12, and comes increasingly from the cold plasma contribution. But the cold plasma contribution is broadened and decreased in amplitude by the evanescent layer, and when $Q(x_{h2})$ becomes significant compared to $q_1(x_{h2})$, which occurs after most of the secondary maxima have decayed away, the main peak broadens significantly, and the whole cone rapidly spreads out.

CHAPTER IV. DAMPING, ENERGY FLOW AND ABSORPTION

Having obtained the general structure of the resonance cones in the bounded slab plasma model, we want to study some features of the energy flow and of the damping and corresponding energy absorption along the cones of interest for plasma heating. Having obtained the potential everywhere as a sum of resonance cones of similar structure, we can concentrate on a single cone structure for each of the X-mode and ion thermal waves, and straightforwardly generalize to all cones. The particular cones we will concentrate on are those coming directly from the source on the $x < x_{h1}$ side of the hybrid layer, because those are the largest amplitude, hence the most important.

Usually it will be more convenient to work with the damping and energy flow for a single Fourier \vec{k} -component of the wave. However, for each cone, k_x is a fixed function of k_z , and in the asymptotic region of the cone structure only a narrow spectrum of k_z centered around the saddle point value contributes to the local cone field. Thus from a determination of the damping associated with each \vec{k} -component, we can determine to a good approximation the damping that arises locally on each part of the cone. Also, these facts will allow us to derive a superposition theorem for the energy flow of individual \vec{k} -components to get energy flow locally on the cone.

4.1 Damping of the Cones

The effect of Landau, cyclotron, and collisional damping on the cones is implicitly contained in the cone potential solutions that we

have obtained in the form of a small imaginary component of the phases (the g's and the h's) of the waves, which we have ignored until now. We will concentrate on the damping of the primary cone from the source in region I that goes into the first hybrid layer, and on the converted ion thermal cone coming out of that layer, since those are the primary cones and the results are easily generalized.

The form of the damping correction to the plasma wave phase is given in Eq. (3.23). If we let r and i indicate the real and imaginary parts, the wave in region I takes the form

$$\tilde{\phi}(x, k_z) \sim \left[\frac{K_{\parallel}(0) K_{\perp}(0)}{K_{\parallel}(x) K_{\perp}(x)} \right]^{1/4} e^{[i|k_z|g_{1r}(x) - |k_z|g_{1i}(x) + i|k_z|^3 q_1(x)]} \quad (4.1a)$$

for the X-mode and

$$\tilde{\phi}(x, k_z) \sim \left[\frac{K_{\parallel}(0) K_{\perp}(0) \beta(x)}{K_{\perp}^3(x)} \right]^{1/4} e^{[ih_{1r}(x) - h_{1i}(x) + i|k_z|^2 p_1(x)]} \quad (4.1b)$$

for the ion thermal wave. (There is also a damping factor in the coefficient of the latter, which comes from the X-mode wave which has converted to the ion thermal wave.) Both of the damping exponents are a function of k_z , the latter through the cyclotron harmonic contribution. There are also "second order" contributions to the damping from the imaginary contributions to $q_1(x)$ and $p_1(x)$. These are normally

considerably smaller than the "first order" damping, but the "second order" contributions to the ion thermal mode include electron Landau damping, which might be important when the "first order" contributions of ion collisional and ion cyclotron harmonic damping are small. Thus, we will include that particular "second order" contribution.

From the form of the damping of the waves as a function of k_z , it is difficult to determine the exact form of the damping on the resonance cone fields, which encompass the whole k_z spectrum, but in the asymptotic regions of the cones only a narrow spectrum of k_z centered around the saddle point contributes locally to the cone field, and the local damping of the cone may be said to be governed by the saddle point value of k_z . More precisely, let

$$\tilde{\phi}(x, k_z) = \tilde{\phi}_0(x, k_z) e^{-\Gamma(x, k_z)} \quad (4.2)$$

where $\tilde{\phi}_0(x, k_z)$ is the undamped field obtained by ignoring damping, and $\Gamma(x, k_z)$ is the damping exponent. Thus, since the exponential factor is slowly varying in k_z compared with ϕ_0 ,

$$\phi(x, z) \sim e^{-\Gamma(x, k_0)} \int \tilde{\phi}_0(x, k_z) e^{ik_z z} \frac{dk_z}{2\pi} \quad (4.3)$$

when the integral may be approximated by its asymptotic form by integrating over the saddle point k_0 . The saddle point for the two modes we are studying may be found from the integral forms of the Airy functions and the Whittaker's function which characterize the cone fields in Eqs. (3.79, 3.81). For the X-mode the appropriate saddle point is

$$k_o = \left[\frac{z - g_{1r}(x)}{3q_1(x)} \right]^{1/2} \quad (4.4a)$$

and for the ion thermal mode

$$k_o = \frac{1}{2} \left[\frac{z - g_{1r}(x_{h1})}{p_1(x_{h1}) - p_1(x)} \right] \quad (4.4b)$$

The form of the damping exponent for the cone potential is

$$\Gamma(x, k_o) = k_o/2 \int_0^x \left[\frac{-K_{\perp 0}(x')}{K_{\perp 0}^3(x')} \right]^{1/2} \text{Im } K_{\perp}(x', k_o) + \frac{\text{Im } K_{\parallel}(x', k_o)}{[-K_{\perp 0}(x') K_{\perp 0}(x')]^{1/2}} \left. \right\} dx' \quad (4.5)$$

for the X-mode and

$$\Gamma(x, k_o) = \frac{1}{2} \int_x^{x_{h1}} \left\{ \frac{\text{Im } K_{\perp}(x', k_o)}{[\beta(x') K_{\perp 0}(x')]^{1/2}} + |k_z|^2 \left[\frac{\beta(x')}{K_{\perp 0}^3(x')} \right]^{1/2} \text{Im } K_{\parallel}(x', k_o) \right\} dx' \quad (4.6)$$

for the ion thermal mode. The latter includes the "second order" electron damping through the imaginary part of K_{\parallel} , and the forms show that the electron damping of the ion thermal cone is negligible compared with the ion damping when

$$\text{Im } K_{\perp} \gg \frac{|k_z|^2 \beta}{K} \text{Im } K_{\parallel} \quad (4.7)$$

which is generally true in the $x \ll x_{h1}$ region except for very low ion

collision frequency and for ω not near any of the ion cyclotron harmonics. The forms of the imaginary parts of K_{\parallel} and K_{\perp} are [see Eqs. (1.16 - 1.18)]

$$\text{Im } K_{\parallel}(x') = \frac{v_e \omega_{pe}^2(x')}{\omega^3} + 2\sqrt{\pi} \frac{\omega_{pe}^2(x') \omega}{k_z^3 v_e^3} e^{-\omega^2/k_z^2 v_e^2} \quad (4.8a)$$

$$\text{Im } K_{\perp}(x') = \frac{v_i \omega_{pi}^2(x')}{3} + \frac{2\omega_{pi}^2(x) \omega_{ci}^3}{\omega k_z^3 k_x^3 v_i^4} \sum_n n^2 e^{-\frac{(\omega - n\omega_{ci})^2}{k_z^2 v_i^2}} \quad (4.8b)$$

The form of k_x that enters the latter equation is

$$k_x = k_z \left[\frac{-K_{\parallel 0}(x)}{K_{\perp 0}(x)} \right]^{1/2} \quad (4.9a)$$

for the X-mode, and

$$k_x = \left[\frac{K_{\perp 0}(x)}{\beta(x)} \right]^{1/2} \quad (4.9b)$$

for the ion thermal mode.

It is seen that for the X-mode the parts of the cone that are farthest from the cold plasma cone line [$z = g_{1r}(x)$] in the $z > g_{1r}(x)$ region (where the oscillating spatial structure of the cone is) are the most severely damped: Γ increases monotonically with $z - g_{1r}(x)$. For $z < g_{1r}(x)$ (where the exponential tail of the cone is), Γ becomes imaginary, so damping merely introduces a spatially dependent phase factor which increases with the distance $z - g_{1r}(x)$ from the cold plasma cone trajectory. This is very similar to the nature of the decay of

that cone in the evanescent layer. These asymptotic forms are strictly valid for

$$z - g_{1r}(x) \gg [3q_1(x)]^{1/3}$$

This form of Γ goes to zero as $z \rightarrow g_{1r}(x)$, i.e., outside the region of its validity, and thus predicts no damping along the cone line. A more accurate numerical evaluation of the effect of damping on the cone field similar to what was done in Chapter 3 for the cone in the evanescent layer shows the damping rate decreases monotonically as $z \rightarrow g_{1r}(x)$, but does not go to zero there. Thus the saddle point damping prediction is too low near the cone line. The behavior of the cone damping arises from the fact that the damping of the individual k_z components increases with increasing k_z .

For the ion thermal mode, the dependence of Γ on $k_z = k_0$, and hence on z , comes only in $\text{Im } K_{\parallel}$ and $\text{Im } K_{\perp}$. This means that the collisional contribution to the damping of this mode is independent of k_0 and thus of the position in z on the cone structures, so that it gives rise to a uniform decay of the whole cone structure, unlike its effect on the X-mode cone. The collisional and Landau contribution increases with $k_z = k_0$, and hence is more severe the greater the distance $z - g_1(x_{h1})$ from the "cold plasma" cone line $z = g_{1r}(x_{h1})$. Thus when collisional damping is the predominant damping mechanism, the whole cone structure decays approximately uniformly in the $-x$ direction, unlike the X-mode cone. If ion cyclotron harmonic and/or Landau damping is the predominant mechanism(s), so that the higher k_z are more highly damped, the "high k_z " secondary maxima decay at a higher rate than the primary

maximum, similar to that of the X-mode cone. For cases for which both collisional and collisionless damping are important, the mean peak may be predominantly collisionally damped, because it is made up of the smaller k_z components for which collisionless damping is small, whereas the higher order maxima, which are made up of increasingly higher k_z components, may be dominated by collisionless damping.

We now want to investigate the damping rates of these modes, particularly that of the ion thermal mode which is responsible for most of the absorption of the wave for more specific cases, since the incoming wave is usually not severely damped. Let us consider the damping of the ion thermal wave near the lower hybrid layer, since that is where most of the energy absorption might be expected to take place. Near that layer we can assume a linear density profile for a thin region

$$\begin{aligned} \text{Re } K_{\perp 0}(x) &\approx \gamma(x_{h1} - x) \\ \omega &\sim \omega_{pi}(x) \sim \omega_{lh}(x) \end{aligned} \quad (4.10)$$

We will neglect the small electron thermal part of (x') :

$$\beta(x) \approx \frac{3}{2} \frac{v_i^2 \omega_{pi}^2(x)}{\omega^4} \sim \frac{3v_i^2}{2\omega^2} \quad (4.11)$$

Divide the damping exponent up into a collisional part Γ_c , a harmonic part Γ_h , and a Landau part Γ_l :

$$\Gamma = \Gamma_c + \Gamma_h + \Gamma_l \quad (4.12)$$

The collisional part includes ion collisional damping and a less important electron collisional damping component:

$$\Gamma_c \approx \frac{1}{2\omega\sqrt{\beta(x_{h1})}} \left\{ v_i \int_x^{x_{h1}} \frac{dx'}{(x_{h1}-x')^{1/2}} + \frac{k_z^2 v_e \beta(x_{h1}) \omega_{pe}^2(x_{h1})}{\gamma \omega^2} \int_x^{x_{h1}} \frac{dx'}{(x_{h1}-x')^{3/2}} \right\} \quad (4.13)$$

To get the electron collisional damping part, as well as the ion cyclotron harmonic and the electron Landau damping parts, we must use the mode conversion point $x = x_0$ as the upper limit of the integral rather than the hybrid layer $x = x_{h1}$, since using the latter will give a divergent integral. The mode conversion point is the correct point from which to integrate, since that is where the ion thermal wave starts and thus the point from which it is damped. (Since $x_{h1} - x_0 \ll x_{h1} - x$, we have normally used x_{h1} as the upper limit of our integrals rather than x_0 , as that gives a negligible error if it does not produce a divergent integral.)

The mode conversion point $x = x_0$ is given by Eq. (3.12) and is a function of k_z . Hence

$$\begin{aligned} x_0 &= x_{h1} - \frac{2k_0(-\beta K_{||0})^{1/2}}{\gamma} \\ &\approx x_{h1} - 2\sqrt{\frac{3m_i}{2m_e}} \frac{k_0 v_i}{\omega\gamma} \end{aligned} \quad (4.14)$$

where $k_z = k_0$ is the saddle point value of ϕ_0 of the ion thermal cone given by Eq. (4.4). Note that now x_0 is a function of the position at which we are measuring the damping because it is a function of those k_z

that produce the field at that position.

The collisional damping exponent now becomes

$$\Gamma_c \approx \frac{1}{\sqrt{6}\gamma v_i} \left\{ 2v_i (x_{h1} - x)^{1/2} + \frac{3k_0^2 v_e v_2^2 m_i}{\gamma \omega^2 m_e} \left[\left(\frac{\gamma}{k_0 v_i} \sqrt{\frac{m_e}{6m_i}} \right)^{1/2} - (x_{h1} - x)^{-1/2} \right] \right\} \quad (4.15)$$

The second term in the electron collisional damping is small compared with the first because we are in the region where $x_{h1} - x_0 \ll x_{h1} - x$. Note that by using x_{h1} as the upper limit of the ion collisional integral rather than x_0 , we neglected a term of order $(x_{h1} - x_0)^{1/2}$, which is small by the same token. The ion cyclotron harmonic and Landau damping contributions to the damping may similarly be calculated using $x = x_0$ as the upper limit of their integrals:

$$\begin{aligned} \Gamma_h &\approx \frac{3\omega_{ci}^3}{2\omega\gamma^2 k_0 v_i^2} \sum_n n^2 e^{-\frac{(\omega - n\omega_{ci})^2}{k_0^2 v_i^2}} \\ &\times \int_x^{x_0} \frac{\exp\left[\frac{\omega^2 \beta(x_{h1})}{v_i^2 \gamma (x - x_{h1})}\right]}{(x - x_{h1})^2} dx' \\ &= \frac{3\omega_{ci}^3}{2\omega^3 \gamma k_0 \beta(x_{h1})} \sum_n n^2 e^{-\frac{(\omega - n\omega_{ci})^2}{k_0^2 v_i^2}} \\ &\times \left\{ \exp\left[\frac{\omega^2 \beta(x_{h1})}{v_i^2 \gamma (x - x_{h1})}\right] - \exp\left[\frac{\omega^2 \beta(x_{h1})}{v_i^2 \gamma (x_0 - x_{h1})}\right] \right\} \quad (4.16) \end{aligned}$$

$$\begin{aligned}
 \Gamma_{\ell} &= \frac{\sqrt{\pi} \omega_{pe}^2(x_{h1}) \omega}{k_0 v_e^3} \left[\frac{\beta(x_{h1})}{\gamma^3} \right]^{1/2} e^{-\frac{\omega^2}{k_z^2 v_0^2} \int_x^{x_0} \frac{dx'}{(x_{h1}-x')^{3/2}}} \\
 &\approx \frac{m_i \sqrt{6\pi^3} \omega^2 v_i}{m_e k_0 v_e^3 \gamma^{3/2}} \left\{ \left[\sqrt{\frac{2m_e}{3m_i}} - \frac{\omega \gamma}{k_0 v_i} \right]^{1/2} - (x_{h1}-x)^{-1/2} \right\} \\
 &\quad \times e^{-\frac{\omega^2}{k_0^2 v_0^2}}
 \end{aligned} \tag{4.17}$$

The second term in the curly brackets in both Γ_h and Γ_{ℓ} is small compared with the first term, especially so for harmonic damping, in our region $x_{h1} - x \gg x_{h1} - x_0$. The significance of this for the Landau damping for given k_z components is that when the smaller terms are neglected, their contribution to Γ no longer depends on x , so that most of the damping that will take place on this mode has already taken place by the time the wave has reached the asymptotic region. Thus the damping rate by this mechanism is very high near the lower hybrid layer and falls off very rapidly as the ion thermal wave moves away from that layer. This can be seen from the general form of the damping rate $d\Gamma/dx$ obtained from Eqs. (4.6) and (4.8):

$$\begin{aligned}
 \frac{d\Gamma}{dx} &= \frac{1}{2} \left\{ \left[\beta(x) K_{10}(x) \right]^{-1/2} \left[\frac{\nu_i \omega_{pi}^2(x)}{\omega^3} + \frac{2\omega_{pi}^2 \omega t_i^3 \beta^{3/2}(x)}{\omega k_0(x) K_{10}^{3/2}(x) v_i^4} \right. \right. \\
 &\quad \times \left. \left. e^{-\omega^2 \beta(x) / K_{10}(x) v_i^2} \sum_n n^2 e^{-\frac{(\omega - n\omega_{ci})^2}{k_0^2 v_i^2}} \right] \right. \\
 &\quad \left. + |k_z|^3 \left[\frac{\beta(x)}{K_{10}^3(x)} \right]^{1/2} \left[\frac{\nu_e \omega_{pe}^2(x)}{\omega^3} + 2\sqrt{\pi} \left(\frac{\omega_{pe}^2(x) \omega}{k_z^2 v_e^3} \right) e^{-\frac{\omega^2}{k_0^2 v_e^2}} \right] \right\}
 \end{aligned} \tag{4.18}$$

The ion collisional and the electron (collisional and Landau) damping contributions fall off as the wave moves away from the mode conversion point because of the K_0 factor in the denominator and the factor proportional to density in the numerator in those terms. However, the ion collisional damping rate falls off much more slowly than the electron damping rates, while the ion cyclotron harmonic damping rate increases rapidly as the wave moves away from the hybrid layer. Thus we would expect that both electron and ion damping are important damping mechanisms near the hybrid layer, with perhaps the electron damping even dominating, but as the wave moves away from the hybrid layer, the electron damping falls off rapidly and the ion damping dominates and, in particular, when ω is sufficiently close to a cyclotron harmonic, ion cyclotron harmonic damping will become the dominant mechanism. It should be noted that the reason ion cyclotron harmonic damping can be an important mechanism is that the wave maintains a finite k_z component, i.e., propagates obliquely to the magnetic field (although, as will be discussed in the next section, the group velocity component along ℓ is large compared with that along z , so that the wave propagates almost perpendicular to the field), since, as is well known, there is no ion cyclotron harmonic damping for ion Bernstein modes traveling perpendicular to \vec{B}_0 .

The total damping exponent, after neglecting the small terms in Γ_c , Γ_h and Γ_ℓ is

$$\Gamma \approx \frac{1}{\sqrt{68} v_i} \left\{ 2\nu_i (\chi_{m1} - \chi)^{1/2} + \frac{3V_e}{\omega^2} \left(\frac{k_0^3 v_i^3}{y} \sqrt{\frac{m_i^3}{6m_e^3}} \right)^{1/2} \right\}$$

$$\begin{aligned}
 & + \frac{3\omega_{ci}^3}{2\omega^3\gamma k_0\beta(\chi_{hi})} \sum_n n^2 e^{-\frac{(\omega-n\omega_{ci})^2}{k_0^2 v_i^2}} \\
 & \times \left[e^{\frac{\omega^2\beta(\chi_{hi})}{v_i^2\gamma(\chi-\chi_{hi})}} - e^{\frac{\omega^2\beta(\chi_{hi})}{v_i^2\gamma(\chi_0-\chi_{hi})}} \right] \quad (4.19) \\
 & + \frac{1}{v_e^3\gamma^2} \left(\frac{\omega^5 v_i}{k_0^3} \sqrt{\frac{2m_e^3}{3m_i}} \right)^{1/2} e^{-\omega^2/k_0^2 v_e^2} \}
 \end{aligned}$$

Certain features of the dependence of the damping on plasma parameters are evident from this form. For given k_z components excited by the source, as the density gradient γ at the hybrid layer decreases, the ion collisional and the electron collisional and Landau damping increase while that of ion cyclotron harmonic damping decreases, with the electron damping increasing in importance relative to both types of ion damping. Thus by increasing γ , we increase the proportion of the absorbed wave that goes to the ions over that which goes to the electrons, and in particular we increase the importance of cyclotron harmonic damping relative to all other types of damping. As the ion temperature increases, the ion cyclotron harmonic damping and both types of electron damping increase, while that of ion collisional damping decreases.

The above observations about the nature of the damping of the ion thermal wave were made for fixed $k_z = k_0$. However, for studying the damping of the cone as a whole, it is more useful to see how a given

peak decays, or how a part of the cone a given distance from the cold plasma line decays. Consider the form of k_0 in the region of assumed linear density profile:

$$\begin{aligned}
 p(x_{h1}) - p(x) &= \frac{1}{2} \left[\frac{\beta(x_{h1})}{\gamma^3} \right]^{1/2} K_{11}(x_{h1}) \int_x^{x_0} \frac{dx'}{(x_{h1} - x')^{3/2}} \\
 &= \sqrt{3/2} \frac{m_i v_i}{\omega \gamma^{3/2} m_e} \left\{ \left(\frac{\gamma}{k_0 v_i} \sqrt{\frac{m_e}{6m_i}} \right)^{1/2} - (x_{h1} - x)^{-1/2} \right\}
 \end{aligned} \tag{4.20}$$

Again, the second term is small compared with the first, so

$$k_0 = \frac{z - g_{1r}(x_{h1})}{p(x_{h1}) - p(x)}$$

becomes constant for fixed z as x decreases, and rapidly just becomes proportional to the distance $z - g_{1r}(x_{h1})$ from the cold plasma cone line. (It should be noted that k_0 does not actually go to zero at the point of mode conversion, as this might suggest; there is another higher order correction like $|k_z|^3 q_1(x)$ to the phase of $\tilde{\phi}(x, k_z)$ which we have ignored in the asymptotic region, but which would become as important as the $|k_z|^2 p(x)$ very near the hybrid layer.) This means that our conclusions for fixed $k_z = k_0$ also hold approximately true for fixed distance $z = g_{1r}(x_{h1})$ from the cold plasma cone line, indeed for fixed z , with the knowledge that the fixed distance from the cone line

is proportional to fixed k_z . Another conclusion that can be drawn from this form of k_o is that the width of the peaks and spatial oscillations of the ion thermal cone approaches a constant as the cone propagates to smaller x ; they do not continue to spread out as they did coming into the hybrid layer (on the X-mode cone), and for a short distance after mode conversion.

Finally, some observations are in order on the damping rate of the cone coming into the hybrid layer. From Eq. (4.5) this is

$$\frac{d\Gamma}{dx} = \frac{k_o}{2} \left\{ \frac{\omega_{pe}^2(x)}{\omega^2 [-K_{\parallel 0}(x) K_{\perp 0}(x)]^{1/2}} \left[\frac{\nu_e}{\omega} + 2\sqrt{\pi} \left(\frac{\omega}{k_o v_e} \right) \right. \right. \\ \left. \left. \times e^{-\omega^2/k_o^2 v_e^2} \right] + \left[\frac{-K_{\parallel 0}(x)}{K_{\perp 0}(x)} \right] \left[\frac{\nu_i \omega_{pi}^2(x)}{\omega^3} + \frac{2\omega_{pi}^2(x) \omega_{oi}^3}{\omega k_o^4 \nu_i^4} \right. \right. \\ \left. \left. \times \left(\frac{-K_{\perp 0}}{K_{\parallel 0}} \right)^{3/2} e^{\omega^2 K_{\perp 0}/k_o^2 K_{\parallel 0} \nu_i^2} \sum n^2 e^{-\frac{(\omega - n\omega_{oi})^2}{k_o^2 \nu_i^2}} \right] \right\} \quad (4.21)$$

which is to be compared with that of the ion thermal cone damping rate in Eq. (4.18). This mode starts out in the low density region of the plasma near the plasma layer (where $K_{\parallel 0}(x) \sim 0$), with virtually no ion damping; only electron collisional and Landau damping is present, and this is strong near the plasma layer. The electron damping rate falls off somewhat as the immediate vicinity of the plasma layer is left, then all types of damping increase in importance as the wave moves into

the plasma interior, with the ion damping increasing at a faster rate than the electron damping. As the mode conversion point is approached [so that $K_0(x)$ becomes very small], the ion damping increases in importance very rapidly relative to the electron damping, with the relative importance of ion cyclotron harmonic damping increasing the most rapidly. This ion damping may rapidly become the dominant mechanism on this mode near the hybrid layer, although both electron and ion damping will probably be important in this region. As previously discussed, the ion damping will continue to increase in importance relative to the electron damping after mode conversion, so that at some point ion damping begins to dominate, and all subsequent absorption goes primarily to the ions.

All forms of the damping given by Eq. (4.22) increase with the distance $z-g_{1r}(x)$ from the cone line, so the higher order maxima decay away the most rapidly. This differential of damping rates for the various peaks is greater for collisionless damping than for collisional damping, and the former is ordinarily quite small on this mode except for the very high k_z components. Thus, the main peak of this mode will typically be primarily damped by electron collisions, except near the hybrid layer, where ion collisions become important, but some Landau damping may be important for the higher order peaks.

Certain aspects of the damping of the resonance cones have been considered previously. P. Bellan and M. Porkolab¹⁹ considered collisional damping of the incoming mode, and concluded that this may become quite large near the hybrid layer for typical collisional

plasmas. Our analysis suggests that collisional damping is the most important mechanism for this mode, but that collisionless damping may also be important for the secondary peaks if the source excites these. Also, the collisional as well as Landau damping is ordinarily rather small far away from the lower hybrid layer, and only gets large near the lower hybrid layer. Even near the hybrid layer, it is primarily the secondary peaks that are strongly damped, so that the main peak should be weakly damped enough to undergo mode conversion. These conclusions are important extensions of Bellan and Porkolab's study.

There has been no previous analytic investigation of the damping of the outgoing cone, but M. Simonutti,²¹ and K. Ho and H. Kuehl²⁰ have done some numerical investigation of that damping. M. Simonutti considered only collisionless absorption and concluded that cyclotron harmonic damping was small on the incoming mode, but may become important on the outgoing mode. Our analysis confirms this conclusion and further implies that ion cyclotron damping will become the predominant mechanism of the outgoing mode if it is not totally absorbed near the lower hybrid layer. Another important conclusion of our analysis is that ion collisional damping is important for this mode near the hybrid layer, and gives rise to a uniform decay of the cone. K. Ho and H. Kuehl concluded that ion cyclotron harmonic damping causes a rapid decay of the outgoing cone. Our analysis confirms this and shows that damping is largest on the secondary peaks of the cone.

4.2 Energy Conservation Theorem for Quasistatic Fields

In order to study the energy flow, we need an energy conservation theorem for quasistatic fields. There are Poynting-type energy conservation theorems for electromagnetic waves in plasmas in the plasma literature,³ but when the quasistatic approximation is used, there is an ambiguity in the proper form of \vec{H} to use in the power flux vector $\vec{E} \times \vec{H}$ in the theorem. This is because the $\nabla \times \vec{E}$ Maxwell equation gives $\vec{H} = 0$, implying zero power flux in the cold plasma limit, whereas the $\nabla \times \vec{H}$ Maxwell equation gives an $\vec{H} \neq 0$. The latter equation turns out to give a good estimate for the power flux, but it will be instructive to develop energy theorems from first principles, which will resolve the ambiguity and confirm the correct form of H to use in the power flux.

There are two forms of the conservation theorem that we will develop, both of which will be useful since they are somewhat complementary. The first will be from the fluid equations. This has the advantage that a Fourier transformation of the fluid quantities is unnecessary, but has shortcomings since it does not include Landau and cyclotron harmonic damping, as fluid theory does not predict those damping mechanisms. We will then develop the theorem in terms of the warm plasma dielectric tensor. This form has the advantage of including collisionless damping and only having one undetermined quantity in it (the wave potential), but can be derived for only a single Fourier k component. For the latter case, the fields will be taken to have an $e^{i(k \cdot r - \omega t)}$ (plane wave) dependence.

We will ignore for simplicity the energy flow associated with zero-order drifts, such as the diamagnetic drift arising from the pressure due to the background density inhomogeneity. This is valid for sufficiently gentle density inhomogeneities. These may be included if necessary in the fluid form of the conservation theorem, but not in the warm plasma dielectric tensor form. This is because the latter, which is obtained in \vec{k} -space, assumes sufficiently slowly varying inhomogeneities so that the dispersion relation is satisfied in the WKB sense, with the wavenumbers being a function of the local density.

Let us start with Poisson's equation

$$-\nabla^2 \phi = \rho / \epsilon_0 \quad (4.22)$$

and the continuity equation

$$\frac{\partial \rho}{\partial t} + \nabla \cdot \vec{J} = 0 \quad (4.23)$$

Taking the time derivative of Poisson's equation, substituting it into the continuity equation, and multiplying by ϕ^* gives

$$\phi^* \nabla \cdot \left(\vec{J} - \epsilon_0 \frac{\partial \nabla \phi}{\partial t} \right) = 0 \quad (4.24)$$

Transforming this with the vector identity $\phi \nabla \cdot \vec{A} = \nabla \cdot (\phi \vec{A}) - \vec{A} \cdot \nabla \phi$, we may put this into the form

$$\frac{\partial}{\partial t} \left(\frac{\epsilon_0}{2} |\nabla \phi|^2 \right) + \nabla \cdot (\phi^* \vec{J} - \epsilon_0 \phi^* \frac{\partial \nabla \phi}{\partial t}) = \nabla \phi^* \cdot \vec{J} \quad (4.25)$$

As it stands, this is a conservation equation for the electric field energy. The first term is the time rate of change of the energy density of the electrostatic field. The second term is the power flux associated with the field, which includes contributions from the displacement current and from the regular currents induced in the plasma by the field. On the right hand side is an $\vec{E} \cdot \vec{J}$ power sink term, which represents the energy transferred from the field to the particles in the plasma.

Equation (4.25) is not yet adequate for finding the wave energy, since the wave energy is made up of both electric field energy and energy of the coherent (wavelike) motion of the plasma particle. Thus we must divide the $\vec{E} \cdot \vec{J}$ particle energy term up into a coherent particle motion part associated with the wave and an incoherent part associated with the irreversible transfer of energy from the wave to the particles by damping mechanisms. To do this we utilize the fluid equations of motion with a phenomenological collision frequency ν assumed to represent collisional damping:

$$N_\alpha m_\alpha \left(\frac{\partial}{\partial t} + \vec{v}_\alpha \cdot \nabla \right) \vec{v}_\alpha = N_\alpha e_\alpha (\vec{E} + \vec{v}_\alpha \times \mathbf{B}) - \gamma K \Gamma_\alpha \nabla N_\alpha - N_\alpha m_\alpha \vec{v}_\alpha \nu_\alpha \quad (4.26)$$

for particle species α , where N_α is the density of species α . Linearizing, there is no zero-order velocity of the particles if we ignore

drifts and macroscopically average the Larmor orbit motion of the particles, and we obtain

$$\vec{E} = \frac{m_\alpha}{e_\alpha} \frac{\partial \vec{v}_\alpha}{\partial t} + \frac{\gamma k T_\alpha}{n_0 e_\alpha} \nabla n_\alpha - \vec{v}_\alpha \times \vec{B}_0 + \frac{v_\alpha m_\alpha}{e_\alpha} \vec{v}_\alpha \quad (4.27)$$

where n_0 is the background plasma density, and n_α is the perturbed density associated with the wave of species α . Thus the time average $\vec{J} \cdot \vec{E}$ power is

$$\vec{J} \cdot \vec{E}^* = \sum_\alpha \left\{ \frac{n_0 m_\alpha}{2} \frac{\partial |\vec{v}_\alpha|^2}{\partial t} + T_\alpha \vec{v}_\alpha \cdot \nabla n_\alpha + n_0 v_\alpha m_\alpha |\vec{v}_\alpha|^2 \right\} \quad (4.28)$$

We may transform the second term by

$$\vec{v}_\alpha \cdot \nabla n_\alpha = \nabla \cdot (n_\alpha \vec{v}_\alpha) - n_\alpha \nabla \cdot \vec{v}_\alpha \quad (4.29)$$

and the linearized continuity equation for α

$$\frac{\partial n_\alpha}{\partial t} + n_0 \nabla \cdot \vec{v}_\alpha = 0 \quad (4.30)$$

With the resulting form of $\vec{J} \cdot \vec{E}$ we may rewrite the Eq. (4.25) in the form

$$\frac{\partial U}{\partial t} + \nabla \cdot \vec{S} = P_R \quad (4.31)$$

where

$$U = U_E + U_K + U_T \quad (4.32)$$

is the energy density of the wave, with

$$U_E = \frac{\epsilon_0}{2} |\nabla \phi|^2 \quad (4.33a)$$

the electrostatic field energy density,

$$U_K = \sum_\alpha \frac{n_0 m_\alpha}{2} \vec{v}_\alpha^2 \quad (4.33b)$$

the particle kinetic energy density,

$$U_T = \sum_{\alpha} \frac{\gamma_{\alpha} T_{\alpha} n_{\alpha}^2}{2n_0} \quad (4.33c)$$

the energy density of the fluid pressure oscillations:

$$\vec{S} = \vec{S}_C + \vec{S}_D + \vec{S}_T \quad (4.34)$$

is the power flux of the wave, with

$$\vec{S}_C = \phi^* \vec{j} \quad (4.35a)$$

the flux produced by regular currents

$$\vec{S}_D = -\epsilon_0 \phi^* \frac{\partial(\nabla\phi)}{\partial t} \quad (4.35b)$$

the flux of displacement currents

$$\vec{S}_T = \sum_{\alpha} \gamma_{\alpha} T_{\alpha} n_{\alpha} \vec{v}_{\alpha} \quad (4.35c)$$

the flux of the pressure oscillations; and

$$P_R = -n_0 \sum m_{\alpha} v_{\alpha} v_{\alpha} \quad (4.36)$$

is the "heating" of the particles produced by collisional damping of the wave.

This fluid form of the energy conservation theorem contains the unknown perturbed quantities n_{α} , \vec{v}_{α} , and ϕ associated with the wave; we could solve the fluid equations to get n_{α} and \vec{v}_{α} in terms of ϕ , and thus U , S , and P_R in terms of ϕ . But we should be able to get these energy-related quantities in terms of ϕ and plasma parameters solely

through a knowledge of the warm plasma dielectric tensor (which is derived from the Boltzmann-Vlasov and other equations). We will derive a conservation theorem in terms of $\bar{K}(\vec{k}, \omega)$ and $\phi(k, \omega)$ which is complementary to our fluid form, in which quantities are a function of r and t . This approach will give us collisionless damping contributions to P_R which arise from microscopic processes and are not present in fluid theory.

The method that we will use is that used by Stix for transverse waves.³ Basically, the approach is to form a quantity from the fields, a dielectric tensor, and dispersion relation that has the units of energy density and has a known value (such as zero). Then, consider a small change in plasma parameters and evaluate the change in this quantity. The changes can be identified with power flux, dissipation, etc. to get a conservation equation.

Let the dielectric tensor (a function of \vec{k}) be written in the form

$$\bar{K}(\vec{k}, \omega) = \bar{K}_h + \bar{K}_a \quad (4.37)$$

where \bar{K}_h is the Hermitian (loss-free) part, and \bar{K}_a is the anti-Hermitian (loss or damping) part. (This will facilitate the separation of wave energy from the energy of dissipation).

Consider now a loss-free plasma which satisfies the quasistatic dispersion relation. Poisson's equation may be written, using $\vec{E} = -i\vec{k}\phi$

$$G\phi = 0 \quad (4.38)$$

where

$$G = \frac{\epsilon_0 \omega}{2} \vec{k} \cdot \vec{\bar{K}}_h \cdot \vec{k} \quad (4.39)$$

G is Hermitian, since the plasma is loss free, so the adjoint Poisson equation may be written

$$\phi^* G^\dagger = G \phi^* = 0 \quad (4.40)$$

Now consider a small perturbation of ω , \vec{k} , and the plasma parameters, which may introduce losses, etc. Denoting the quantities of the new state by primes, Poisson's equation here takes the form

$$G' \phi' = 0 \quad (4.41)$$

where G is no longer necessarily Hermitian, since losses may now be present. The linearized relation of \vec{G}' to the old \vec{G} is

$$G' \approx G + \delta\omega \frac{\partial G}{\partial \omega} + \delta\vec{k} \cdot \frac{\partial G}{\partial \vec{k}} + \delta G \quad (4.42)$$

where $\delta\omega$, $\delta\vec{k}$, δG are assumed small. Use this form in Eq. (4.41) and take $\phi^*(4.41) - \phi'(4.40)$ to get

$$\phi^* \vec{k} \cdot \left\{ \delta\omega \frac{\partial G}{\partial \omega} + \delta\vec{k} \cdot \frac{\partial G}{\partial \vec{k}} + \delta G \right\} \cdot \vec{k} \phi' = 0 \quad (4.43)$$

Now we can replace $\phi' = \phi + \delta\phi$ by ϕ in this equation, since this is just neglecting a nonlinear term. We can write G in the form

$$\begin{aligned} \delta G &= \frac{\epsilon_0 \omega}{2} \vec{k} \cdot \delta \vec{\bar{K}}_h \cdot \vec{k} \\ &= \frac{\epsilon_0 \omega}{4} \vec{k} \cdot \left\{ [\delta \vec{\bar{K}}_h - (\delta K_h)^\dagger] + [\delta \vec{\bar{K}}_h + (\delta K_h)^\dagger] \right\} \cdot \vec{k} \end{aligned} \quad (4.44)$$

The first term is anti-Hermitian and represents the losses introduced by our change in plasma parameters. The second term is Hermitian and gives rise to reactive energy terms, which time average to zero. Then

$$\frac{\epsilon_0}{2} |\phi|^2 \left\{ \vec{k} \cdot \left[\frac{\partial}{\partial \omega} (\omega \bar{K}_h) \right] \cdot \vec{k} \delta \omega + \omega \vec{k} \cdot \left[2 \bar{K}_h + \frac{\partial \bar{K}_h}{\partial \vec{k}} \cdot \vec{k} \right] \cdot \delta \vec{k} + \frac{\omega}{2} \vec{k} \cdot \delta \bar{K}_a \cdot \vec{k} + \text{reactive terms} \right\} = 0 \quad (4.45)$$

This is a Fourier transformed version of Eq. (4.31), so we immediately can identify the energy density, flux and dissipation terms in \vec{k} -space:

$$\begin{aligned} U &= -\frac{\epsilon_0}{2} |\phi|^2 \vec{k} \cdot \left[\frac{\partial}{\partial \omega} (\omega \bar{K}_h) \right] \cdot \vec{k} \\ \vec{S} &= -\omega \epsilon_0 |\phi|^2 \left[\vec{k} \cdot \bar{K}_h + \frac{1}{2} \vec{k} \cdot \frac{\partial \bar{K}_h}{\partial \vec{k}} \cdot \vec{k} \right] \end{aligned} \quad (4.46)$$

$$P_R = \frac{\epsilon_0 \omega}{4} \vec{k} \cdot \bar{K}_a \cdot \vec{k} |\phi|^2$$

This new form of the energy conservation theorem for quasistatic waves is quite similar to Stix's form for transverse waves. The difference comes in that the Poynting's vector flux $\vec{E} \times \vec{H}$ of Stix is replaced by the "quasistatic" power flux $\vec{k} \cdot \bar{K}_h |\phi|^2$. We can recover the latter result (approximately) if we replace the \vec{H} in $\vec{E} \times \vec{H}$ by the solution of the $\nabla \times \vec{H}$ Maxwell equation, but not from the \vec{H} in the $\nabla \times \vec{E}$ Maxwell equation.

We may compare this "kinetic" form of the energy conservation equation with the fluid form if we assume a single Fourier component in the

fluid equations. Then we may compare and equate terms. To facilitate this, divide $\bar{\kappa}_h$ up into a cold plasma part and a thermal part:

$$\bar{\kappa}_h = \bar{\kappa}_0 + \bar{\kappa}_T \quad (4.47)$$

Then

$$U_K = \sum_{\alpha} \frac{n_{\alpha} m_{\alpha} \bar{v}_{\alpha}^2}{2} = \frac{-\epsilon_0 |\phi|^2}{2} \vec{k} \cdot \left[(\bar{\kappa}_0 - 1) + \omega \frac{\partial \bar{\kappa}_0}{\partial \omega} \right] \cdot \vec{k}$$

$$U_T = \sum_{\alpha} \frac{\gamma K T_{\alpha} n_{\alpha}}{2 n_0} = \frac{-\epsilon_0 |\phi|^2}{2} \vec{k} \cdot \left[\frac{\partial}{\partial \omega} (\omega \bar{\kappa}_T) \right] \cdot \vec{k}$$

$$\vec{S}_c = \phi^* \vec{J} = -\omega \epsilon_0 |\phi|^2 \vec{k} \cdot (\bar{\kappa}_0 - 1)$$

$$\begin{aligned} \vec{S}_T &= -\frac{\omega \epsilon_0}{2} |\phi|^2 \frac{\partial}{\partial \vec{k}} \left[\vec{k} \cdot \bar{\kappa}_T \cdot \vec{k} \right] \\ &= \sum_{\alpha} \gamma K T_{\alpha} n_{\alpha} \vec{v}_{\alpha} \end{aligned} \quad (4.48)$$

$$P_R = -n_0 \sum_{\alpha} n_{\alpha} \bar{v}_{\alpha} \gamma_{\alpha} = \frac{\epsilon_0 \omega}{4} \vec{k} \cdot \bar{\kappa}_a \cdot \vec{k}$$

with U_E and S_D having the same form as before.

The above set of equations summarizes the relation between the kinetic and dielectric tensor form of the energy conservation theorems, and by dividing up the dielectric tensor into its contributions from species α , we have an expression for the fluid quantities \bar{v}_{α}^2 ,

$n_{\alpha} \vec{v}_{\alpha}$, n_{α}^2 for each species α in terms of ϕ and the dielectric tensor.

We can straightforwardly obtain these quantities for the form of the linearized warm plasma dielectric tensor we used to obtain the forms of ϕ in our model. These are

$$\begin{aligned}
 n_i^2 &= \left(\frac{n_0 e}{m_i} \right)^2 \frac{k_x^2 E_x^2}{\omega^4} \\
 n_e^2 &= \left(\frac{n_0 e}{m_e \omega^2} \right)^2 \left[3 E_z^2 k_z^2 - \left(\frac{\omega}{\omega_{ce}} \right)^4 E_x^2 k_x^2 \right] \\
 \vec{v}_e &= \left(\frac{e}{m_e \omega} \right) \left\{ \frac{\omega^2}{\omega_{ce}^2} E_x \hat{x} + E_z \hat{z} \right\} \\
 \vec{v}_e &= \left(\frac{e}{m_e \omega} \right) \left[E_x \hat{x} + E_z \hat{z} \right]
 \end{aligned} \tag{4.49}$$

A solution of the fluid equations under the approximation in our model for each v_{α} and n_{α} will confirm these relations.

For our purposes, it is more useful to use the kinetic (dielectric tensor) form of the conservation theorem to obtain the power flow and dissipation along the resonance cones, but we would like to get expressions for these as a function of \vec{r} , rather than of \vec{k} , in order to see how these quantities vary along the cone structure. This can be done with the aid of the fluid energy equation. For example, we may write the power flux in the form (in \vec{k} -space):

$$\vec{S}(\vec{k}) = \vec{\alpha}(\vec{k}) |\phi(\vec{k})|^2 \quad (4.50a)$$

where $\alpha(\vec{k})$ may be identified in Eq. (4.46). However, from the fluid equation, the real space form of $S(\vec{r})$ in Eq. (4.34) is

$$\vec{S}(\vec{r}) = \phi^*(\vec{r}) \vec{J}_{\text{tot}}(\vec{r}) + \text{flux of thermal oscillations} \quad (4.50b)$$

where \vec{J}_{tot} is the sum of the real and displacement currents. Writing $\vec{J}_{\text{tot}}(\vec{r})$ in its Fourier transform form

$$\vec{J}_{\text{tot}}(\vec{r}) = \epsilon_0 \omega \int_{-\infty}^{\infty} |\mathbf{K} \cdot \vec{k}| \phi(\vec{k}) e^{i\vec{k} \cdot \vec{r}} d^3\vec{k} \quad (4.51)$$

Now it is easy to see from our derivation of $S(\vec{k})$ from the dispersion relation that when we include the flux due to thermal effects that the appropriate form of $\vec{S}(\vec{r})$ is

$$\vec{S}(\vec{r}) = \phi^*(\vec{r}) \int \vec{\alpha}(\vec{k}) \phi(\vec{k}) e^{i\vec{k} \cdot \vec{r}} d^3\vec{k} \quad (4.52)$$

Now $\phi(\vec{k})$ is proportional to $\delta(k_x - k_{x0})$, where k_{x0} is the appropriate k_x from the dispersion relation for the particular mode of interest and is a function of k_z . Upon doing the k_x integration, we may then do the integration of k_z by considering $\alpha(k_z)$ to be slowly varying and utilizing the familiar saddle point method to get

$$\vec{S}(\vec{r}) = \vec{\alpha}(k_z = k_0) |\phi(\vec{r})|^2 \quad (4.53)$$

where k_0 is the saddle point value of k_z that creates the asymptotic form of ϕ . This expression is valid as long as α does not vary greatly over

the range of k_z that makes a significant contribution to $\phi(\vec{r})$.

Equation (4.53) is a superposition theorem for the power flow in real space. A similar derivation gives a similar result for the dissipated power P_R .

As a final note on these conservation theorems, Eq. (4.46) gives a value for the group velocity of the waves if the plasma is virtually loss free:

$$\vec{v}_g = \frac{\partial \omega}{\partial \vec{k}} \approx \frac{-\omega \vec{k} \cdot \left[2\vec{k}_h + \frac{\partial \vec{k}_h}{\partial k} \cdot \vec{k} \right]}{\vec{k} \cdot \left[\frac{\partial}{\partial \omega} (\omega \vec{k}_h) \right] \cdot \vec{k}} = \frac{\vec{S}_e + \vec{S}_D + \vec{S}_T}{u_E + u_K + u_T} \quad (4.54)$$

This is well defined only for a narrow wavepacket centered around \vec{k} . In our model, the source excites the whole spectrum of k_z , and hence a spectrum of \vec{k} is present. However, in the asymptotic regions of the cone structure, only a narrow spectrum of k_z centered around the saddle point contribute to the field, so that a well-defined \vec{v}_g exists in those regions, and Eq. (4.50) may be used to determine it.

4.3 Energy Flow and Absorption along the Cones

We want to apply the energy conservation equations just derived for quasistatic fields to study the direction and concentration of energy flow along the cone and the (irreversible) absorption of that energy by damping mechanisms.

The expression for the power flux that we obtained (in \vec{k} -space) in terms of the dielectric tensor is given in Eq. (4.46) by

$$\vec{S} = -\omega\epsilon_0 |\phi|^2 \left\{ \vec{k} \cdot \bar{\bar{K}}_0 + \frac{1}{2} \frac{\partial}{\partial k} [\vec{k} \cdot \bar{\bar{K}}_T \cdot \vec{k}] \right\} \quad (4.55)$$

where again $\bar{\bar{K}}_0$ represents the cold plasma part of the dielectric tensor, and $\bar{\bar{K}}_T$ is the thermal part. The dielectric tensor we are using is, of course, given by Eq. (1.11). Thus

$$\vec{k} \cdot \bar{\bar{K}}_T \cdot \vec{k} = -k_x^4 \beta - \frac{3}{2} - \frac{3}{2} \frac{\omega_{pe}^2 v_e^2 k_z^2}{\omega^4} \quad (4.56)$$

$$\vec{k} \cdot \bar{\bar{K}} = k_x K_{\perp} \hat{x} + k_z K_{\parallel} \hat{z}$$

so

$$\begin{aligned} \vec{S} = & -\omega\epsilon_0 |\phi|^2 \left\{ k_x (K_{\perp 0} - 2k_x^2 \beta) \hat{x} \right. \\ & \left. + k_z \left(K_{\parallel 0} - \frac{3k_z v_e^2 \omega_{pe}^2}{\omega^4} \right) \hat{z} \right\} \end{aligned} \quad (4.57)$$

Now the cone is made up of a whole spectrum of k_z , so that this form of the power flux in \vec{k} -space gives rise to a well-defined power flux in

\vec{r} -space only when a narrow spectrum of k_z contributes to the local cone field, which is true in the asymptotic region of the cones, where a narrow spectrum of k_z centered around the saddle point is the primary contribution to the local cone field. In that case we may obtain an approximate form for \vec{S} in \vec{r} -space by using the saddle point value $k_z = k_0$, and of course the form of k_x appropriate for the particular cone we are considering.

When the losses and inhomogeneities in the plasma are small, then the group velocity direction is the same as that of the power flux \vec{S} , seen from Eq. (4.54). Thus the group velocity angle θ is given by

$$\tan \theta = \frac{v_{gx}}{v_{gz}} \approx \frac{S_x}{S_z} = \frac{k_x (K_{\perp 0} - 2k_x^2 \beta)}{k_z (K_{\parallel 0} - \frac{3k_z^2 v_e^2 \omega_{pe}^2}{\omega^4})} \quad (4.58)$$

In the limit of zero temperature, $v_\alpha \rightarrow 0$, this just becomes the cold plasma resonance cone angle. In that limit, the cold plasma X-mode cone angle is, using k_x from Eq. (3.9),

$$\tan \theta \approx \left[\frac{-K_{\perp 0}(x)}{K_{\parallel 0}(x)} \right]^{1/2} \quad (4.59a)$$

while for the ion thermal mode,

$$\tan \theta \approx - \left[\frac{K_{\perp 0}^3(x)}{\beta k_z^2 K_{\parallel 0}(x)} \right]^{1/2} \xrightarrow{v_\alpha \rightarrow 0} \infty \quad (4.59b)$$

In the strict limit $v_\alpha \rightarrow 0$, the ion thermal cone does not exist, as the

wavelength and damping length goes to zero, but if we let $v_\alpha \rightarrow \epsilon_\alpha$, where ϵ_α is a very small value, then a resonance cone for the ion thermal mode exists with cone angle $\theta \approx \pi/2$ which is very highly damped when $\omega \gg \omega_{\text{LH}}(x)$. Of course as $\omega \rightarrow \omega_{\text{LH}}(x)$, then $K_0 \rightarrow 0$ and $\theta \rightarrow 0$, which is to be expected because at the point of mode conversion v_g must be parallel to the field, since that is where the incoming cone turns around to propagate back out of the hybrid layer.

For the X-mode the warm plasma group velocity angle is

$$\tan \theta = \left[\frac{K_{10} - (K_{10}^2 + 4\beta k_z^2 K_{110})^{1/2}}{2\beta k_z^2} \right] \frac{(K_{10} + 4\beta k_z^2 K_{110})^{1/2}}{(K_{110} - \frac{3k_z^2 v_e^2 \omega_{pe}^2}{\omega^4})} \quad (4.60)$$

Since $K_0 \rightarrow 0$ is our propagating region, we see that θ is everywhere decreased to a smaller value from its value for a cold plasma by thermal effects. In cold plasma theory the cone starts out at $\theta = \pi/2$ at the plasma frequency layer $\omega = \omega_{pe}(x)$ near the boundary. However, for the warm plasma every narrow k_z -packet along the warm plasma resonance cone starts out at angle

$$\tan \theta \sim \frac{\omega^2}{k_z v_e \omega_{pe}(x)} \sim \frac{\omega}{k_z v_e} \quad (4.61)$$

which is large, since $k_z v_e \ll \omega$, so θ is slightly smaller than $\pi/2$, with the deviation from $\pi/2$ increasing with electron temperature and with k_z . From our discussion about the saddle point value of increasing the distance from the cold plasma cone line, this means not only is the

main peak shifted from the $\theta = \pi/2$ of the cold plasma cone to a smaller angle, but the second peak is shifted to an even smaller angle, the third peak is smaller than that, etc. This explains from the standpoint of group velocity why the resonance cone structure spreads out as it moves away from the source.

As the cone moves far away from the plasma layer, but before it reaches the lower hybrid layer, i.e., for $\omega_{pe}(x) \gg \omega \gg \omega_{lh}(x)$, the cone angle is given by

$$\tan \theta \approx \left[\frac{K_{10} - (K_{10}^2 + 4\beta k_z^2 K_{110})^{1/2}}{2\beta k_z^2} \right] \frac{(K_{10}^2 + 4\beta k_z^2 K_{110})^{1/2}}{\left(K_{110} - \frac{3k_z^2 V_0^2 \omega_{pe}^2(x)}{\omega^4} \right)} \quad (4.62)$$

Thus the group velocity angle decreases as the density increases, with the second thermal factor causing θ to decrease with k_z as before. Thus the peaks of the cone structure move increasingly along the magnetic field and continue to spread out as they move into the plasma. The cone peaks move into the hybrid region $\omega \lesssim 3\omega_{lh}(x)$ at an angle

$$\tan \theta \sim \theta \sim \frac{\omega}{\omega_{pe}(x)} \sim 1/14 \quad ((4.63)$$

The peaks become parallel to the field, i.e., $\theta \rightarrow 0$ at the mode conversion point where $k^2 = -4\beta k_z^2 K_{11}$ which is a function of k_z , with the higher the k_z the greater the distance from the lower hybrid layer $x - x_{h1}$, i.e., the lower the density at which mode conversion of that component occurs. This means the highest order peaks of the cone undergo

mode conversion first at the lowest density, with the main peak undergoing conversion at the highest density nearest the hybrid layer. Indeed, each of the k_z components undergoes mode conversion onto the ion thermal mode at different positions, and the net result of the whole spectrum of such k_z is a mode conversion of the cone structure, with the oscillatory structure of the X-mode cone connecting onto a similar oscillatory structure of a mode of a completely different character.

For the ion thermal cone, the group velocity angle is given by

$$\tan \theta \approx \frac{\left(K_{\perp 0} + [K_{\perp 0}^2 + 4\beta b_z^2 K_{\parallel}]^{1/2} \right)^{1/2}}{2\beta b_z^2} \frac{(K_{\perp 0}^2 + 4\beta b_z^2 K_{\parallel})^{1/2}}{\left(K_{\parallel 0} - \frac{3b_z^2 v_e^2 \omega_{pe}^2}{\omega^4} \right)} \quad (4.64)$$

This angle starts out at $\theta = 0$ (parallel to the magnetic field) at the mode conversion point $K_{\perp 0}^2 = -4\beta k_z^2 K_{\parallel}$ and becomes negative for a smaller density than the mode conversion density, because the group velocity of the wave has turned around and is now pointing away from the hybrid layer (v_{gx} is now negative while v_{gz} is still positive). As the cone moves out of the hybrid region where $\omega \gtrsim 3\omega_{\text{LH}}(x)$,

$$\tan \theta \approx \frac{-\omega}{k_z \sqrt{\beta} \omega_{pe}^2} \sim \frac{-\omega^3}{k_z v_e \omega_{pi} \omega_{pe}} \quad (4.65)$$

Thus in this region the magnitude of $\tan \theta$ is much greater than one, so

θ is rather large and somewhat less than $\pi/2$, with the angle decreasing in magnitude as k_z increases for a given x . This is to be expected, since the higher k_z components undergo conversion at a lower density, and thus have had less distance to "turn around" from a group velocity parallel to the field to one perpendicular to it. Thus for a given x , the higher order peaks are aligned more along the field than the primary peak. As the cone moves toward lower density (smaller x) the cone angle continues to increase and asymptotically approaches $-\pi/2$, with the smallest k_z components approaching it the most rapidly. Thus the whole ion thermal cone structure comes out of the hybrid layer almost perpendicular to the field.

In Fig. 4.1 the group velocity angle θ_0 is shown as a function of $\omega_{\text{LH}}(x)/\omega$. It is seen that as the incoming wave gets far away from the plasma frequency layer, all of the k_z components move at the same small angle. Thus the whole cone goes into the hybrid layer with a well-defined group velocity angle. After mode conversion, all of the k_z for a given x travel at a slightly different angle, but as the outgoing wave gets far away from the hybrid layer, the whole cone again moves in a well-defined group-velocity angle $\theta_0 \approx \pi/z$.

We would also like to evaluate the magnitude as well as the direction of the power flux. This is well defined in the asymptotic region of the cone, where we can use the superposition theorem given by Eq. (4.49). The form of $\alpha(\vec{k})$ from the dielectric tensor used in our model is

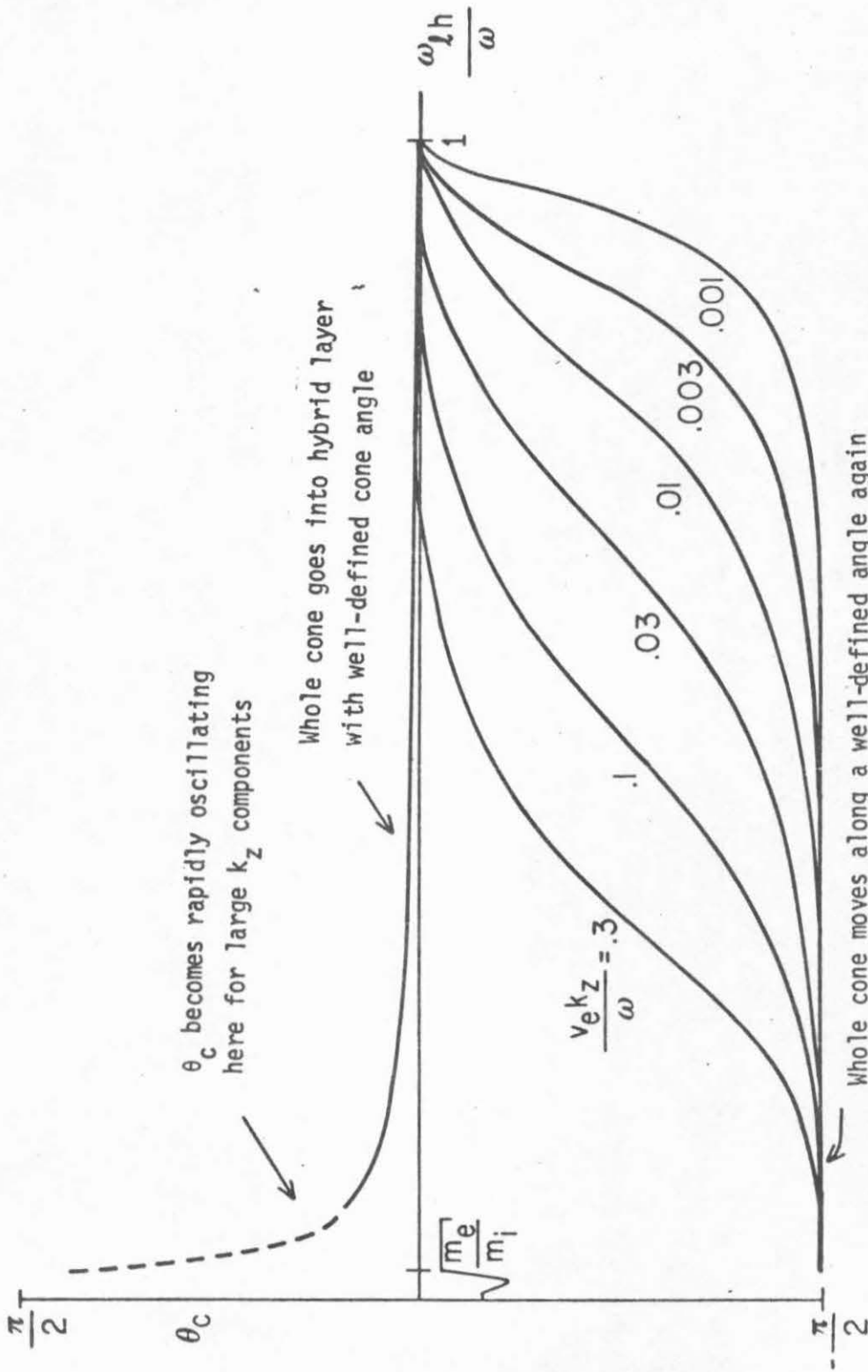


Fig. 4.1 Graph of power flux or group velocity angle vs. normalized density for small spectrum of k_z centered around the k_z indicated. $\theta_c > 0$ for the incoming mode, and $\theta_c < 0$ for the converted mode.

$$\begin{aligned} \vec{\alpha}(\vec{h}) &= -\omega \epsilon_0 \left[\vec{h}_0 \cdot \vec{K}_h + \frac{1}{2} \vec{h}_0 \cdot \frac{\partial \vec{K}_h}{\partial \vec{h}} \cdot \vec{h} \right] \\ &= -\omega \epsilon_0 \left\{ k_x (K_{10} - 2k_x^2 \beta) \hat{x} + k_z \left(K_{110} - \frac{3k_z^2 v_e^2 \omega_{pe}^2}{\omega^4} \right) \hat{z} \right\} \end{aligned} \quad (4.66)$$

For the incoming mode, the components of k at the saddle points are

$$k_z = k_0 = \left\{ \frac{z - g_1(x)}{[3q_1(x)]^{1/3}} \right\} \quad k_x = \left[\frac{-K_{11}}{K_{10}} \right]^{1/2} |k_z| \quad (4.67)$$

so we obtain

$$\begin{aligned} \vec{S}(\vec{r}) &\approx \omega \epsilon_0 \left| F \left(\frac{z - g_1(x)}{[3q_1(x)]^{1/3}} \right) \right|^2 \left[\frac{z - g_1(x)}{3q_1(x)} \right]^{1/2} x \\ &\quad \times \left\{ [-K_{110} K_{10}]^{1/2} \hat{x} + K_{110} \hat{z} \right\} \end{aligned} \quad (4.68)$$

where we have neglected the small thermal terms in the curly brackets (valid in region away from the hybrid layer), and $|F(\zeta)|^2 = \text{Ai}^2(\zeta) + \text{Gi}^2(\zeta)$. This form shows that the maxima in power flow occur at the field maxima and the minima at the minima of the field. If we consider the power flow for fixed x, it is proportional to

$$|S(\vec{r})| \sim \zeta^{1/2} |F(\zeta)|^2 \quad (4.69)$$

where $\zeta = [z - g_1(x)]/[3q_1(x)]^{1/3}$. Then the relative power flow along the

maxima and minima are summarized in the following table:

	ζ	$ F(\zeta) $	$\zeta^{1/2} F(\zeta) ^2 \sim S(\vec{r})$
First maximum	1.83	.60	.486
Second maximum	5.47	.425	.422
Third maximum	7.82	.375	.394
First minimum	4.10	.32	.210
Second minimum	6.83	.30	.237
Third minimum	9.05	.29	.253

Table 9. Field magnitudes and power flow magnitudes compared for the maxima and minima on the cones

The table shows that the power flow density along the peaks falls off slowly with increasing order of the maxima, much more slowly than the square of the potential falls off with peak order. We also see, somewhat surprisingly, that the power flux along the minima of the cone increases with increasing order of the minima, or increasing distance from the cold plasma cone line. Thus the power flow density smooths out with increasing distance from the cold plasma cone line, since the disparity between the local maximum and minimum of power flux decreases.

For the outgoing ion thermal mode we have for k_x and the saddle point value of k_z ,

$$k_x \approx \left[\frac{K_{10}(x)}{\beta(x)} \right]^{1/2}, \quad k_z = k_0 \approx \frac{z - g_1(x_{h1})}{2[p(x_{h1}) - p(x)]} \quad (4.70)$$

We thus obtain

$$\vec{S}(\vec{r}) = \frac{\omega \epsilon_0}{2[p(x_{h1}) - p(x)]} \left| D^{-1/2} \left[\frac{z - g_1(x_{h1})}{\sqrt{2[p(x_{h1}) - p(x)]}} \right] \right|^2 \\ \times \left\{ - \left[\frac{K_{10}(x)}{\beta(x)} \right]^{1/2} \hat{x} + \frac{[z - g_{1,z}(x_{h1})] K_{110}(x)}{2[p(x_{h1}) - p(x)]} \hat{z} \right\} \quad (4.71)$$

The component along \hat{x} is large compared with the \hat{z} component near the cold plasma cone line except for x near the hybrid layer, but the \hat{z} component increases with distance from the cold plasma cone line, while the \hat{x} component does not, for given x . Also for given x , the power flow density is proportional to the square of the potential. Thus the power flux at the maxima (and minima) of the potential falls off approximately as the square of the potential (ignoring the small \hat{z} -component), with the magnitude of this flux density in general increasing as x decreases (as the cone moves to lower density); the \hat{x} component of flux increases with decreasing x , while the z component decreases with decreasing x , for a given point on the cone, i.e., for fixed

$$\zeta = \frac{z - g_1(x_{h1})}{\sqrt{2} [p(x_{h1}) - p(x)]^{1/2}} \quad (4.72)$$

The approximate relative magnitude of the power flux along the maxima and minima of the ion thermal cones is summarized in the following table:

	ζ	$ D_{-1/2}(i^{3/2}\zeta) ^2 \sim S(\vec{r})$
First Maximum	1.55	3.06
Second Maximum	4.0	1.49
Third Maximum	5.15	1.12
Fourth Maximum	6.2	0.05
First Minimum	3.1	.05
Second Minimum	4.6	.04
Third Minimum	5.85	.04
Fourth Minimum	6.9	.04

Table 10. Relative power flux density along maxima and minima of ion thermal resonance cones

We see that the power flux density along the peaks of the cone falls off rather rapidly with increasing order of the peak, while the power flux along the valleys stays approximately constant. This is in contrast to the power flow magnitudes deduced along the peaks and valleys of the X-mode cone, in that the ion thermal cone has a greater portion of the power flow concentrated near the mean peak than the X-mode cone.

It should be noted that the calculated power flow along the cones is for a point source, which is a reasonable approximation for a very small source. But we can see how these calculations are modified

for a finite source from the previous analysis (Chapter II) which we made for finite sources. For a finite source the thermal wave is more subdued and the secondary maxima are of smaller amplitude, while the main peak itself is broadened. This would mean that more energy flow is concentrated along the main peak, but this main peak energy flow will be spread out to an extent determined by the source size.

The energy flow along the maxima and minima of the cone that has tunneled through a thin evanescent layer is summarized in Table 11. This shows that the power flux magnitude along the tunneled cone maxima fall off more rapidly with the order of the maxima than it did for the source cone. This means more power is concentrated along the main peak, although the main peak will be spread out.

	ζ_r	$ F(\zeta) $	$(-\zeta)^{1/2} F(\zeta) \sim S(\vec{r})$
First Maximum	-1.83	2.6	3.51
Second Maximum	-5.47	0.9	2.10
Third Maximum	-7.82	0.6	1.68
First Minimum	-4.10	0.2	.40
Second Minimum	-6.82	0.2	.51
Third Minimum	-9.05	0.2	.60

Table 11. Relative field and power flow along cones that tunneled through evanescent layer of $\mathcal{G}(x_{h2}) = [3q_1(x_{h1})]^{1/3}$

The power absorption in \vec{k} -space was found to be

$$\begin{aligned}
 P_R(\vec{k}) &= \frac{\epsilon_0 \omega |\phi|^2}{4} \vec{k} \cdot \vec{K}_0 \cdot \vec{k} = \frac{\epsilon_0 \omega |\phi|^2}{4} \{k_x^2 \text{Im} K_{\perp} + k_z^2 \text{Im} K_{\parallel}\} \\
 &= \frac{\epsilon_0 \omega |\phi|^2}{4} \left\{ \frac{\nu_i \omega_{pi}^2(x) b_x^2}{\omega^3} + \frac{2 \omega_{pi}^2 \omega_{ci}^3}{\omega b_z b_x^3 \nu_i^4} e^{-\omega^2 / b_x^2 \nu_i^2} \right. \\
 &\quad \left. \times \sum_n n^2 e^{-\frac{(\omega - n \omega_{ci})^2}{k_z^2 \nu_i^2}} + \frac{\nu_e \omega_{pe}^2(x) b_z^2}{\omega^3} + 2 \sqrt{\pi} \left[\frac{\omega_{pe}^2(x) \omega}{b_z \nu_e^3} \right] e^{-\frac{\omega^2}{b_z^2 \nu_e^2}} \right\}
 \end{aligned}
 \tag{4.73}$$

We can make an argument quite similar to the one we did for the power flux, that we can get an expression for $P_R(\vec{r})$ in real space (in the asymptotic region of the cone potential) by replacing $\phi(\vec{k})$ by the real space $\phi(\vec{r})$, and evaluating the coefficient $k_x^2 \text{Im} K_{\perp} + k_z^2 \text{Im} K_{\parallel}$ at the appropriate k_x for the mode and at the saddle point value $k_z = k_0(x, z)$ of the potential. Thus for the X-mode the power absorption density is

$$\begin{aligned}
 P_R(\vec{r}) &\cong \frac{\epsilon_0 \omega |F(x)|^2}{4 [q_1(x)]^{2/3}} \left\{ \frac{\nu_i \omega_{pi}^2(x) K_{110}(x) b_0^2}{\omega^3 K_{10}(x)} \right. \\
 &\quad + \frac{2 \omega_{pi}^2 \omega_{ci}^3 K_{10}^{1/2}}{\omega b_0^2 \nu_i^4 K_{110}^{1/2}} \sum_n n^2 e^{-\frac{(\omega - n \omega_{ci})^2}{k_0^2 \nu_i^2}} + \frac{\nu_e \omega_{pe}^2(x) b_0^2}{\omega^3} \\
 &\quad \left. + 2 \sqrt{\pi} \left(\frac{\omega_{pe}^2(x) \omega}{b_0 \nu_e^3} \right) e^{-\frac{\omega^2}{b_0^2 \nu_e^2}} \right\}
 \end{aligned}
 \tag{4.74}$$

with k_0 given by Eq. (4.67), and for the ion thermal mode

$$\begin{aligned}
 P_R(\vec{r}) \approx & \frac{\epsilon_0 \omega |D - \frac{1}{2}(i^{3/2} f)|^2}{4 [\rho(\chi k_i) - \rho(\chi)]} \left\{ \frac{\nu_i \omega_{pi}^2(\chi) K_{L0}(\chi)}{\omega^3 \beta(\chi)} \right. \\
 & + \frac{2\omega_{pi}^2(\chi) \omega_{ci}^3}{\omega k_0^4 \nu_i^4} \left(\frac{\beta(\chi)}{K_{L0}(\chi)} \right)^{3/2} \sum_n n^2 e^{-\frac{(\omega - n\omega_{ci})^2}{k_z^2 \nu_i^2}} + \frac{\nu_e \omega_{pe}^2 k_0^2}{\omega^3} \\
 & \left. + 2\sqrt{\pi} \left(\frac{\omega_{pe}^2(\chi) \omega}{k_0 \nu_e^3} \right) e^{-\omega^2/k_z^2 \nu_e^2} \right\} \quad (4.75)
 \end{aligned}$$

with k_0 given by Eq. (4.70). These forms can be compared with the damping rates of the cone potential $d\Gamma/dx$ given in Eq. (4.22) and (4.18), and confirms from the standpoint of energy absorption many of the conclusions drawn from a study of the damping. We see that the term in the braces in both forms of $P_R(\vec{r})$ are directly proportional to the corresponding $d\Gamma/dx$, which gives rise to such properties deduced as the fact that on the X-mode the relative portion of the absorbed energy that goes into the ions over that to the electrons continuously increases as the mode goes in, and that this continues to increase after mode conversion and as the ion thermal mode comes out, so that at some point ion damping begins to totally dominate over electron damping.

By comparing the equations for $P_R(\vec{r})$ and $d\Gamma/dx$, we see the relation

$$P_R(\vec{r}) = \frac{\epsilon_0 \omega |D - \frac{1}{2}(i^{3/2} f)|^2}{4} \left[\frac{K_{L0}^3(\chi)}{\beta(\chi)} \right]^{1/2} \frac{d\Gamma(\chi, z)}{dx} \quad (4.76)$$

for the ion thermal mode, and

$$P_R(\vec{r}) = \frac{\epsilon_0 \omega |F(\beta)|^2}{2 [3q_1(x)]^{2/3}} \left[\frac{-K_{110}^3(x)}{K_{10}(x)} \right]^{1/2} k_0 \frac{d\Gamma(x, z)}{dx} \quad (4.77)$$

for the X-mode. It should be noted that for each cone, $d\Gamma/dx$ increases in severity with the distance from the cold plasma cone (usually at a more rapid rate for the X-mode cones than for the ion thermal cone), while the square of the potential at the peaks steadily decreases with distance. Thus the product of these two quantities, which gives $P_R(\vec{r})$ will have a maximum value at or near some peak, and this peak will not necessarily be the primary peak.

CHAPTER V: SUMMARY AND CONCLUSIONS

The structure of the quasistatic warm plasma resonance cones excited by a point gap source (which yields the Green's function for finite gap-type sources) in an inhomogeneous magnetized bounded slab plasma was calculated and elucidated in this thesis. First, we obtained the structure of the multiply-reflected warm plasma resonance cones for a homogeneous or slightly inhomogeneous slab plasma with no turning points in order to study the basic structure and properties of resonance cones in the model that we chose (because it has many of the features of bounded plasmas created in the laboratory) and to contrast it with the guided wave description of the fields of that model. We then generalized this to the case that two (symmetric) lower hybrid resonance turning points exist in the inhomogeneous plasma, which is a case of interest to lower hybrid heating, and deduced the manner in which mode conversion of the cones occurs, the structure of the resonance cones in our model for this case, and properties of the cones such as damping and energy flow along them.

In the general analysis of the warm plasma resonance cone structure in our model, we generalized a previous result by R. Gould that the potential in a slab model can be found as a sum of multiply-reflected resonance cone singularities to include warm plasma effects, collisional and collisionless damping, and inhomogeneities in the plasma. The potential was obtained as a sum of warm plasma resonance cones, each of which has a similar cross-sectional structure but a different size, amplitude, and position. This characteristic

structure was seen to be a form that is well-known from previous study of resonance cones in a warm plasma: an exponentially decaying tail on the large angle side of the "cold plasma cone line" and an oscillatory structure with a primary maximum and other secondary (smaller amplitude) maxima on the small angle side. (Recall, e.g., Fig. 2.3.) Each cone potential was shown to be decomposable in the asymptotic region into a cold plasma Coulomb-like cone and a thermal wave which interfere to cause the oscillating structure.

An important new result was the revelation of an interference between nearby multiply-reflected cones, which is most important near the boundaries, and which arises because the warm plasma resonance cones are of finite extent, so that their structures overlap. This interference was seen to take on two different forms. When the two cones are sufficiently separated and distinct, the interference takes on the form of a small high frequency modulation of one of the cones by its neighbor. This was identified as the interference of the thermal wave (with a rapidly oscillating phase) of one cone with the second (primarily with the cold plasma contribution to that cone). However, when the cones come very close together, as they do near the boundaries, the two individual cones no longer are distinguishable, and the two cones together form a single interference pattern that is different than the structure of either cone.

It was shown that in general the resonance cones are relatively localized structures near the source, but spread out and decrease in amplitude as they propagate away from the source and undergo multiple reflections from the boundary. (The cones reflect per-

fectly off of the boundaries with a π phase shift in the cone field for an infinitely conducting boundary, but undergo a loss of amplitude and a different phase shift for reflection off of a finite conductivity surface.) Thus the higher order cones become increasingly less localized and interference becomes greater, so individual resonance cones become harder to distinguish, as several cones may contribute to the field at a given point. Thus the resonance cone point of view is not as useful far from the source. This was compared with the complementary guided wave form, in which an infinite number of the (nonlocal) modes contribute to the fields near the source, but damping causes the highest order modes to decay away rapidly from the source, so that the far field is made up only of the lowest order modes. A conclusion that was drawn was that the resonance cone form is the most useful for the relatively near field solutions, where the electrostatic approximation is best, but that the guided mode form may be more useful in the far field, where the electrostatic approximation begins to break down.

The quantitative dependence of the cone structure width and shift in cone angle on position, cone order, and plasma temperature was determined. The dependence on the last quantity was the same as that found by Fischer and Gould² and others for a point charge source. The dependence on the other quantities is a new result for our model, and was expressed in a form that could be compared to previous results through the use of an "effective vertical distance from the source".

An asymptotic analysis of the damping of the resonance cones for the homogeneous case revealed that a decay of the fields is produced

on the "propagating side" of the cold plasma resonance cone line (i.e. on the small angle side, where the oscillatory structure is), with the important conclusion that the rate of decay increases with the distance from the cold plasma cone line; thus the higher order maxima of the cone decay away faster than the primary maximum. On the "evanescent side" of the cone, damping merely introduces a phase change in the potential. It was seen that Landau damping was quite small for the frequencies far above the lower hybrid considered, except for the very high order peaks of the cone. Collisional damping was found to decrease with increasing temperature, for fixed collision frequencies, in contrast to Landau damping, which increases with increasing temperature.

Our warm plasma resonance cone picture was generalized to find the potential for our model for an inhomogeneous plasma with lower hybrid resonance layers present. It was found that the resonance cone method is much more useful than the guided wave approach in this case for several reasons: the resonance cone form is easier to calculate in analytic form; the hybrid layer in the plasma interior causes the cones to be strung out along the background magnetic field so that there is little overlap or interference between the individual cones, and the field at a given point usually has significant contribution only from a single cone; and, the presence of an evanescent layer between the lower hybrid layers causes the higher order cones to be significantly reduced in amplitude, so that only the lowest order resonance cones need be considered, unlike the case of a guided wave solution.

An important result of this calculation was the demonstration that the potential in our model with lower hybrid layers present could be solved as an infinite sum of multiply-reflected, multiply-tunnelled warm plasma X-mode and ion thermal (mode converted) resonance cones, the cross-section of the potential of each of which has a characteristic structure which is qualitatively the same as that discussed above for warm plasma resonance cones in general. The higher order cones, which have undergone tunnelling through the evanescent layer, are considerably reduced in amplitude, so that the effectively infinite sum of cones can be quickly truncated at some low order. The potential as a sum of resonance cones was summarized by a diagram scheme in Tables 7-8.

An interesting new conclusion was that the cones maintain the general structure characteristic of warm plasma resonance cones upon tunnelling through the evanescent layer. If the layer is thin, i.e. the cones may tunnel through the evanescent layer, and warm plasma "evanescent cones" may exist in this layer. The effect of the evanescent layer was seen to be a decay in the cone amplitude, with the parts of the cone structure that are the farthest from the cold plasma cone line decaying the fastest. (The decay rate at a given point increases with the distance from the cold plasma cone line.) Thus the secondary peaks become more subdued relative to the main peak, and the main peak is broadened and shifted closer to the cold plasma cone line. This is caused by the rapid decay of the thermal contribution to the cone in that layer. For a thick enough layer the thermal wave decays away and

the secondary peaks disappear, while the main peak broadens and eventually becomes so diffuse that the term resonance cone loses its meaning.

Another new aspect of this work was the obtaining of the transformation properties across back-to-back lower hybrid layers. The problem of mode conversion at the lower hybrid has been treated before by several investigators: Rabenstein³⁵ solved the basic mathematical problem involved, and Stix¹² solved the physical problem of mode conversion, which is an application of the mathematical solution of the differential equation involved. Fig. 3.5 summarizes the linearly independent mode conversion solutions, one of which is well-known, and three of which are hard to find in the literature, although all four can be obtained by finding appropriate linear combinations of the solutions in Rabenstein. However, the obtaining of the transformation properties across back-to-back hybrid layers is a new result. The cone solutions we obtained are valid for any evanescent layer thick enough so the conjugate regions do not overlap for the k_z that satisfy our small thermal velocity approximation.

Mode conversion of the resonance cones has been discussed previously, e.g. by Simonutti,¹⁸ Bellan and Porkolab⁸, and Ko and Kuehl²⁰, who point out that the individual k_z components undergoing mode conversion recombine to form an outgoing cone. However, by combining the structure of our solutions with the group velocity analysis, we can give a picture as to why the whole cone undergoes conversion, i.e. why the general cone structure is maintained.

The incoming cone approached the hybrid layer so that the various

maxima and minima of the cone approach parallel movement to the magnetic field, so that the distance from the cold plasma cone line on a perpendicular cross-section of the cone just becomes the distance from the lower hybrid layer. But we determined that the local saddle point value of k_z on the cone increases with the distance from the cold plasma cone line, and also that the higher the particular k_z component of the wave, the further from the lower hybrid at which that component undergoes mode conversion. Thus the whole narrow spectrum of k_z making up, say, a given peak on the cone, undergoes conversion within a narrow region, and in general the peak as a whole undergoes mode conversion, with the distance of the mode conversion of the peak from the lower hybrid layer increasing with the order of the peak. The highest order peaks convert first far away from the hybrid layer, and the main peak converts last very near the hybrid layer, and this causes the whole cone to turn around.

The form of the resonance cone fields that we obtained when lower hybrid layers are present in the plasma reveals various features about the way the cones transform across the hybrid layers and evanescent region, which is supplemented by the group velocity analysis. The incoming X-mode cone moves into the layer almost parallel to the field, and bifurcates into an ion thermal cone, which moves back out of the hybrid layer on the propagating side, and X-mode and ion thermal evanescent cones which move into the evanescent layer. The ion thermal cone on the propagating side is almost perpendicular to the field. The "cold plasma cone line" for this cone does move perpendicular to B_0 ,

but the group velocity analysis shows the cone propagates almost perpendicular to B_0 , asymptotically approaching perpendicular as it moves far away from the hybrid layer, with the main peak moving the closest to perpendicular to B_0 for a given x .

The X-mode cone that continues into the evanescent layer moves in a perpendicular sense, i.e. with a cold plasma cone line perpendicular to \vec{B}_0 and decays away, with the higher order peaks decaying faster. The basic cone nature is preserved if the layer is thin, and the cone bifurcates at the second hybrid layer, producing both an X-mode and an ion thermal cone propagating out of the hybrid layer on the propagating side. They come out initially along \vec{B}_0 , but the latter rapidly turns to propagate almost perpendicular to \vec{B}_0 .

Some important conclusions about the damping of these resonance cones were also reached by the inclusion of a small amount of ion and electron collisional, electron Landau, and ion cyclotron harmonic damping. One new result was that all forms of the damping on the incoming X-mode cone increase with the distance from the cold plasma cone line, (as noted above), while on the ion thermal cone all forms of damping increase with the distance from the cold plasma cone line, except for ion collisional damping, which was seen to cause a uniform decay over the whole cone structure. It was also found that collisionless damping is not very important on the incoming mode in most cases, except for the higher order peaks of the cone and sometimes very near the hybrid layer, where ion cyclotron harmonic damping may become important when the source frequency is sufficiently close to a cyclotron harmonic. This confirms and extends Simonutti's result obtained by numerical methods, that collisionless

damping is usually not very strong on the incoming mode. Our analysis shows electron collisional damping to usually be the most important mechanism far away from the hybrid layer, with ion collisional damping becoming important or dominating near the hybrid layer, for typical collisional plasmas for this mode. The results are in general agreement with the study of collisional damping on the incoming mode made by Bellan and Porkolab¹⁹, who concluded that for typical collisional plasmas the collisional damping may be sufficient to absorb most of the energy of the incoming near the lower hybrid layer. However, our results suggest that for the small localized sources considered in this work, this is true only for the secondary peaks of the cone, so that there may still be some of the main peak that reaches the mode conversion point and converts to the outgoing mode. On the outgoing mode our analysis suggests that ion collisional damping is the most important mechanism near the hybrid layer with cyclotron harmonic damping being strong on the higher order peaks. Simonutti concluded from the numerical computation of collisionless damping that harmonic damping may be quite important for this mode. Our results agree with this and further imply that this becomes the dominant mechanism far away from the hybrid layer if the mode propagates that far before completely damping out.

Energy conservation theorems were derived for quasistatic fields and used to analyze the energy flow and absorption along the cones. The form of power absorption by the various damping mechanisms confirmed the conclusions we drew based on the form of the damping calculated on the cone fields; a relation between the energy absorption

rates and the damping rate was derived. For the X-mode cone it was found that the power flow along the peaks falls off rather slowly with increasing peak order, while that along the valleys unexpectedly increases with the order or distance from the cold plasma cone line. For the ion thermal cone, however, the power flow along the peaks was seen to fall off more rapidly with peak order, while the power flow along the valleys remains relatively constant, so that there is a greater concentration of the power flow near the main peak for the ion thermal cone than for the X-mode cone.

As a final note on the cone-potential structure, most experiments studying the structure tend to see secondary maxima that are considerably smaller than the main peak, although some experiments, such as that of Gonfalone⁴, see more pronounced secondary peaks. The simple model of undamped cones from a point source predicts secondary maxima that are only moderately smaller than the primary maxima, although the theory predicts a faster falloff of the peak magnitude for a charge source than for the gap source used here. However, three mechanisms which would modify this prediction when included in the model were studied: finite source size, damping, and the presence of evanescent layers. All of these factors will subdue the secondary maxima relative to the main peak, and it is probably primarily finite source effects in combination with some small contributions from the other two mechanisms that account for the experimentally observed structure.

Suggestions for Further Work

The most obvious area in which further work on this general problem is needed is the experimental area. There have been experiments measuring the X-mode resonance cones, and experiments in which absorption of the incoming wave at the lower hybrid layer occurred, sometimes but not always accompanied by measurable particle heating, but there has not been any positive identification of mode conversion as the heating or absorption mechanism or measurements of the ion thermal cone coming out of the hybrid layer. The theory presented in this work and by other researchers suggests that observation of the ion thermal cone should be possible (although probably only the main peak) in plasmas with sufficiently low ion collision frequency, and may prove to be useful in an experimental determination as to whether mode conversion is an important process in lower hybrid heating, or whether it is observable or dominated by other mechanism such as parametric instabilities and nonlinear effects.

On the theoretical side, a useful extension of this work would be to look at the same problem with an inhomogeneous magnetic field, the inclusion of which would more closely model a tokamak geometry. (Periodic boundary conditions in the z direction would also be necessary.) In that case the group velocity and resonance cone trajectory is more complicated. In addition, with an inhomogeneous magnetic field, there will most probably be a layer between the lower hybrid layer and the boundary where the source frequency ω becomes equal to some harmonic of the ion cyclotron frequency, and the ion thermal mode may undergo mode conversion again at this layer onto a (higher'

order) ion Bernstein mode, which turns around and propagates back into the interior of the plasma. However, as this layer is approached, ion cyclotron harmonic damping becomes great and the actual analytic form of the damping very near this layer is not known, so that it is not clear how much of this wave is absorbed by cyclotron damping and how much by the second mode conversion process.

Other extensions of the present work include the inclusion of parametric and nonlinear ponderomotive force effects in our model, which may be important for sufficiently large fields excited by the source.

APPENDIX A: TABLE OF NOTATION

$\omega_{p\alpha}$	plasma frequency for species α (ions or electrons)
$\omega_{c\alpha}$	cyclotron frequency for species α
$v_{\alpha} = (2kT_{\alpha}/m_{\alpha})^{1/2}$	thermal velocity for species α
$\phi(x, z)$	potential of wave field
$\tilde{\phi}(x, k_z)$	Fourier transform of ϕ in z
\bar{K}	dielectric tensor of plasma
K_{\parallel}	parallel component of dielectric tensor
K_{\perp}	perpendicular component of dielectric tensor
θ_c	resonance cone angle
$\alpha(k_z) k_z $	value of k_x for X-mode for homogeneous plasma [Eq. (2.11)]
D	cold plasma part of α
$E k_z^2$	thermal part of α
$a_i^{(j)}$	coefficient of the i th solution in region j
$ k_z g_1(x)$	phase of the X-mode from $x=0$ to x [Eq. (3.20)]
$h_1(x)$	phase of ion thermal mode from 0 to x [Eq. (3.20)]
$ k_z g(x)$	exponent of X-mode from x_{h1} to x [Eq. (3.25)]
$\mathcal{A}(x)$	exponent of ion thermal mode from x_{h1} to x [Eq. (3.25)]
$ k_z g_2(x_{h1})$	phase of X-mode from x_{h2} to x [Eq. (3.30)]
$h_2(x)$	phase of ion thermal mode from x_{h2} to x [Eq. (3.30)]
$ k_z ^2 q_1(x)$	thermal corrections to $g_1(x)$ [Eq. (3.21)]
$ k_z ^2 p_1(x)$	thermal corrections to $h_1(x)$ [Eq. (3.21)]
$ k_z ^2 \mathcal{P}(x)$	thermal corrections to $g(x)$ [Eq. (3.27)]
$ k_z ^2 \mathcal{Q}(x)$	thermal corrections to $\mathcal{A}(x)$ [Eq. (3.27)]
$ k_z ^2 q_2(x)$	thermal corrections to $g_2(x)$ [Eq. 3.31]]

- $|k_z|^2 p_2(x)$ thermal corrections to $h_2(x)$ [Eq. (3.31)]
- $\overline{M}^{(J)}$ transfer matrix from region J-1 to J [Eq. (3.)]
- γ inverse scale length of density gradient at the hybrid layers [Eq. (3.33)]
- $A(x), B(x)$ slowly varying factors of the WKB forms of the X-mode and ion thermal mode potential, respectively [Eq.(3.19)]
- $U = |k_z| g_1(x_{h1})$
- $V = h_1(x_{h1})$
- $P = |k_z| g(x_{h2})$
- $Q = \mathcal{A}(x_{h2})$
- $W = |k_z| g_2(a)$
- $Y = h_2(a)$
- $F(\zeta) = Ai(\zeta) - iGi(\zeta)$ Airy function combination occurring in X-mode cone potential
- $u_1 = (\gamma/\beta)^{1/3}(x_{h1}-x)$ rescaled variably near $x=x_{h1}$ [Eq. (3.36)]
- $u_2 = (\gamma/\beta)^{1/3}(x-x_{h2})$ rescaled variably near $x=x_{h2}$ [Eq. (3.36)]
- $u = -(\beta/\gamma^4)^{1/3} k_{||}(x, k_z) k_z^2$ [Eq. (3.39)]
- ϵ damping correction to u
- $\mathcal{F}[z, g(x), q(x)]$ general form of X-mode cone field which combines a $z>0$ cone with its mirror image $z<0$ cone [Eq. (3.82)]
- $\mathcal{D}[z, g(x_h), s(x)]$ general form of an ion thermal cone which originates at $x=x_h$, combining a $z>0$ cone with its mirror image [Eq. (3.82)]
- U_E, U_K, U_T energy density stored in the electrostatic field, kinetic energy density, and energy density of pressure waves, respectively [Eq. (4.48)]
- $U = U_E + U_K + U_T$ total energy density, when energy is being discussed

- $\vec{S}_C, \vec{S}_D, \vec{S}_T$ power flux vector for regular currents, displacement currents, and pressure oscillations, respectively [Eq. (4.48)]
- $\vec{S} = \vec{S}_E + \vec{S}_D + \vec{S}_T$ total power flux
- \bar{K}_h, \bar{K}_a symmetric and antisymmetric parts of \bar{K}
- $\Gamma(x, k_z)$ damping exponent of $\phi(x, k_z)$
- $\Gamma_c, \Gamma_h, \Gamma_l$ contributions to Γ from collisional, harmonic, and Landau damping, respectively

APPENDIX B: DERIVATION OF WKB SOLUTIONS

The WKB solutions to Poisson's equation, Eq. (3.2), can be obtained quite simply from the dispersion relation and the quasi-static power flux associated with that equation by a method discussed by T. Stix³ for the "transport of amplitudes" of waves in inhomogeneous media.

From the power flux vector $\vec{S}(\vec{k})$, given by Eq. (4.46), we see $|\mathcal{P}|$ is proportional to $\sqrt{S_x}$, where S_x is the power flow in the x-direction. Thus we may write \mathcal{P} in the form

$$\mathcal{P}(x, k_z) = f[\omega, \vec{k}(x)] \sqrt{|S_x(x)|} \quad (\text{B.1})$$

since \vec{k} is a function of x.

Now momentarily consider only a lossfree plasma. Then the energy flow past each x=constant surface must remain the same because there is no accumulation of energy between surfaces. Then between the points x_0 and x

$$|S_x(x)| = |S_x(x_0)| \quad (\text{B.2})$$

so

$$\mathcal{P}(x, k_z) = \left[\frac{f[x, \vec{k}(x)]}{f[x_0, \vec{k}(x_0)]} \right] \mathcal{P}(x_0, k_z) = \left| \frac{f[x, \vec{k}(x)]}{f[x_0, \vec{k}(x_0)]} \right| e^{i \int_{x_0}^x k_x dx} \quad (\text{B.3})$$

where we have introduced the WKB phase factor between x and x_0 .

The latter form can be easily generalized to a lossy medium by introducing a small imaginary part to k_x , which gives a valid result if $\text{Im } k_x \ll \text{Re } k_x$.

From Eq. (4.46), we have an expression for $|f[x, \vec{k}(x)]|$:

$$|f[x, \vec{k}(x)]| = [k_x K_{\perp} + 2\beta k_x^3]^{1/2} \quad (\text{B.4})$$

The value of k_x for the X-mode and ion thermal mode is given by Eq. (3.9). Taking $x_0=0$, we obtain the slowly varying coefficients $A(x)$ and $B(x)$ in

$$\psi(x, k_z) = A(x) e^{i \int k_x dx} \quad (\text{B.5a})$$

for the X-mode, and

$$\psi(x, k_z) = A(x) e^{i \int k_x dx} \quad (\text{B.5b})$$

for the ion thermal mode. These are (with a slight change in a constant factor):

$$\begin{aligned} A(x) &= \left[\frac{K_{\parallel}(0) K_{\perp}(0)}{K_{\parallel}(x) K_{\perp}(x)} \right]^{1/4} \\ B(x) &= \left[\frac{K_{\parallel}(0) K_{\perp}(0) \beta(x)}{K_{\perp}^3(x)} \right]^{1/4} \end{aligned} \quad (\text{B.6})$$

The WKB solutions in all regions are thus determined by taking the form of k_x appropriate for each region that we desire it, from Eq. (3.9).

REFERENCES

1. H. Kuehl, "Electromagnetic Radiation from an Electric Dipole in a Cold Anisotropic Plasma", *Phys. Fluids* 5, 1095 (1962).
2. R. Fisher and R. Gould, "Resonance Cones in the Field Pattern of a Radio Frequency Probe in a Warm Anisotropic Plasma", *Phys. Fluids* 14, 857 (1971); R. Fisher, "Resonance Cones in the Field Pattern of a Short Radio Frequency Probe in a Warm Anisotropic Plasma", Ph. D. Thesis, California Institute of Technology, April, 1970.
3. T. H. Stix, The Theory of Plasma Waves (McGraw-Hill, New York, 1962).
4. A. Gonfalone, "Density and Electron Temperature Deduced from the Observation of Resonance Cones of an Antenna in a Magnetoplasma", *J. Phys. (Paris)* 33, 521(1972).
5. R. J. Briggs and R. R. Parker, "Transport of RF Energy to the Lower Hybrid Resonance in an Inhomogeneous Plasma", *Phys. Rev. Lett.* 29, 852' (1972).
6. K. Burrell, "Resonance Cones in a Warm Plasma for a Finite Magnetic Field", *Phys. Fluids* 18, 1716 (1975); K. Burrell, "An Investigation into the Resonance Cone Structure in a Warm Anisotropic Plasma", Ph. D. Thesis, California Institute of Technology, **May**, 1974.
7. P. Colestock, "Measurement and Analysis of Resonance Cone Structure from a Finite Sized Source at the Lower Hybrid Frequency", Second Topical Conference on RF Plasma Heating (Lubbock, Texas, 1974).
8. P. Bellan and M. Porkolab, "Experimental Studies of Lower Hybrid Wave Propagation", *Phys. Fluids* 19, 995 (1976).
9. P. Bellan, "Resonance Cones Below the Ion Cyclotron Frequency: Theory and Experiment", *Phys. Rev. Lett.* 37, 903 (1976).
10. T. Ohnuma, T. Kuwabara, K. Shibata, and S. Adachi, "Observation of the Low Frequency Resonance Cones", *Phys. Rev. Lett.* 57, 206 (1976).

11. P. Javel, G. Müller, U. Wever, and R. R. Weynants, "The Resonance Cones of Electron Plasma Waves in Toroidal, Inhomogeneous Plasmas", *Plasma Physics* 18, 51 (1976).
12. T. Stix, "Radiation and Absorption via Mode Conversion in an Inhomogeneous Collision-Free Plasma", *Phys. Rev. Lett.* 15, 878 (1965).
13. Clemmow and Dougherty, Electrodynamics of Particles and Plasmas", (Addison-Wesley, London, 1969).
14. I. Bernstein, "Waves in a Plasma in a Magnetic Field", *Phys. Rev.* 109, 10 (1958).
15. V. E. Golant, "Plasma Penetration Near the Lower Hybrid Frequency", *Zh. Tekh. Fiz.* 41, 2492 (1971) [*Sov. Phys.-Tech. Phys.* 16, 1980 (1972)].
16. B. Moore and M. Oakes, "Mode Conversion in an Inhomogeneous Plasma", *Phys. Fluids* 15, 144 (1972).
17. I. Fidone, "Linear Wave Conversion at the Lower Hybrid Resonance", Symposium on Plasma Heating in Toroidal Devices, Varenna, Italy (Editrice Compositori, Bologna, 1974).
18. M. Simonutti and R. Parker, "Numerical Solution for Linear Wave Conversion near Lower Hybrid Resonance", Second Topical Conference on RF Plasma Heating (Lubbock, Texas, 1974).
19. P. Bellan and M. Porkolab, "Propagation and Mode Conversion of Lower Hybrid Waves Generated by a Finite Source", *Phys. Fluids* 17, 1592 (1974).
20. K. Ko and H. Kuehl, "Excitation and Linear Mode Conversion of Lower Hybrid Resonance Cones in an Inhomogeneous Plasma", *Phys. Fluids* 18, 1816 (1975).
21. M. Simonutti, "Propagation and Collisionless Absorption of Linearly Converted Lower Hybrid Waves", *Phys. Fluids* 18, 1524 (1975).
22. M. Brambilla, "Propagation and Absorption of Waves at the Lower Hybrid Resonance", *Plasma Physics* 18, 669 (1976).

23. B. Fried and S. Conte, The Plasma Dispersion Function (Academic Press, New York, 1961).
24. Abramowitz and Stegun, Handbook of Mathematical Functions (National Bureau of Standards, Washington, D. C., 1964).
25. D. Baldwin and G. Rowlands, "Plasma Oscillations Perpendicular to a Weak Magnetic Field", *Phys. Fluids* 9, 2444 (1966).
26. L. Pearstein and D. Bhadra, "Dispersion of the Upper Hybrid Mode in a Spatially Inhomogeneous Plasma", *Phys. Fluids* 12, 213 (1969).
27. F. Troyan and F. Perkins, "Lower Hybrid Heating in Large Tokamaks" in Proceedings of the Second Topical Conference on RF Plasma Heating (Texas Tech. U., Lubbock, Tex., 1974).
28. R. W. Gould, "On the Connection between Resonance Cones and Guided Wave Modes" in U.S.-Australia Plasma Waves Conference (Sydney, Australia, 1974).
29. C. L. Grabbe, "Resonance Cones in a Warm Magnetized Bounded Plasma", *Phys. Fluids* 20, 599 (1977).
30. N. Froman and P. Froman, The JWKB Approximation (North Holland, Amsterdam, 1965).
31. H. Kuehl, B. O'Brien and G. Stewart, "Resonances and Wave Conversion below the Second Electron Cyclotron Harmonic", *Phys. Fluids* 13, 1595 (1970).
32. T. Tang, "Mode Conversion in a Weakly Inhomogeneous Collisionless Magnetoplasma", *Phys. Fluids* 13, 121 (1970).
33. D. Gorman, "Plasma Waves at Singular Turning Points", *Phys. Fluids* 9, 1262 (1966).
34. S. J. Buchsbaum and A Hasegawa, "Longitudinal Plasma Oscillations near Electron Cyclotron Harmonics," *Phys. Rev.* 143, 303 (1966).
35. A. Rabenstein, "Asymptotic Solution of $u^{(iv)} + \lambda^2 [zu'' + \alpha u' + \beta u] = 0$ for Large $|\lambda|$ ", *Arch. Natl. Mech. Anal.* 1, 418 (1958).